Remote Sensing Solutions, Inc.

PROJECT: Operational SFMR-NAWIPS Airborne Processing and Data Distribution Products

NOAA Award Number: NA05OAR4171101

Final Report

Prepared By: Dr. James Carswell

Date: 10/18/2007

Table of Contents

List of Figures

List of Tables

1 Introduction

1.1 Scope

This document serves as the final report for the Joint Hurricane Testbed (JHT) project entitled, “Operational SFMR-NAWIPS Airborne Processing and Data Distribution Products”. It provides recommendations aimed at improving the accuracy and quality of the operational NOAA SFMR ocean surface wind speed and column rain rate retrievals, while also reducing the uncertainty of these measurements.

1.2 Applicable Documents

The following is a list of references for citations from within this report:

- Operational SFMR-NAWIPS Airborne Processing and Data Distribution Products: Annual Report – Year 1.
- Jiang et al, 2006, “Validation of Rain-rate Estimation in Hurricanes from the Stepped Frequency Microwave Radiometer: Algorithm Correction and Error Analysis,” J. Atmos. Sci. Vol. 63 pp 252-267.
- Uhlhorn et al, “Hurricane Surface Wind Measurements from an Operational Stepped Frequency Microwave Radiometer”, Monthly Weather Review, Vol. 135, pp 3070—3085, 2007.
- Esteban et al, “Remote Sensing of the Ocean and the Atmospheric Boundary Layer within Tropical Cyclones,” Dissertation, Univeristy of Massachusetts, Amherst, 2005.
- Esteban et al, “IWRAP: The Imaging Wind and Rain Airborne Profiler for Remote Sensing of the Ocean and the Atmospheric Boundary Layer within Tropical Cyclones,” IEEE TGARS, Vol. 43, No 8, pp 1775—1787, 2005.

1.3 Document Breakdown

This document contains three sections. Section 1 contains the introduction. Section 2 reviews the work performed and results obtained during the second year of this effort. Section 3 presents recommendations for how to proceed forward based on the results obtained.

2 Second Year – Work Performed & Results Obtained

During the second year effort, the JHT SFMR team focused on analyzing the SFMR observations and retrievals obtained during the 2006 Hurricane season. The objectives included: identifying and explaining anomalies; identifying and removing the sources of RFI that increased the uncertainty in the SFMR estimates during the 2006 hurricane season; and reducing uncertainty and biases in the SFMR wind and rain retrievals caused by errors in the SFMR absorption geophysical model function (GMF) along with the sequential sampling approach utilized by the SFMR to measure the frequency response of the observed scene. These efforts are summarized in the following sections. RSS also developed and deployed a real-time GIS and time series display and analysis application that enabled users at NHC and HRD to visualize and interact with the SFMR and flight level data. This application was presented at the NHC conference in 2006. A short summary of this application is given. If more information is desired on this particular application, please contact Jim Carswell at carswell@remotesensingsolutions.com.

2.1 2006 Hurricane Season - SFMR Anomalies

Remote Sensing Solutions (RSS) reviewed the SFMR measurements and retrievals from the 2006 hurricane season. Based on notes compiled from email communications between HRD and NHC forecasters during the 2006 season, RSS pinpointed locations within the data which correspond to probable errors in the SFMR retrievals. RSS identified anomalies in the SFMR retrievals during missions through Hurricane Ernesto on the 29th and 31st of August.

Figures 1 and 3 map the SFMR wind retrievals for the flights on August 29 and 31, 2006. The NOAA N42RF WP-3D aircraft was flown for these missions with the US002 AOC SFMR. The time stamps, shown in green, mark the regions where problems in the SFMR retrievals were discovered. Figures 2 and 4 show the corresponding multiple time series plots of the SFMR retrievals (wind and rain rate). More detailed time series plots will be shown and a quick summary is given below:

- *August 29th mission*: The 10 second averaged SFMR wind retrievals exceeded the storm force threshold but did not reach hurricane force. Five anomalies were noted.
- *August 31st mission*: This was the second landfall mission. The 10 second averaged SFMR wind retrievals exceeded the storm force threshold but did not reach hurricane force. Five anomalies in the SFMR wind retrievals were observed.

In the subsections to follow, the observed anomalies are presented and their causes explained. Depending on the case, the anomalies are believed to be due to either low water depth or caused by limitations in the precipitation model used in the SFMR retrieval process and the manner in which it samples the scene.

Recall that in our 1st annual JHT report (dated 07/10/2006), we showed that errors in the rain retrieval could translate into errors in the wind retrieval. Solutions to eliminate or lessen such anomalies are address in sections 2.3 and 2.4 of this report.

Before discussing these cases, however, it should be noted that some concern raised by forecasters may have occurred due to the high resolution SFMR retrievals, as well as the averaged retrievals, made available to NHC through RSS' Real-time Display Application. These high resolution measurements exhibit more variance than NHC may be accustomed to seeing. The variance is caused by a shorter integration time (3 seconds versus ten or 30 seconds). We calculated the expected standard deviation for these retrievals based on the performance specifications of the AOC SFMR and found the measured standard deviation for the retrievals agreed well with the predictions.

2.1.1 Anomalies - 29 August 2006

Six anomalies in the SFMR retrievals were observed during the August 29th mission. Each anomaly is presented below and its causes explained. In **Figure 5** through **Figure 9**, and **Figure 11**, the ten second averaged SFMR and flight level winds are plotted as red and purple lines, respectively. The high resolution SFMR wind speed retrievals are plotted as points. The SFMR rain rate retrievals are plotted as a blue line. The collocated water depth estimate (2 minute resolution bathymetry data) is shown as a green line. If not present, the water depth is greater than 100 m.

Figure 5 shows the observed anomaly at approximately 15.975 hours. At this time a rain event occurred. The SFMR wind speed retrieval decreased by more than 10 kts at the beginning of the rain event and increased to approximately 60 kts following the rain event. The flight level winds were relatively flat. We believe that the SFMR wind speed estimates derived from this situation are in error. This wind speed error is due to the current limitations in the SFMR precipitation model and the stepped frequency sampling approach employed by the SFMR. That is, the current precipitation model does not adequately describe the absorption due to precipitation, and because the SFMR does not simultaneously sample all six frequencies, but rather sequentially samples each, slightly different scenes can be observed by each frequency channel. At lower wind speeds (below hurricane force winds) this issue can cause a convergence problem in the retrieval process and oscillating errors. A characteristic of these errors is that the wind speed retrievals will dip down and rise up (i.e. oscillate) as a rain band is entered or exited. By looking for a dip as well as a rise in the wind speed and comparing them against the flight level wind speeds, these errors can be detected. Likewise, at 16.05 hrs (Figure 5), the SFMR winds also excessively increased during a precipitation event and did not reflect the true surface wind. A similar event to this occurred again at 17.12 hours and at 17.55 hours (Figure 8 and Figure 9). Once the precipitation model and sampling have been corrected, we expect that these types of anomalies will not occur.

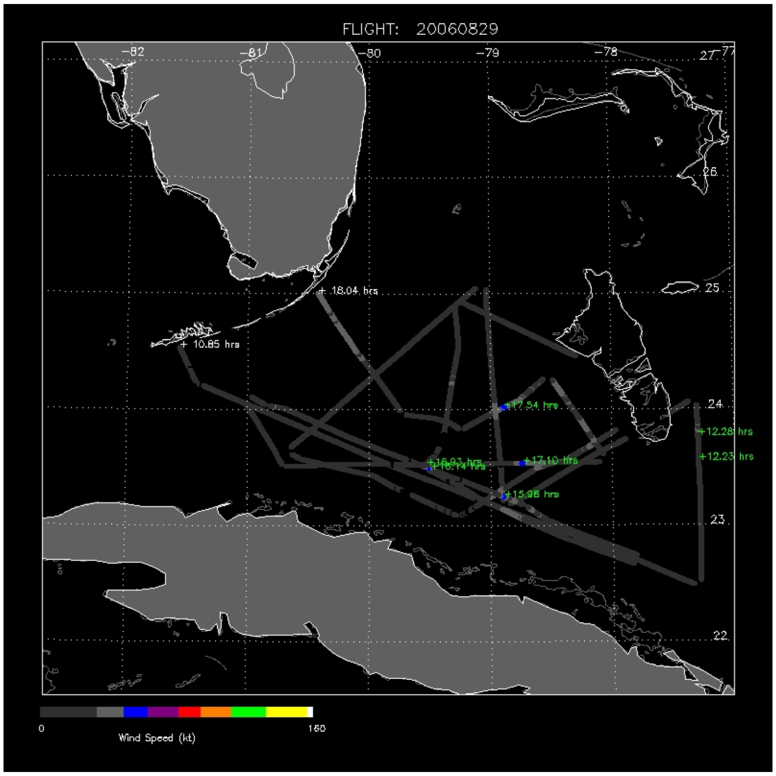

Figure 1: Geolocated SFMR winds estimates from 29 August, 2006.

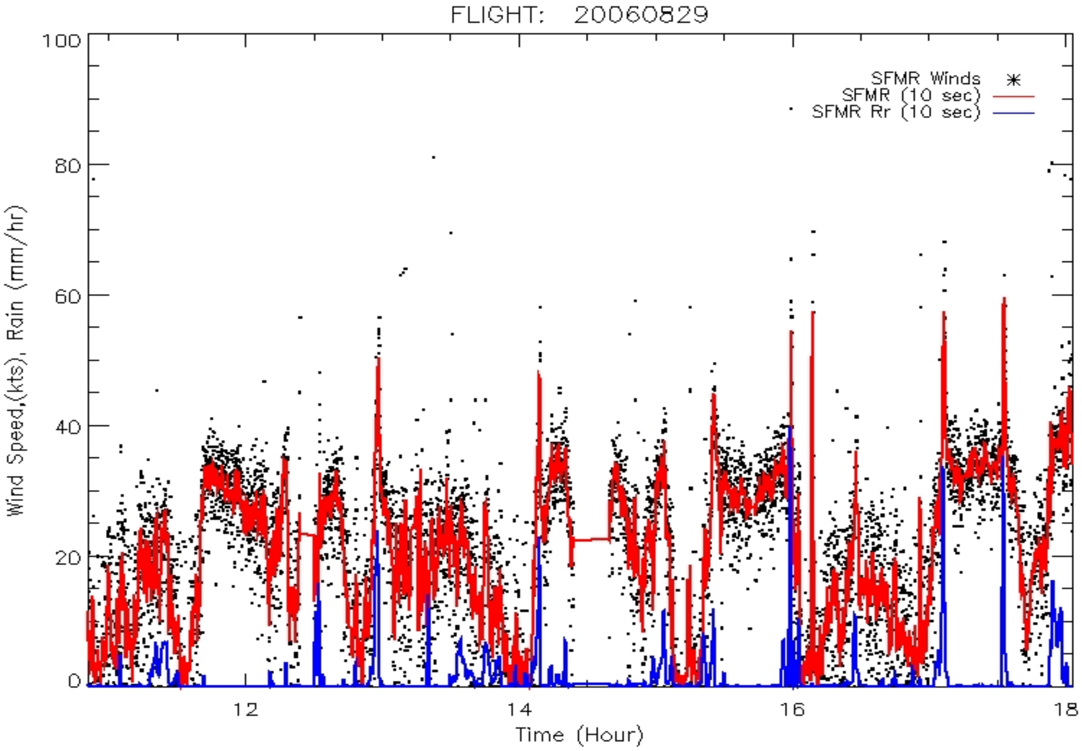

Figure 2: Time series plot of the SFMR wind retrievals (points) with averaged SFMR wind speed and rain rate retrievals (red, blue) acquired on 29 August, 2006.

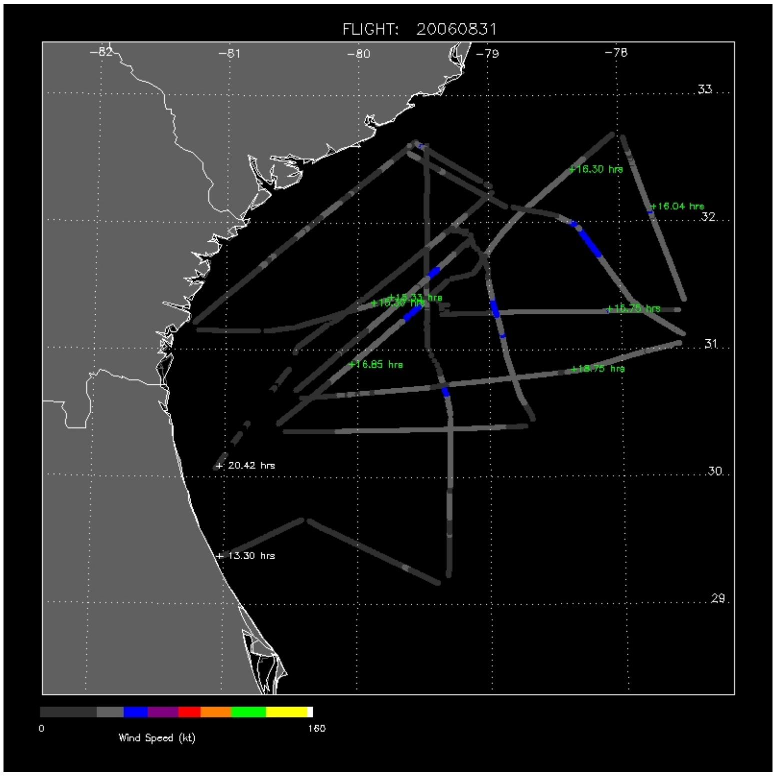

Figure 3: Geolocated SFMR winds estimates from 31 August, 2006

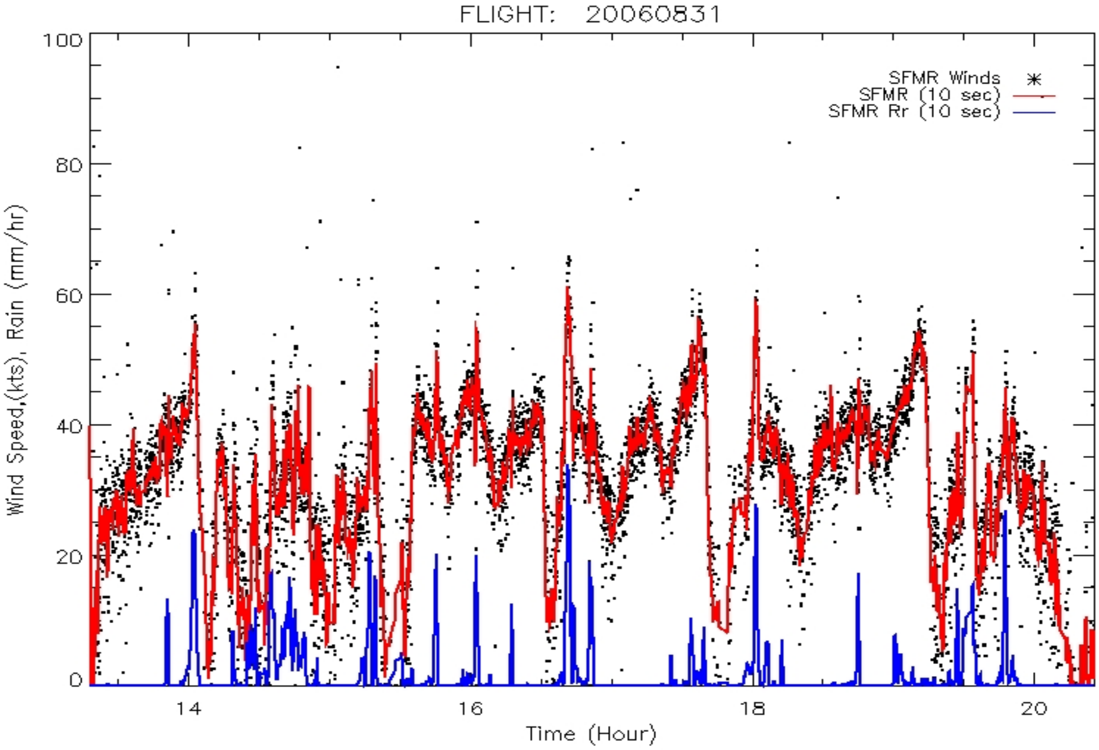

Figure 4: Time series plot of the SFMR wind retrievals (points) and averaged SFMR wind speed and rain rate retrievals (red, blue) acquired on 31 August, 2006.

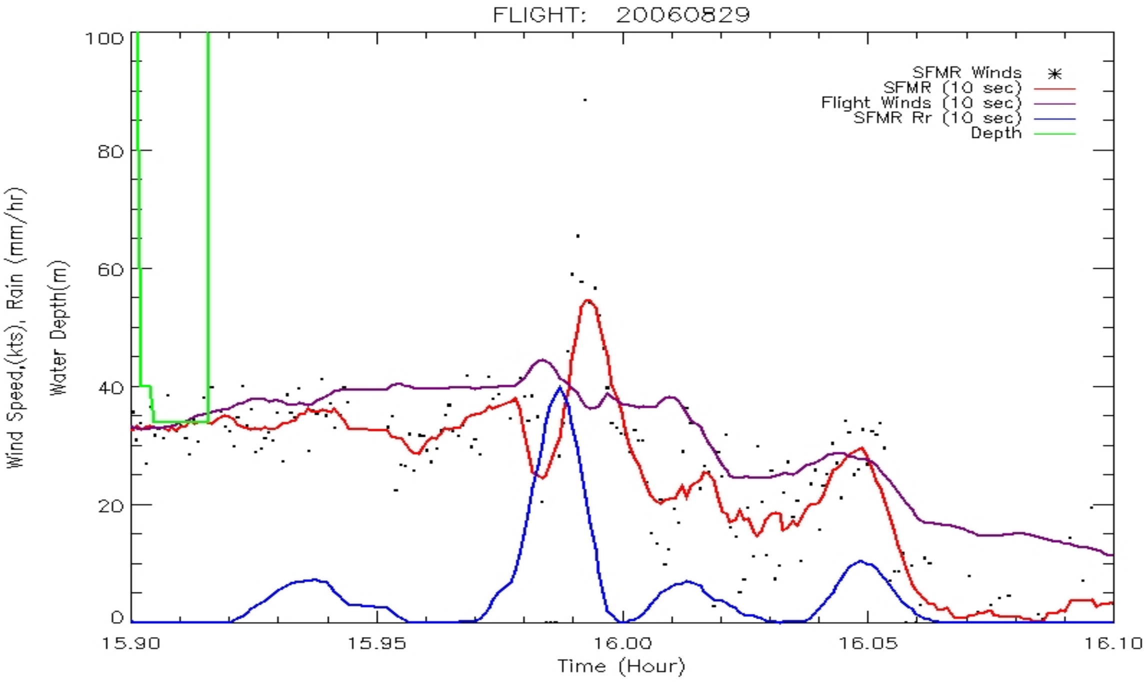

Figure 5: Anomaly in the SFMR wind retrieval is shown at approximately 15.975 hours on 29 August 2006.

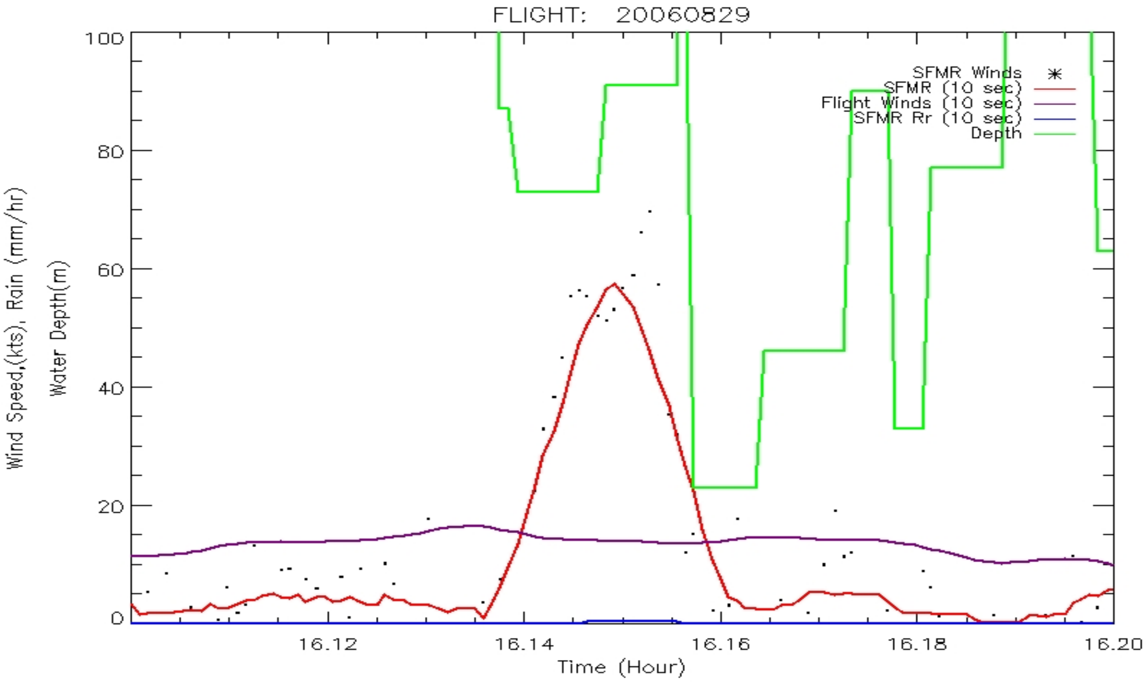

Figure 6: Anomaly in the SFMR wind retrieval is shown at approximately 16.15 hours on 29 August 2006.

As mentioned previously, low water depth can also cause an artificial increase in the SFMR wind speed retrievals by causing enhanced wave breaking and thus more foam generation. We believe that this explains the anomalies at 16.15 hrs (figure 8) and 16.94 hrs (figure 9) where the SFMR winds significantly increased as the water depth became shallow (less than 30 m). Note that in Figure 8, the water depth at 16.15 hrs appears to be approximately 70 m and then drops to 20 m. The spatial resolution / sampling of the bathymetry data are on the order of 3 km.

The 70 m measurements are more than 1.5 km from the track whereas the 20 m water depth measurements are within 500 m. The enhanced SFMR winds at 17.12 hrs may have also been partially attributed to a sharp decrease in the water depth. It is difficult to discern this however since both rain and low water depths occurred at this time.

To illustrate the complexity of bathymetry effects, **Figure 10** shows a picture taken from the WP-3D aircraft at 12:14 GMT (12.23 hours). In this image, small land features and the effects of bathymetry can be seen. The shallow water and land features prevent the long wave structure seen in the lower half of the image from propagating to the area in the upper half. Wave breaking events that generate foam are seen in the lower part of the image but are not seen in the upper half even though the wind is believed to be fairly constant. In such a situation, the SFMR would retrieve different winds in these two areas. Further, the small land features are not detected in our current land mask and may contaminate the brightness temperature measurements, and thus contaminate the SFMR retrievals. **Figure 11** presents the SFMR retrievals around the time that this picture was taken. At 12.23 hours, the wind appears to increase. It is difficult to discern whether the wind actually increased, land contamination occurred or enhanced wave breaking occurred due to shallow water. Note that the flight level winds do not show a corresponding increase.

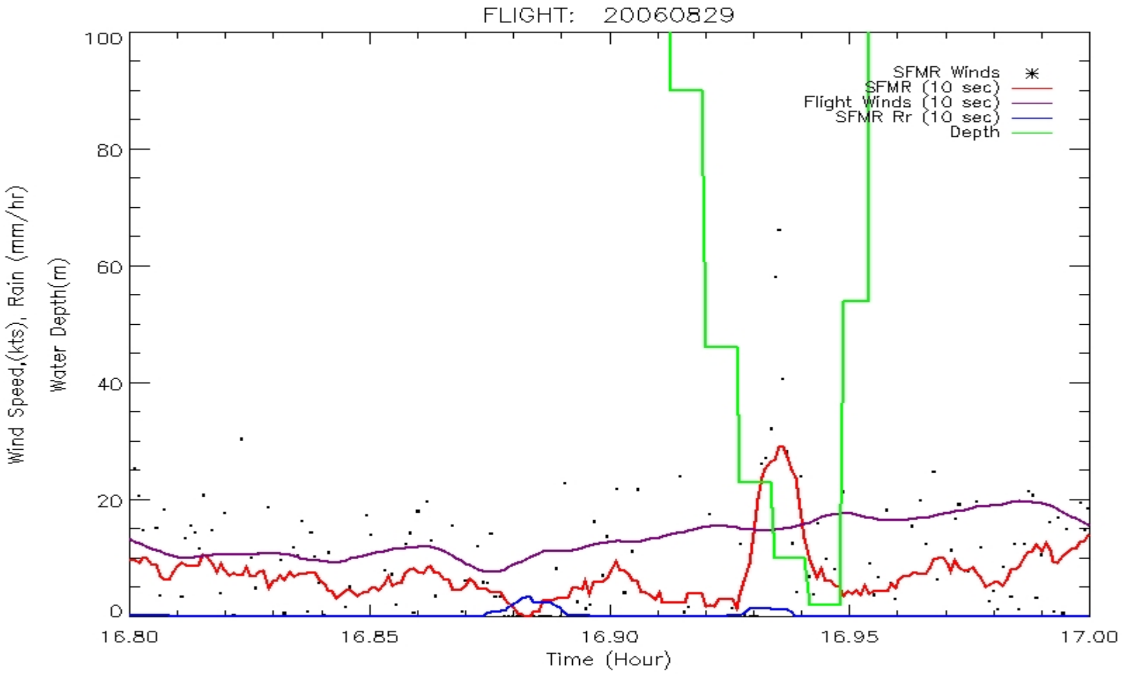

Figure 7: Anomaly in the SFMR wind retrieval is shown at approximately 16.94 hours on 29 August 2006.

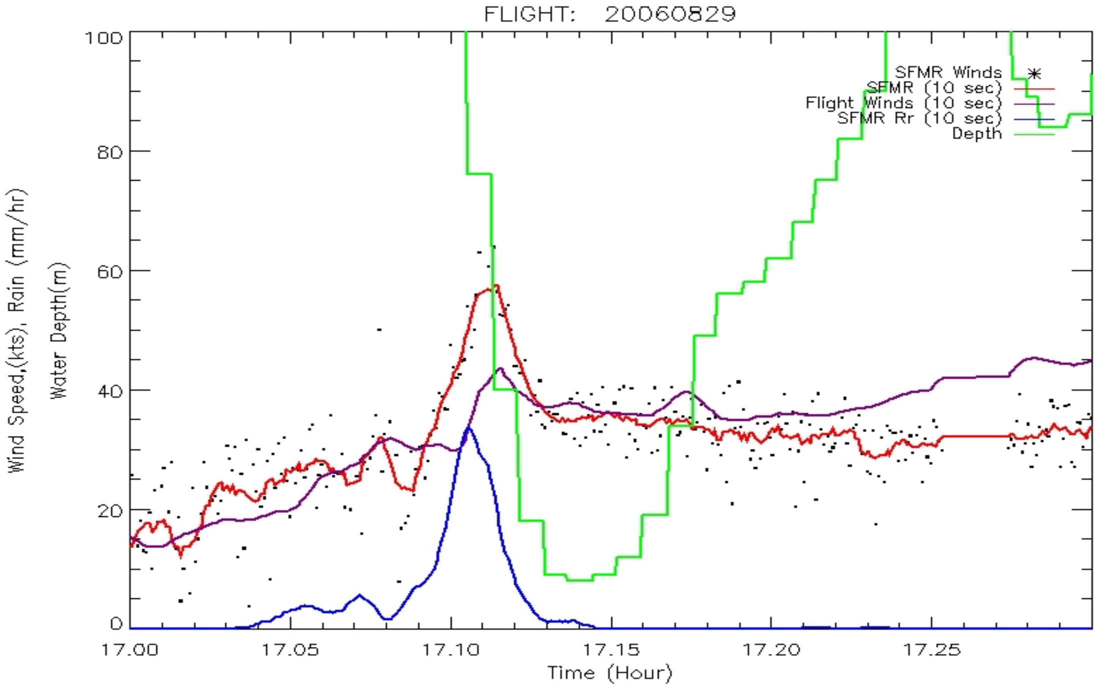

Figure 8: Anomaly in the SFMR wind retrieval is shown at approximately 17.12 hours on 29 August 2006.

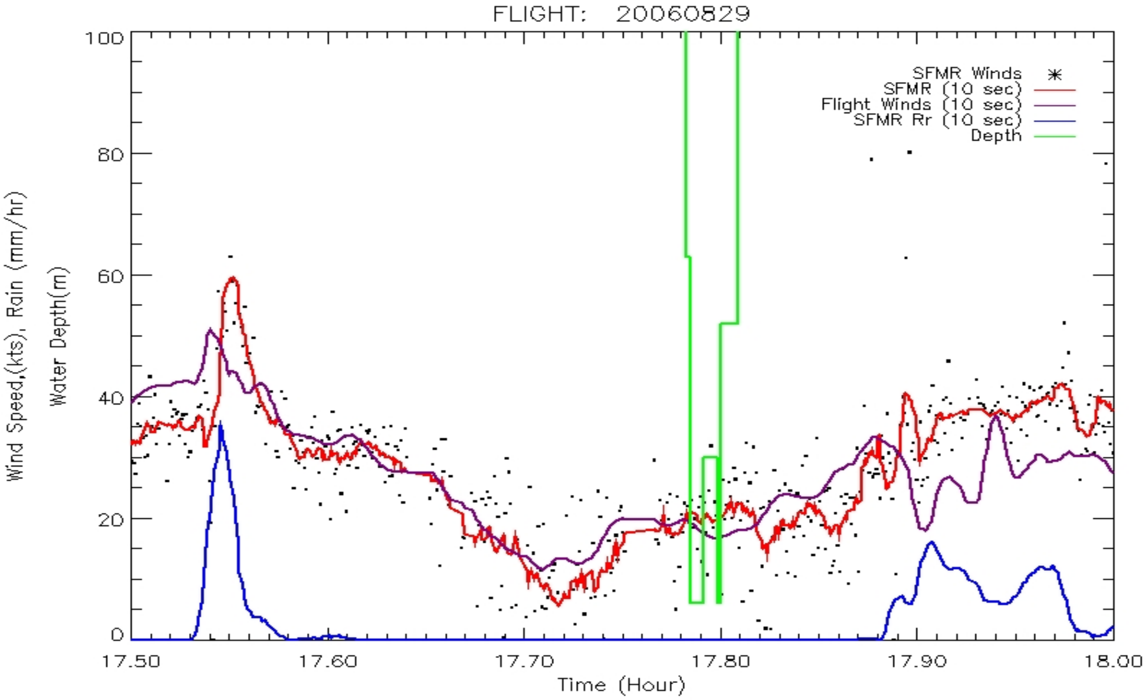

Figure 9: Anomalies in the SFMR wind retrieval are shown at approximately 17.55 and 17.9 hours on 29 August 2006.

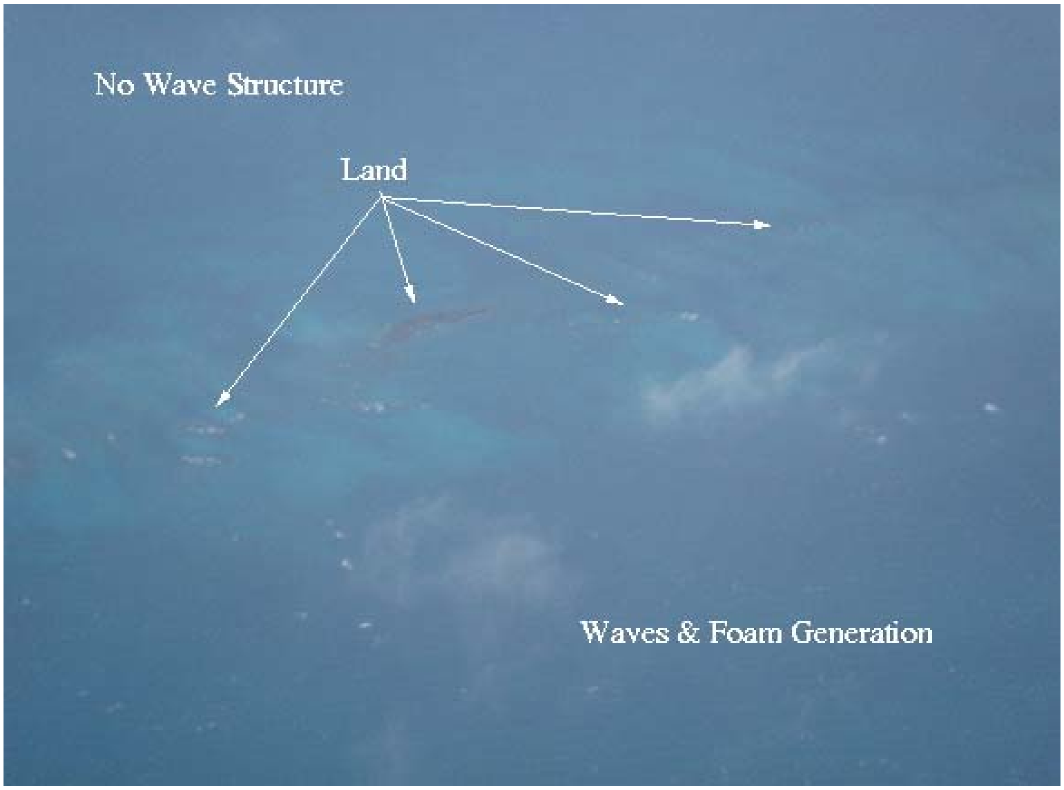

Figure 10: Picture taken from WP-3D aircraft at 12:14 on 29 August, 2006.

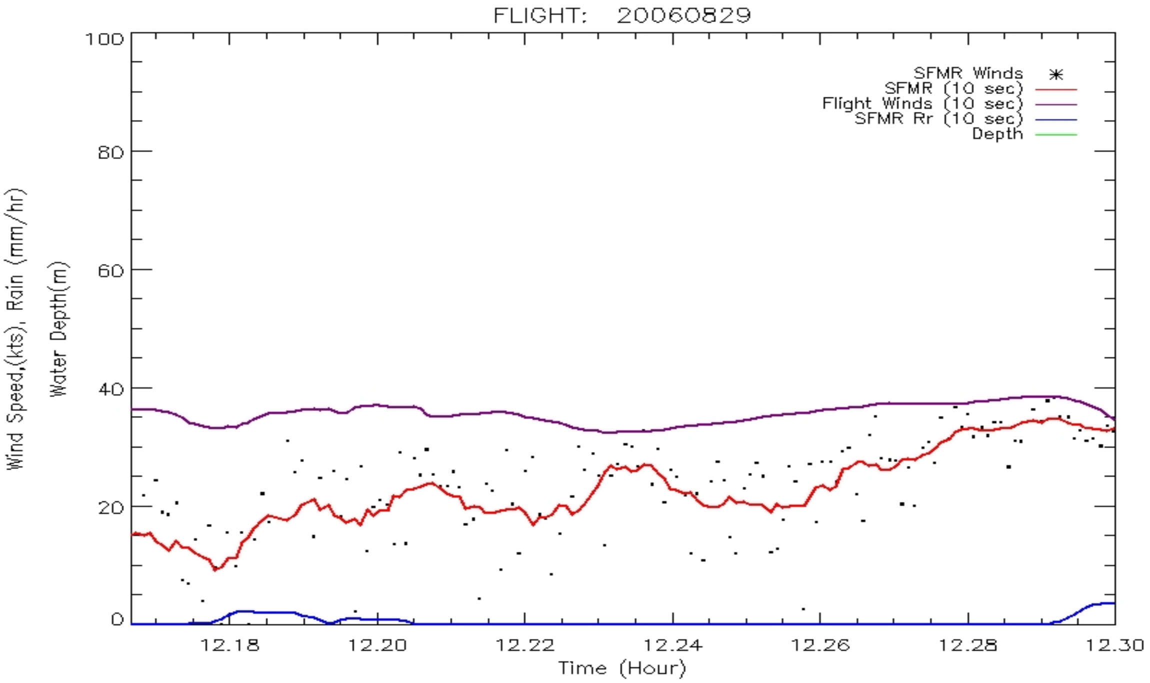

Figure 11: An anomaly in the SFMR wind retrieval is shown at approximately 12.23 hours on 29 August 2006.

2.1.2 Anomalies - 31 August 2006

The mission on 31 August 2006 occurred over deep water. During this mission, the observed anomalies in the SFMR wind speed retrievals occurred in the presence of precipitation. These features can be noted in **Figure 12** at 15.30 and 15.33 hours, **Figure 13** at 15.76 hours, **Figure 14** at 16.04 hours and **Figure 15** at 18.75 hours. Note that the response at 15.76 hours is a little less obvious. We believe the small dip in the winds is caused by the errors in the precipitation model.

Figure 16 shows the SFMR retrievals during a precipitation event and stronger wind speeds. In this case (i.e. stronger winds), the SFMR wind retrievals do not appear to be effected. We believe that for most cases where the winds are at hurricane force, this will be the situation or that the impact of precipitation will be less. Note however that there are still errors in the wind speed and rain rate retrievals because the absorption model used in the SFMR retrieval process is incorrect. As stated before, section 2.3 will address this particular issue. Finally, once the precipitation model is corrected, errors in the wind retrievals caused by precipitation will be removed or significantly reduced.

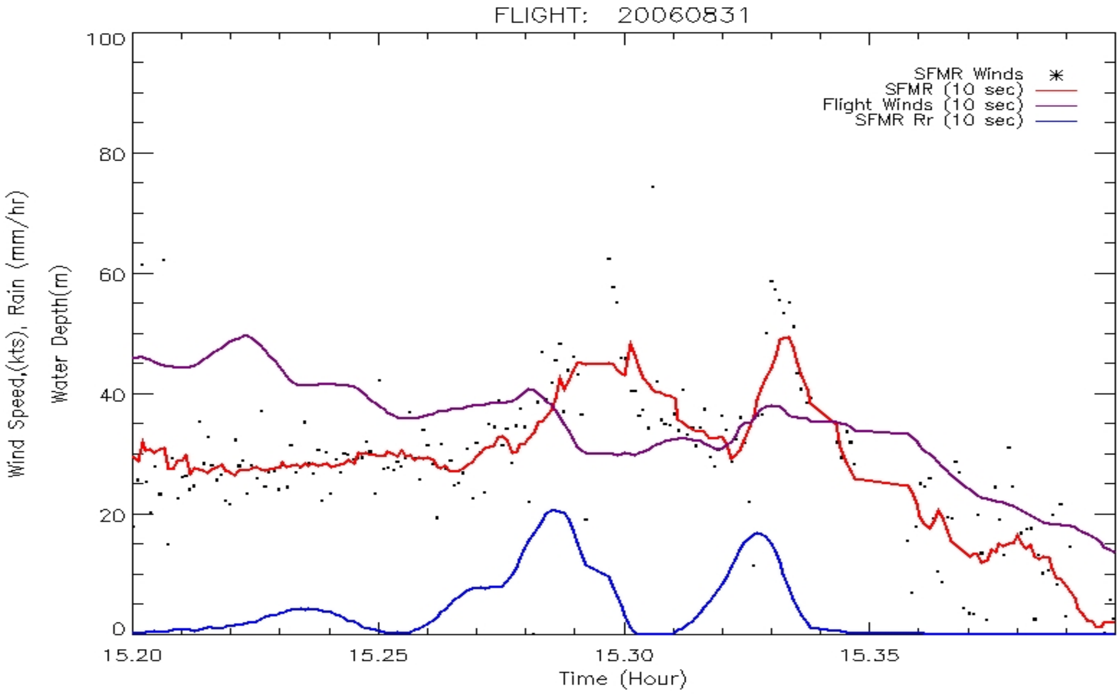

Figure 12: Anomalies in the SFMR wind retrieval are shown at approximately 15.3 and 15.33 on 31 August 2006.

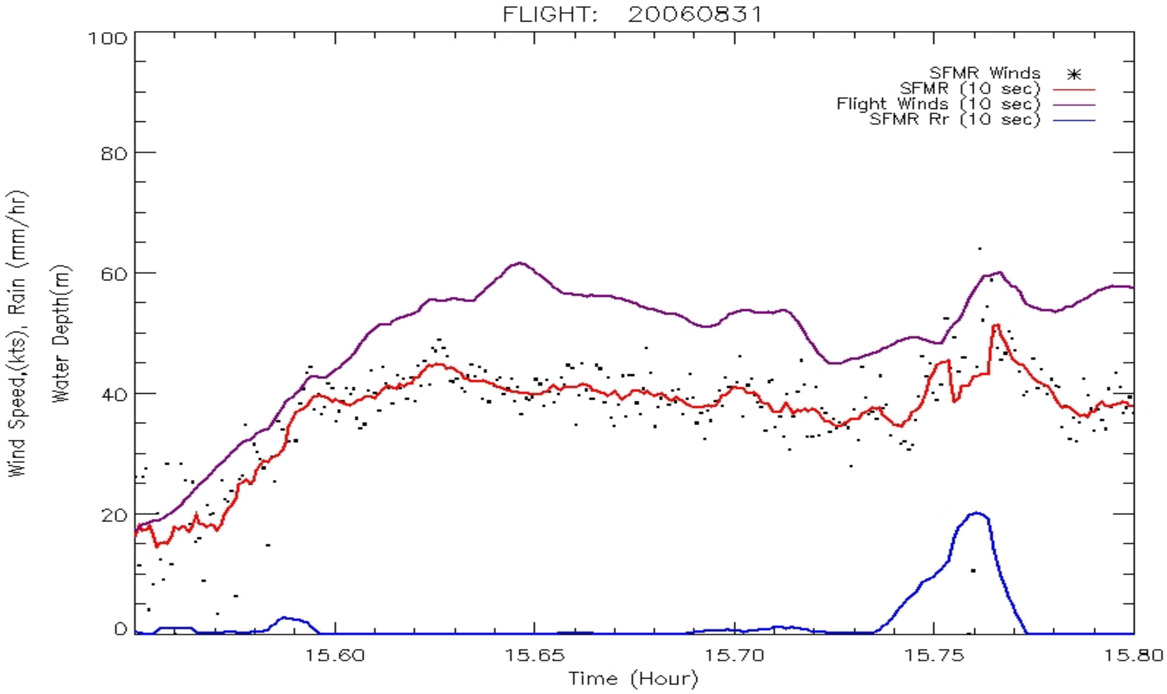

Figure 13: Anomaly in the SFMR wind retrieval is shown at approximately 15.76 hours on 31 August 2006.

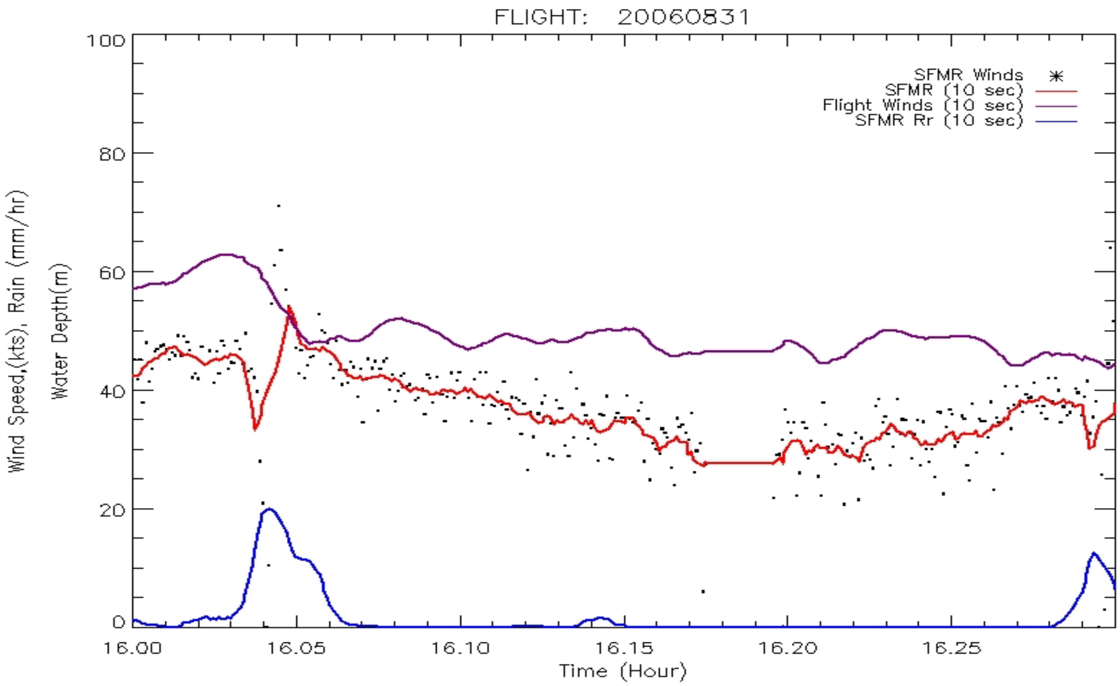

Figure 14: Anomalies in the SFMR wind retrieval are shown at approximately 16.05 and 16.3 hours on 31 August 2006.

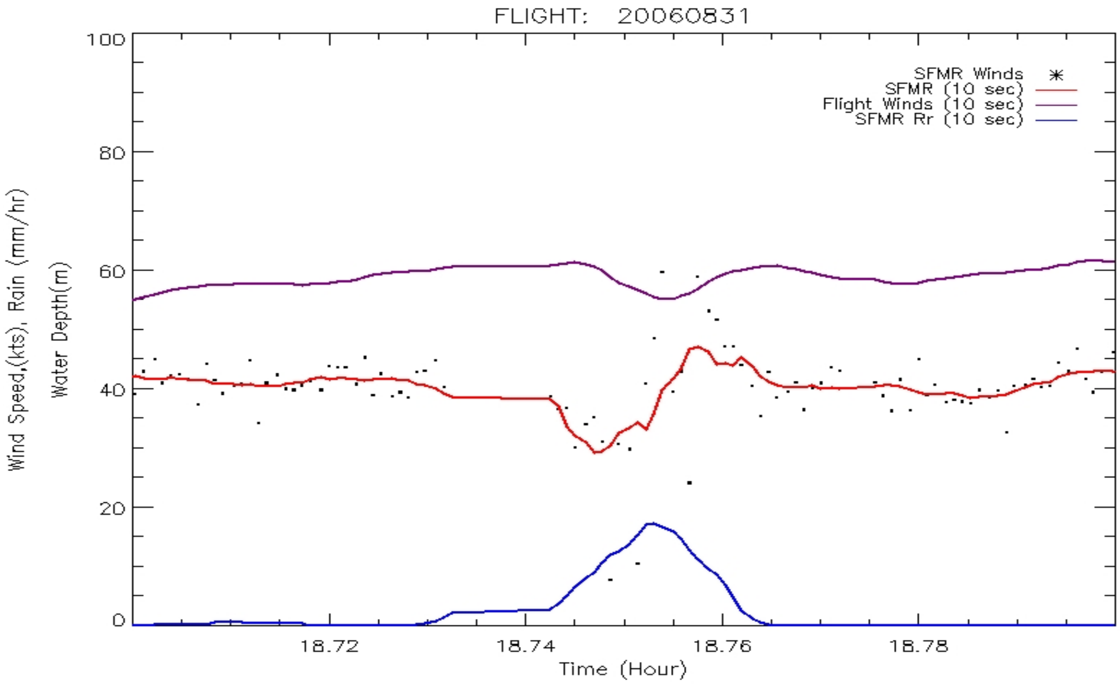

Figure 15: Anomaly in the SFMR wind retrieval is shown at approximately 18.75 hours on 31 August 2006.

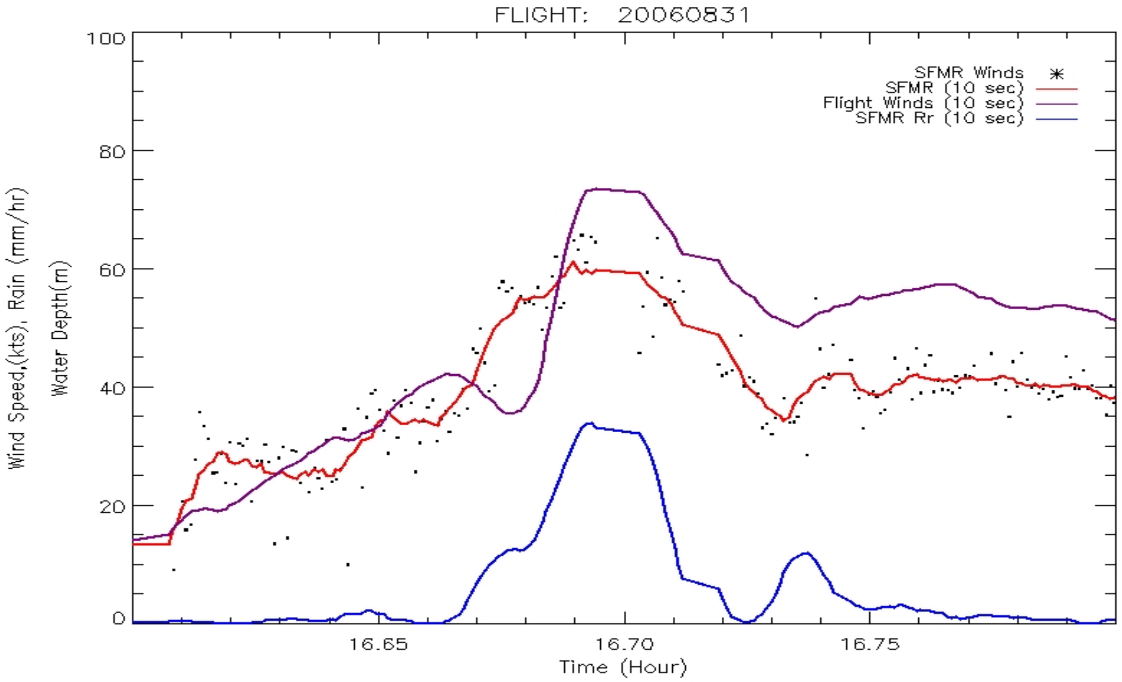

Figure 16: Example of SFMR wind retrievals unaffected by precipitation for stronger winds.

2.2 IWRAP – SFMR interference

In 2006, the IWRAP C-band transceiver was operated during some of the hurricane reconnaissance missions. IWRAP's lowest frequency channel transmitted at 4.985 GHz. When transmitting at this frequency, interference was noted in the lower frequency channel of the AOC SFMR (4.74 GHz). Because IWRAP operates at 20 KHz pulse repetition frequency and because AOC SFMR uses a fixed blanking period, the AOC SFMR could not be blanked during IWRAP transmission. The blanking technique is used by the SFMR to avoid being affected by radio frequency interference (RFI) from local radar systems (i.e. the C-band Lower Fuselage Radar). By viewing its internal loads rather than antenna port (i.e. blanking) while the interfering radar is transmitting and for some time thereafter, the AOC SFMR prevents viewing any RFI.

Since the SFMR could not use a blanking technique with IWRAP, the lower two channels were not used in the retrieval process. Note that the second lowest AOC SFMR channel falls in the middle of the IWRAP frequency band. This allowed the SFMR to retrieve the surface winds without contamination from IWRAP, but it also increased the variance in the wind speed retrievals. The reason is two fold. First, by using only four channels rather than six, the number of samples used in the retrieval decreases by 33 percent. This effectively increases the noise in the retrieval process because fewer samples are used to reduce the normal random noise in the measurements. Second, and more important, is that the maximum frequency separation of the measurements is decreased by 0.83 GHz. As a result, the retrieval process becomes more sensitive to the measurement noise. Recall that the retrieval process is a coupled problem where the wind and rain rate are solved for simultaneously. The rain signature is strongly frequency dependent. By reducing the frequency separation in the measurements, measurement noise can be mistaken for rain causing both a wind speed and rain rate error. Because the measurement noise is random, a bias does not occur, but the variance of the retrievals increases.

Simulations were run to determine the amount that the standard deviation of the wind speed retrievals would increase with the lower two frequency channels disabled. **Figure 17** presents the results. The upper plot shows the standard deviation in the wind speed retrievals as a function of wind speed when only the upper four SFMR frequency channels are used (dashed line) and when all six channels are used (solid line). The lower plot shows the percent increase in the standard deviation as a function of wind speed. These results are averaged over all rain rates because we found that there was no significant dependence on rain rate. As can be seen, when operating with only the four upper channels there is approximately a 75 percent increase in the wind speed retrieval uncertainty (i.e. standard deviation in the wind speed retrievals). When the winds exceed storm force, the resultant standard deviation is less than 2 knots. Although this meets the original requirement for the SFMR, this additional error was prevented for the 2007 hurricane season.

Working with UMass and NOAA, a series of measurements were acquired during the Winter 2007 Ocean Winds Experiment. Using a RF synthesizer, the IWRAP C-band transceiver was stepped through a series of frequencies from 4.7 GHz to 5.2 GHz in 50 MHz steps, dwelling for approximately 1 minute at each frequency, while the AOC SFMR collected its Tb measurements. All other IWRAP internal local oscillators were powered off. The SFMR Tb measurements were then analyzed when RFI was present.

Figure 18 plots the AOC SFMR 4.74 GHz Tb measurements and the IWRAP frequency versus time. For frequencies below 5 GHz, RFI can be seen. To see the finer details, the mean Tb value for each IWRAP frequency interval was determined and subtracted from the Tb values. **Figure 19** plots this difference. This procedure was repeated for the other five AOC SFMR frequency channels. **Figure 20** through **Figure 29** show the results. Note that the spikes seen at approximately 18.7, 18.75 and 18.977 hours are present in all six channels and are related to the synthesizer switching frequencies. From these results, we concluded that IWRAP should not transmit below 5 GHz and that a high pass filter should be installed with a cutoff frequency of 4.9 GHz to ensure that the IWRAP will not interfere with the lower channel of the SFMR. Working with NOAA and UMass, this filter was selected, purchased and installed. No interference was found after installing the filter.

In the future, radar systems deployed on the NOAA WP-3D aircraft should not be allowed to operate between approximately 4.6 GH and 4.9 GHz and should also require a filter to reject out-of-band noise in this frequency range from the transmitted spectrum.

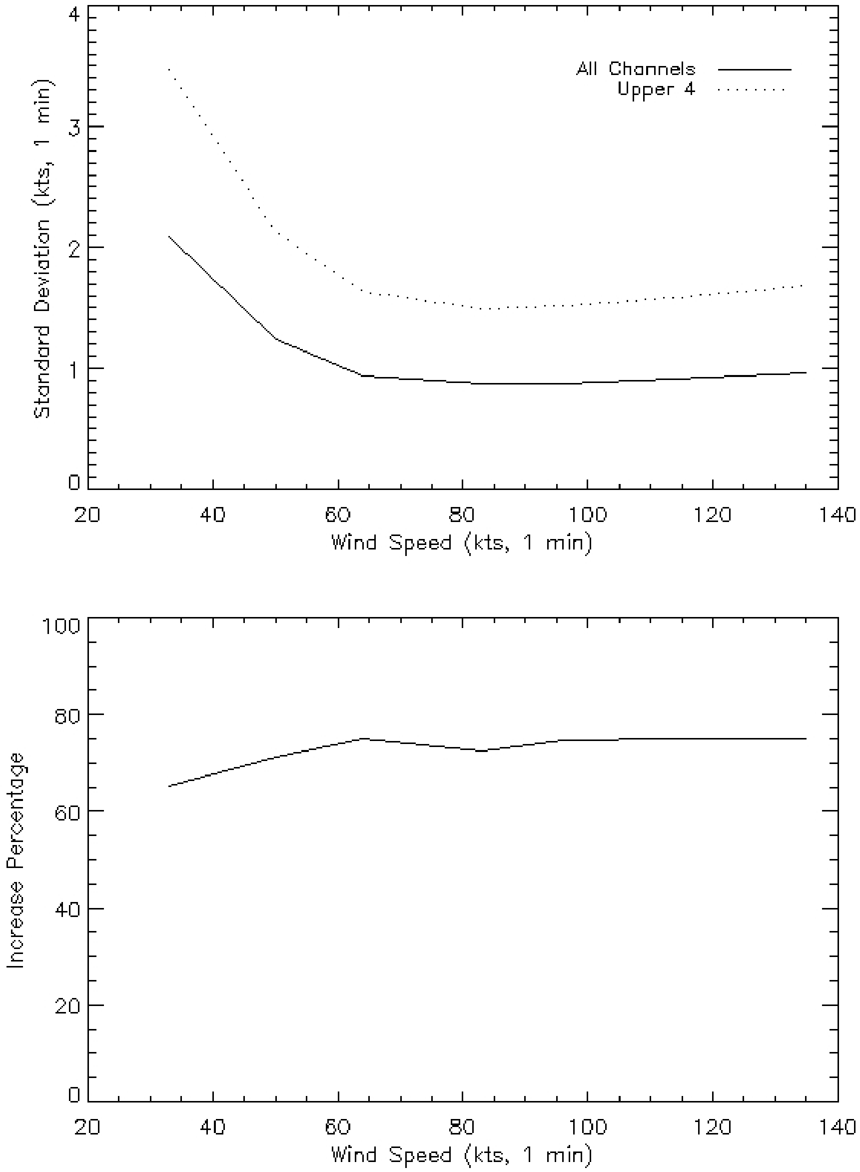

Figure 17: Effects on the SFMR wind speed retrievals caused by disabling lower two AOC SFMR frequency channels.

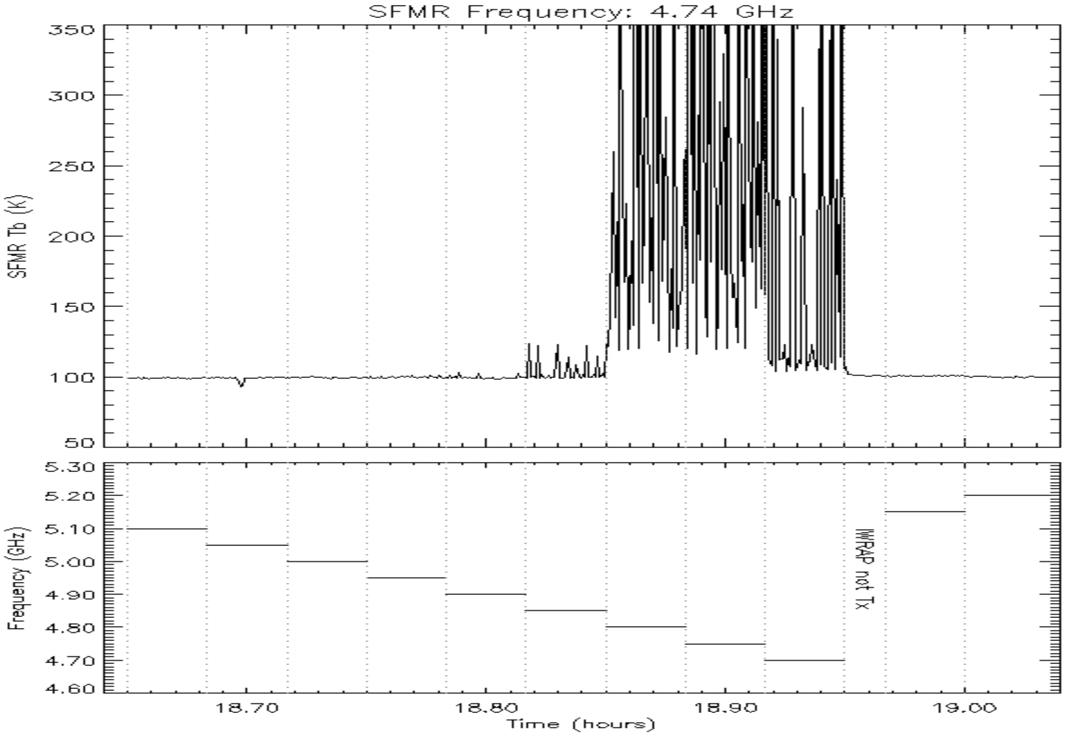

Figure 18: SFMR 4.74 GHz Tb measurements and IWRAP transmit frequency plotted versus time.

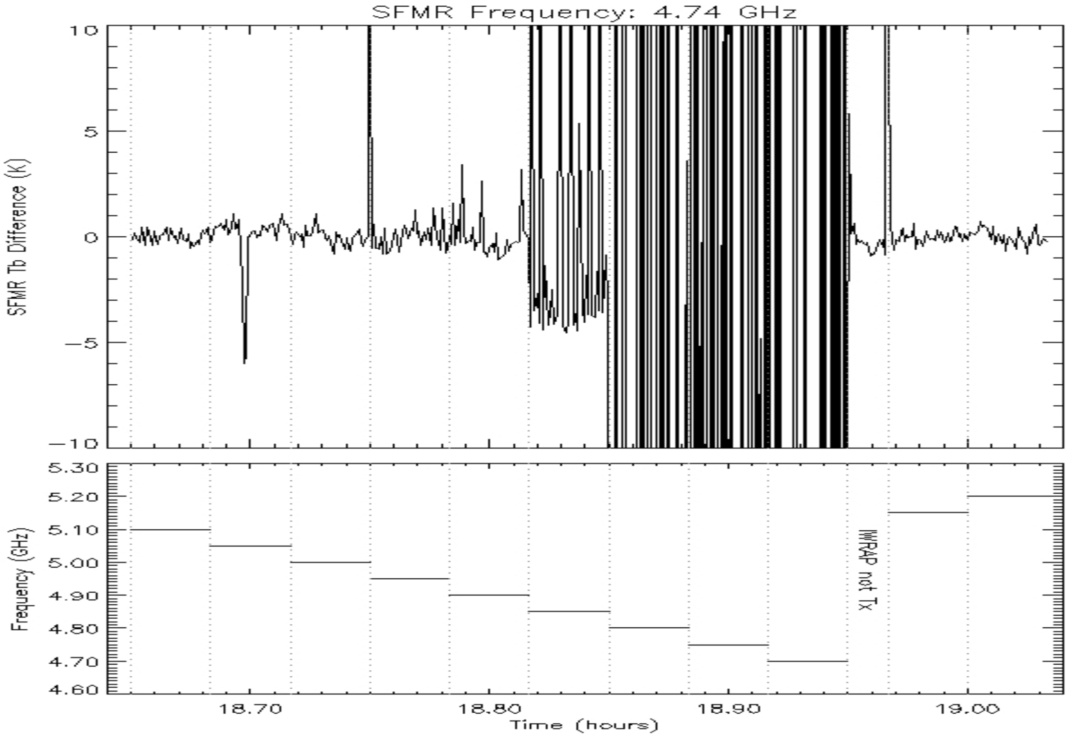

Figure 19: Difference in SFMR 4.74 GHz Tb measurements plotted versus time. Difference is calculated based on mean Tb for each IWRAP frequency interval.

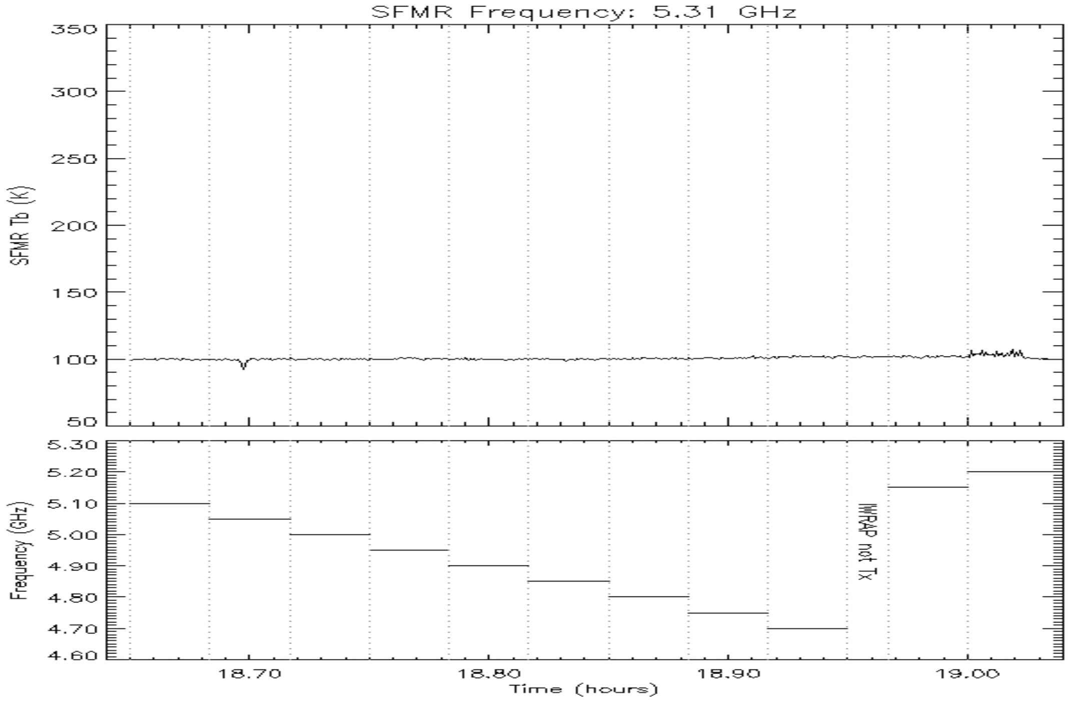

Figure 20: SFMR 5.31 GHz Tb measurements and IWRAP transmit frequency plotted versus time.

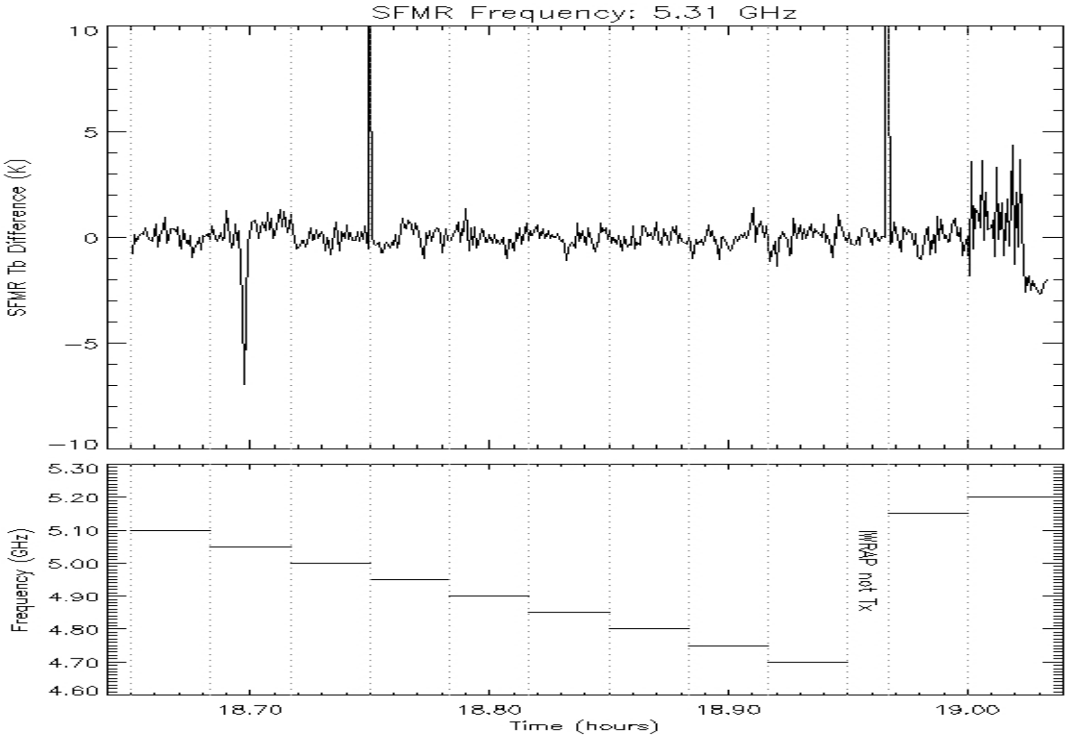

Figure 21: Difference in SFMR 5.31 GHz Tb measurements plotted versus time. Difference is calculated based on mean Tb for each IWRAP frequency interval.

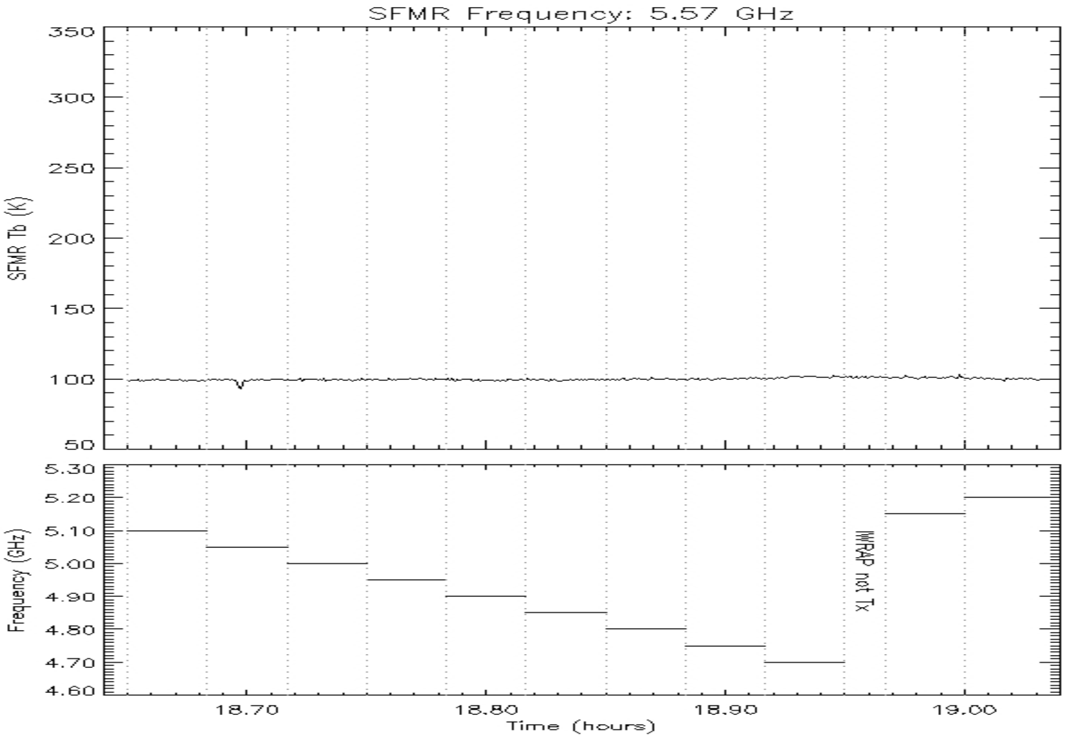

Figure 22: SFMR 5.57 GHz Tb measurements and IWRAP transmit frequency plotted versus time.

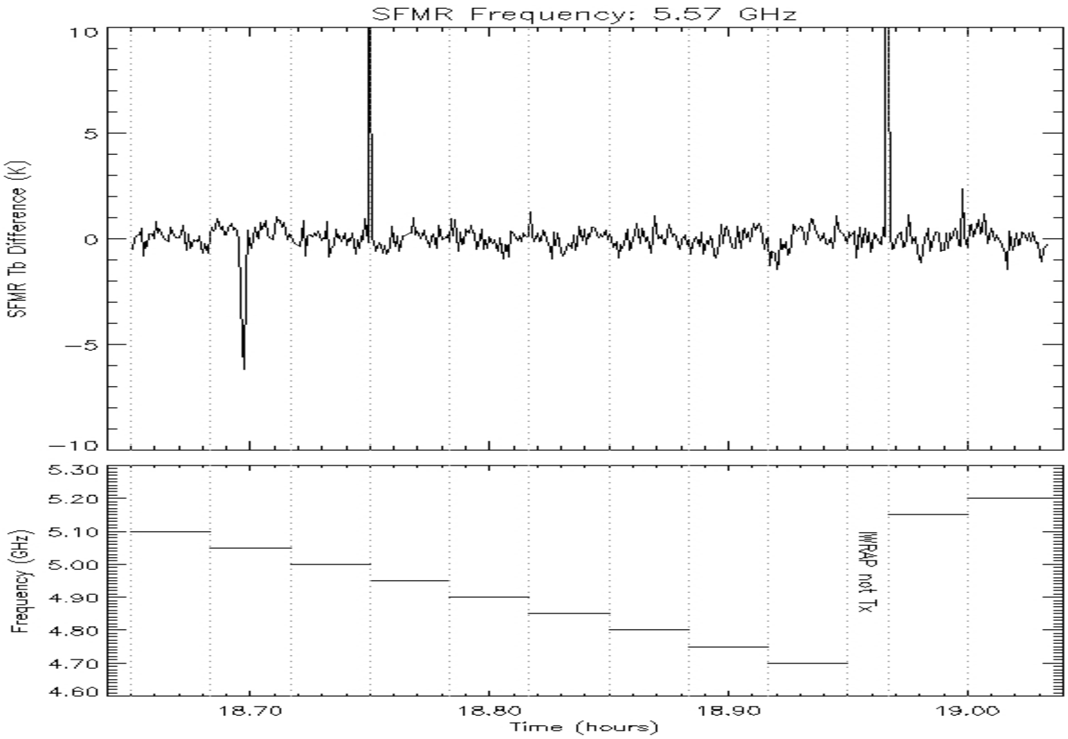

Figure 23: Difference in SFMR 5.57 GHz Tb measurements plotted versus time. Difference is calculated based on mean Tb for each IWRAP frequency interval.

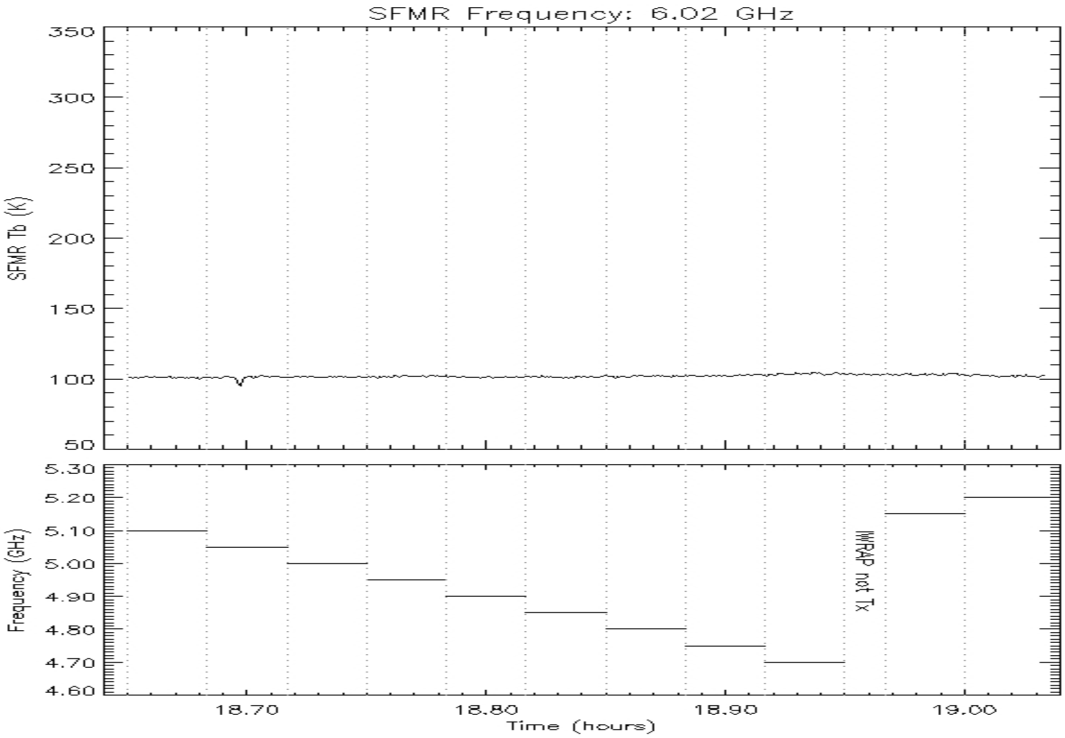

Figure 24: SFMR 6.02 GHz Tb measurements and IWRAP transmit frequency plotted versus time.

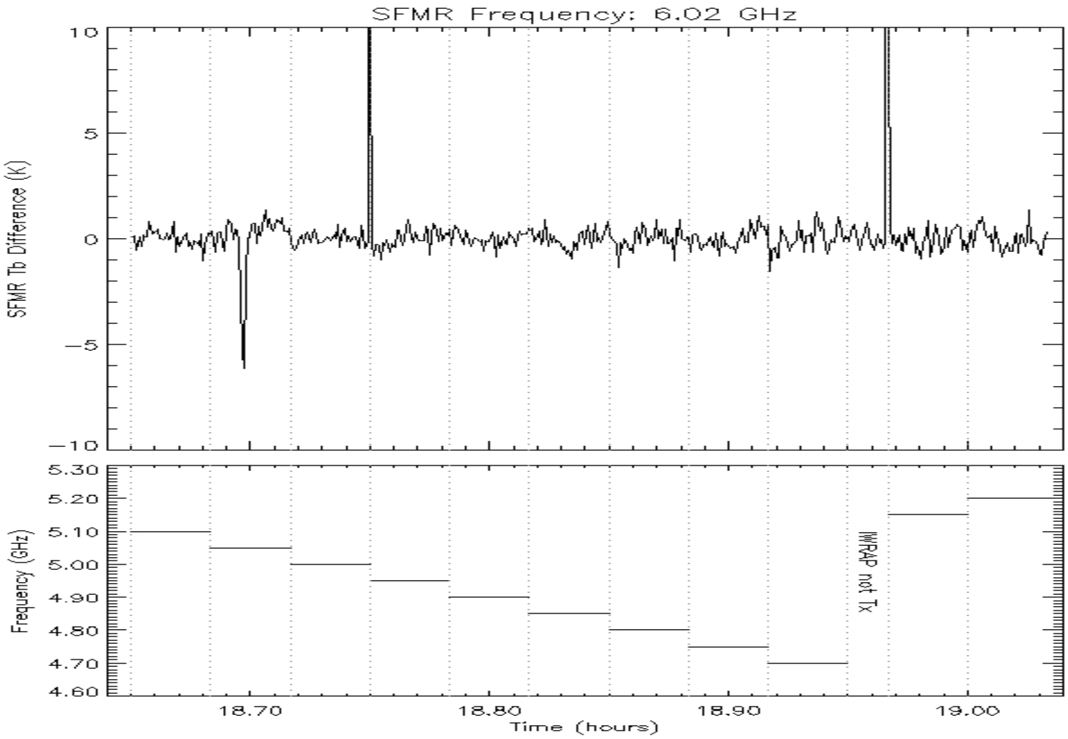

Figure 25: Difference in SFMR 6.02 GHz Tb measurements plotted versus time. Difference is calculated based on mean Tb for each IWRAP frequency interval.

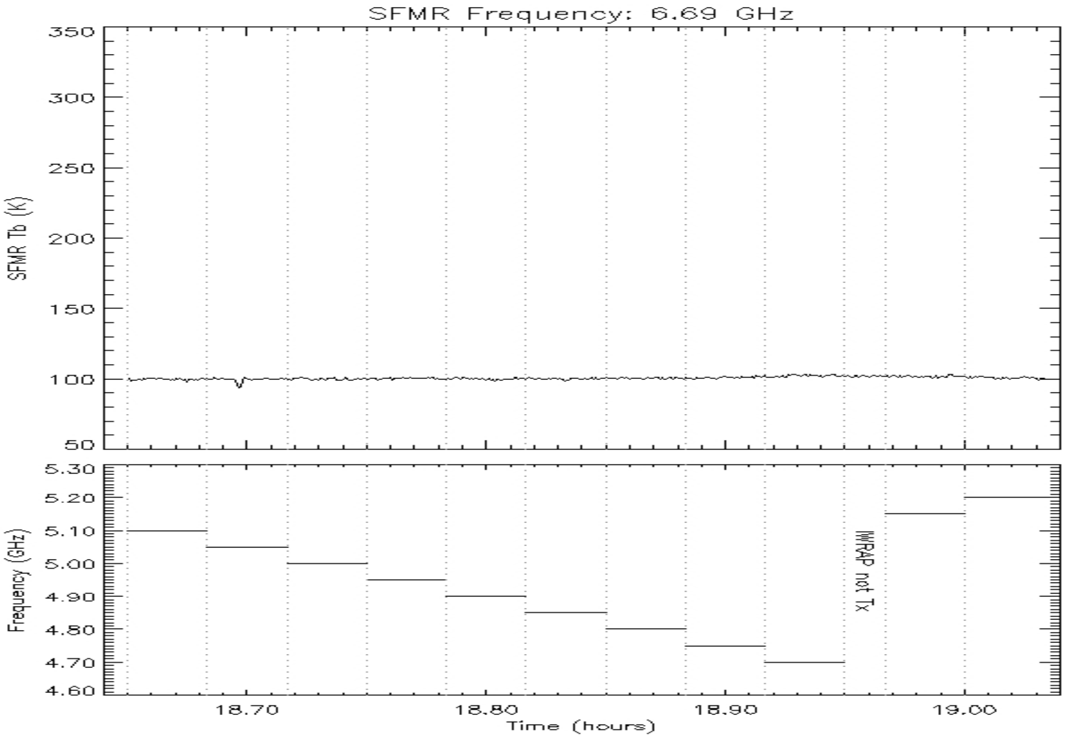

Figure 26: SFMR 6.69 GHz Tb measurements and IWRAP transmit frequency plotted versus time.

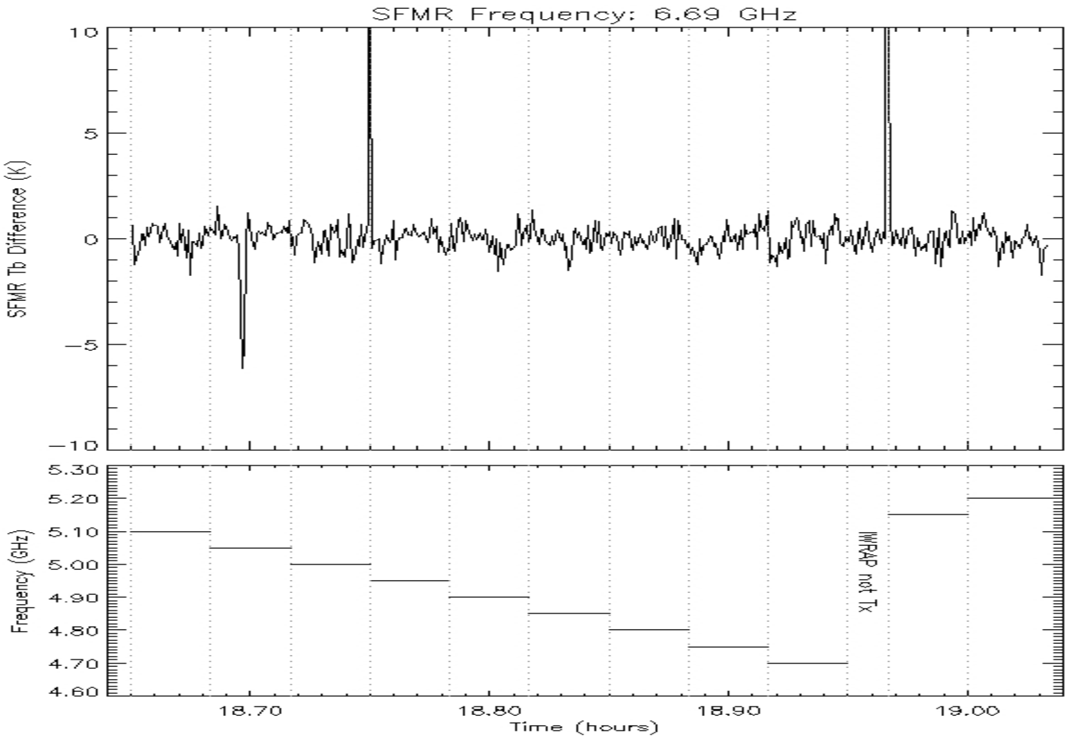

Figure 27: Difference in SFMR 6.69 GHz Tb measurements plotted versus time. Difference is calculated based on mean Tb for each IWRAP frequency interval.

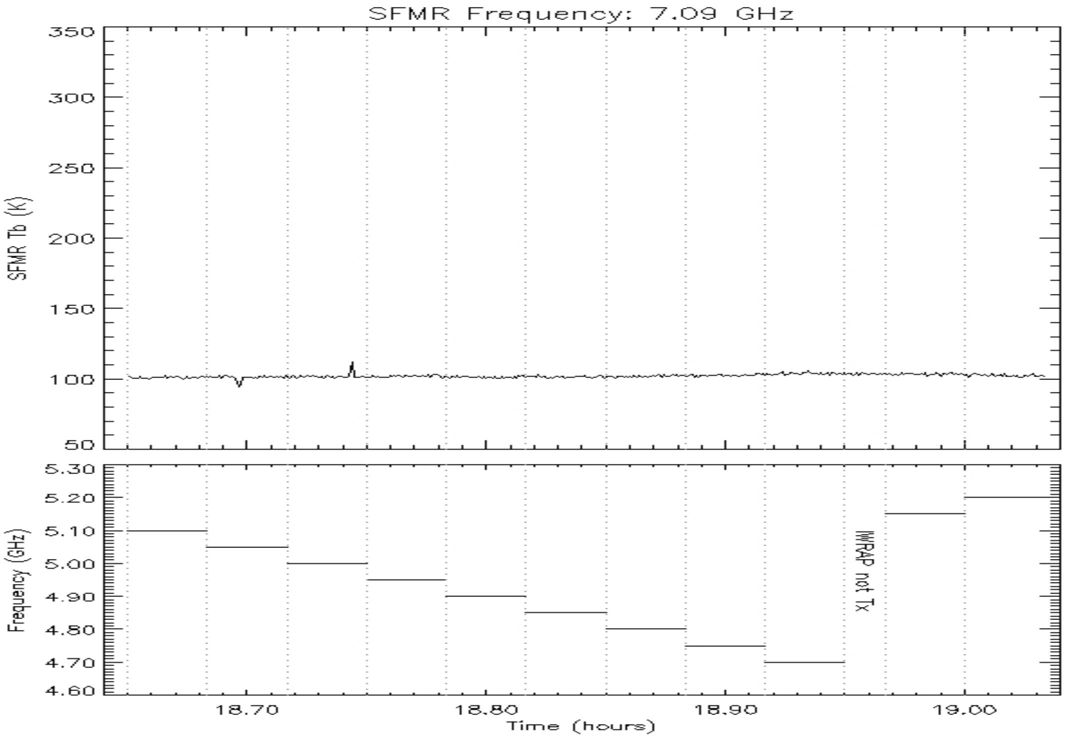

Figure 28: SFMR 7.09 GHz Tb measurements and IWRAP transmit frequency plotted versus time.

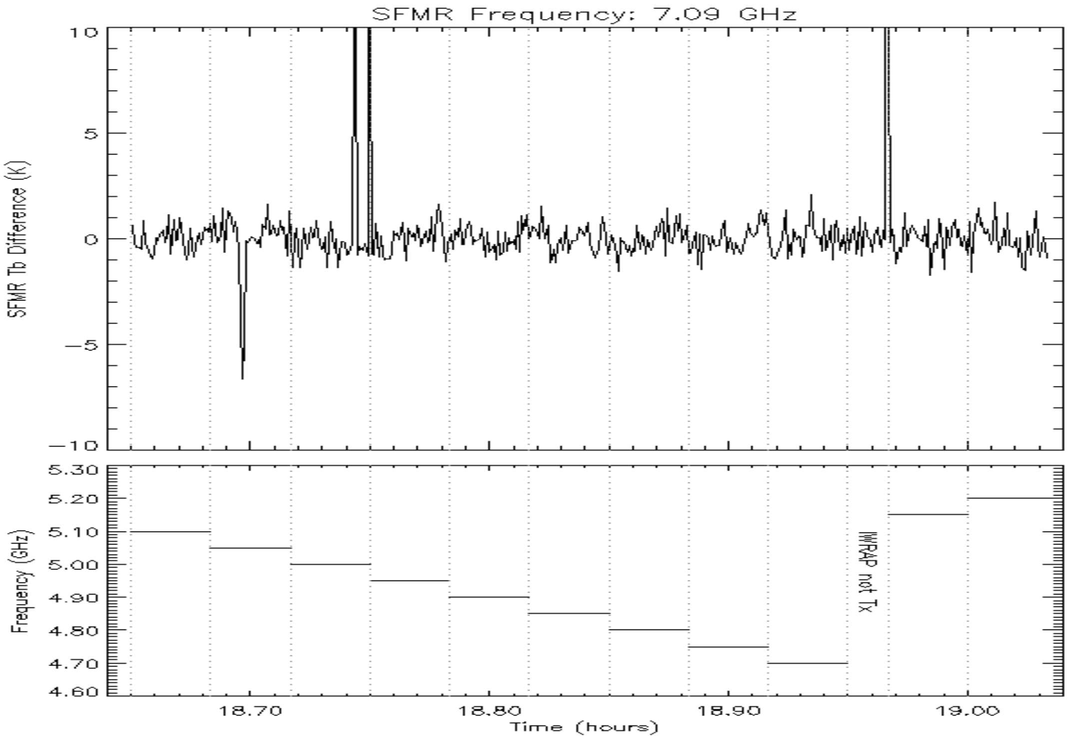

Figure 29: Difference in SFMR 7.09 GHz Tb measurements plotted versus time. Difference is calculated based on mean Tb for each IWRAP frequency interval.

2.3 New SFMR Absorption GMF

One of the primary objectives of the 2nd year JHT effort was to improve the absorption geophysical model function (GMF) used by the SFMR retrieval process. This GMF predicts the absorption at C-band caused by precipitation. Since the brightness temperature measurements are affected by atmospheric absorption (i.e. it contributes to the measurements and attenuates the surface measurements), errors in the absorption GMF not only produce rain rate retrieval errors, but also produce ocean surface wind speed retrieval errors that depend on the rain rate, wind speed and altitude (see 1st year annual reports for more detail).

[Jiang et al, 2006] performed a comparison between the SFMR rain rate retrievals and those derived from the NOAA Lower Fuselage (LF) Radar and the NOAA Tail Doppler (TA) Radar. They reported a 5 mm/hr high bias in SFMR retrieved rain rates compared to the rain rate estimates derived from the LF and the TA radars, and found that the retrieved SFMR rain rates were approximately 60% lower than the collocated LF and TA rain rate estimates. The majority of their comparisons were for 5 to 30 mm/hr as derived by the radars. The authors concluded that the bias may be due to errors in the assumed height of the melting layer and in the way in which radar data are used to estimate average rain between the radiometer and the ocean surface. A representative measurement of rain by the TA and LF radars at one altitude was used to estimate the average mean rain rate for the vertical profile (i.e. SFMR volume). Without any other information, they argue that these two effects result in the systematic bias observed.

However, our analysis documented in the 1st year annual report and the results to follow, showed that biases in the SFMR rain rate retrieval can be caused by errors in the SFMR absorption GMF. This fact combined with the apparent under reporting of the rain rates and the anomalies in the SFMR retrievals, as noted in the previous section of this report, warranted a more thorough analysis and verification of the SFMR absorption GMF.

2.3.1 IWRAP Comparison

To gain a better understanding of this problem, the University of Massachusetts (UMass) Imaging Wind and Rain Airborne Profiler (IWRAP) [Esteban et al, 2005] was used to provide an independent, collocated estimate of the precipitation. This instrument was flown with the UMass SFMR on N42RF during the 2003 hurricane season and with the AOC SFMR (US002) during the 2005 hurricane season. It is a dual wavelength, conically scanning radar that simultaneously profiles the atmosphere and ocean surface at C and Ku-band and at two incidence angles. Because it conically scans, the volume it samples can be matched exactly to the SFMR volume. Using differential attenuation profile measurements, IWRAP can also directly measure the mean rain rate beneath the aircraft. Thus, the uncertainties in the assumptions that [Jiang et al, 2006] were required to make when deriving rain rate estimates from the LF and TA do not limit the IWRAP rain rate retrievals and their comparison to the SFMR rain rate retrievals. Further, a single flight can realize thousands of collocated IWRAP-SFMR estimates providing the most thorough comparison data set.

Using the IWRAP measurements obtained in 2003 during flights through Hurricane Isabel, the Ku-band specific attenuation estimates were derived using differential attenuation techniques and collocated with the UMass SFMR rain rate estimates [Esteban, 2004]. Figure 30 (a) plots the Ku-band specific attenuation versus the UMass SFMR derived rain rate estimates. Note that the UMass SFMR acquires brightness temperature measurements at six frequencies over a very similar frequency range as the AOC SFMR. Further, it simultaneously measures all six frequency channels at 20 Hz resulting in a 0.06 K precision per channel over the same integration period as the AOC SFMR which has a 0.5 K precision. Overlaid on this plot is a power law model function that predicts the specific attenuation as a function of rain rate at two different temperatures. As this figure shows, the SFMR rain rates under predict the “true” rain rate, assuming the specific attenuation models are correct. Scaling the SFMR rain rates by a factor of 2.5 and subtracting an offset of 5 mm/hr, the specific attenuation measurements are plotted versus the “corrected” SFMR rain rate estimates in Figure 30 (b). The data now agrees well with the models. Figure 31 plots the corrected SFMR rain rate estimates and IWRAP rain rate estimates versus time. The agreement is excellent. The IWRAP rain rates show more variation only because the IWRAP spatial resolution is much greater. Note that the 5 mm/hr offset is the exact same bias as reported by [Jiang et al, 2006] even though they used a different approach and different instruments.

Following this comparison, rain rate estimates from IWRAP were derived from measurements collected from the NOAA N42RF WP-3D aircraft during a flight through Hurricane Rita on 22 September 2005. These estimates were collocated with the AOC SFMR rain rate estimates to within +/- 75 m in the along track direction (center of the pixels). More than 2000 collocated rain rate estimates (above 10 mm/hr) were found and these measurements spanned 10 mm/hr to 70 mm/hr. The collocated rain rate estimates were divided into 2.5 mm/hr bins, based on the IWRAP rain rate estimates, and averaged. Each bin contained a minimum of 30 pairs of collocated rain rate estimates. Figure 32 plots the results. A fit to this data set (linear regression) showed, once again, that the SFMR rain rates have an approximate bias of 5 mm/hr (4.6 mm/hr) and that they under estimate the rain rate by a factor of 2.5 compared to the IWRAP rain rate estimates. That is, the slope and offset of the linear regression between the SFMR and IWRAP rain rate estimates were 0.4 and 1.85 mm/hr, respectively.

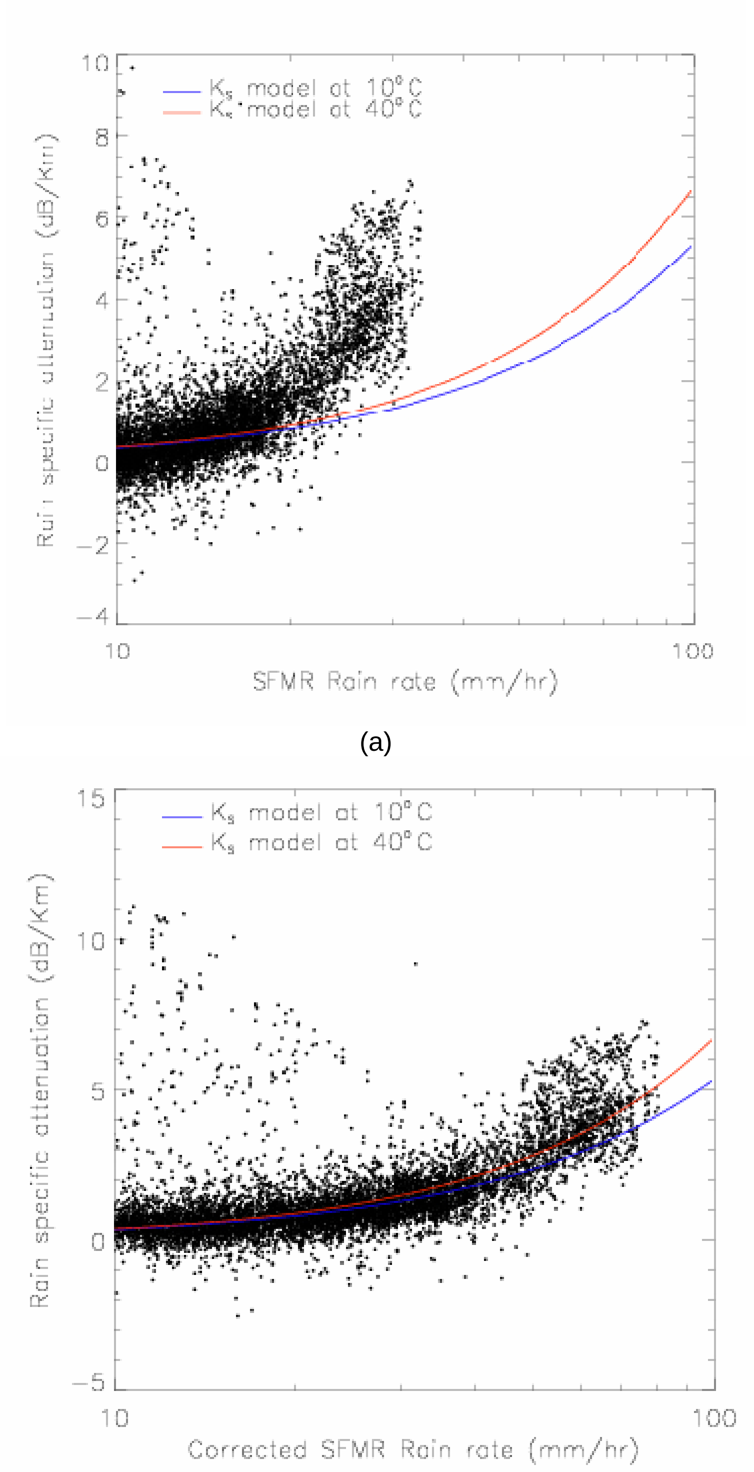

(a)

(b)

Figure 30: IWRAP derived specific attenuation plotted versus the UMass SFMR rain rate estimates (a) and corrected rain rate estimates (b). These observations were collected through a series of flights through Hurricane Isabel in 2003.

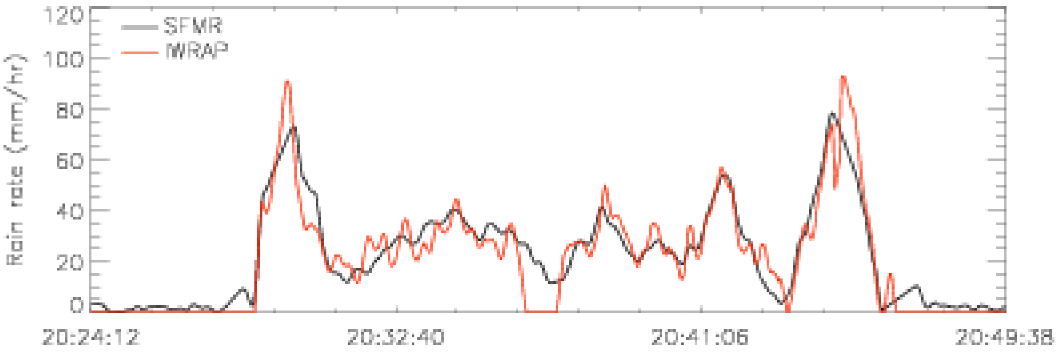

Figure 31: Time series plot of IWRAP (red) and corrected SFMR (black) rain rate estimates are shown. The corrected SFMR rain rates were derived by subtracting 5 mm/hr from the original SFMR rain rates and multiplying by 2.5.

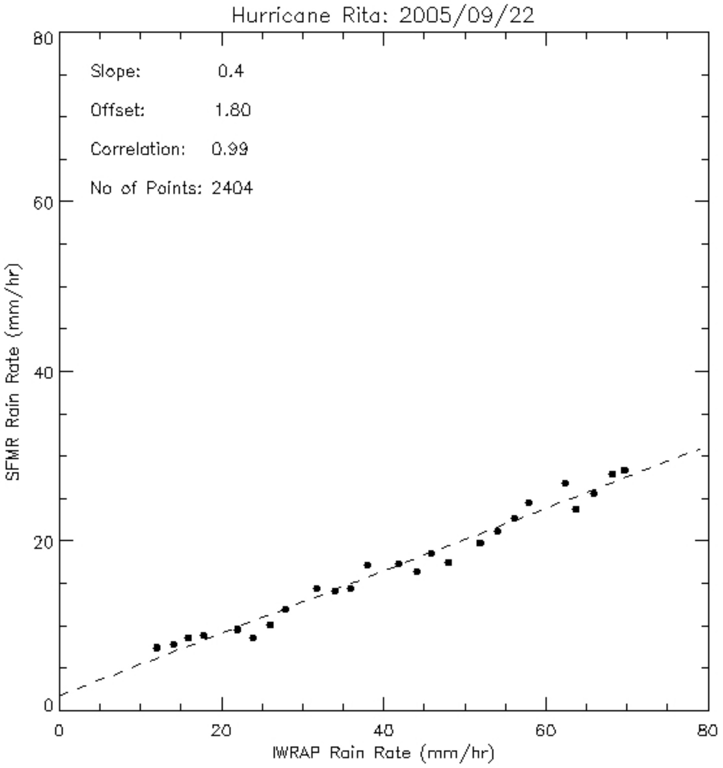

Figure 32: SFMR bin averaged rain rate estimates are plotted versus IWRAP rain rate estimates. The dashed line is a linear regression with the slope, offset and correlation coeffients given in the legend.

These independent results agree with those obtained from the 2003 data and are consistent with the results reported by [Jiang et al, 2006]. Furthermore, the correlation between these two sets of retrievals (IWRAP and the SFMR) is 98 percent. The high correlation shows that the precipitation sampled by these two instruments is the same, and the agreement between the comparison of the 2003 and 2005 data verifies that this approach is robust and consistent. Finally the difference between the IWRAP and SFMR rain rate estimates did not exhibit any dependence on the retrieved wind speed. This is consistent with our simulations that show that modeling errors in the absorption GMF produce rain rate errors that are independent of wind speed

2.3.2 Deriving New SFMR Absorption GMF

The SFMR retrieval process currently uses an absorption model that was reported in [Jiang et al, 2006]. This model has three empirically derived parameters (R_m, R_e and F_e) and is given below:

$$K = \alpha \left(f^{R_m R_r^{F_e}} \right) \left(R_r^{R_e} \right) \tag{1}$$

where,

R_r = rain rate (mm/hr)
α = 1.87x10^{-6} Np / km (constant)
f = frequency (GHz)
R_m = rain multiplier coefficient
R_e = rain exponent coefficient
F_e = frequency exponent coefficient

[Jiang et al, 2006] suggest that the parameter R_e should have a value of 1.15. Starting in 2005, all SFMR retrievals were derived using the 1.15 value for R_e. Using a Monte-Carlo analysis that is described below, the three empirically derived parameters were analyzed and found to not provide an optimal solution. New values were sought that would remove the bias in the SFMR rain rate retrievals, provide a stable solution and improve the accuracy of the SFMR wind speed and rain rate retrievals.

2.3.2.1 Monte-Carlo Analysis

As the equation (1) shows, the absorption increases with both rain rate and frequency. In order to assess the accuracy of different rain model parameters, RSS implemented a Monte-Carlo analysis that varied the empirically derived parameters, R_m, R_e and F_e, in equation (1) around their current values: 2.6, 1.15 and 0.0736, respectively, to seek a solution that would optimize the slope and offset between the comparison of the collocated IWRAP and SFMR rain rate estimates and maintain a correlation better than 97 percent between these two data sets. For each potential solution of R_m, R_e and F_e, the collocated SFMR rain rates were plotted versus the IWRAP rain rates and the slope and offset were calculated. Plotting the solutions in R_e, F_e and R_m space, we found a grouping for which the offset was less than 0.15 m/hr, the slope was greater than 0.9 and the correlation between the two retrieval data sets was greater than 97 percent. These solutions are given in Table 1.

Table 1: Solution set for absorption GMF coefficients.

Re	Fe	Rm	Slope (m)	Offset (b)
0.76	0.0676	2.75	0.947	0.110
0.74	*0.0696*	*2.75*	*0.950*	*0.138*
0.74	0.0716	2.8	0.900	0.015
0.72	0.0736	2.8	0.910	-0.109
0.7	0.0756	2.8	0.915	-0.074

Figure 33 plots the absorption GMF, as described by equation (1) and the coefficients in Table 1. The frequency was set to 6.02 GHz (middle SFMR channel) and each line represents a set of coefficients. The results were similar for the other SFMR frequencies as well. The blue curve represents the highlighted solution in Table 1. It is the chosen solution since it provides the lowest offset (-0.074 mm/hr) and represents roughly the average solution in Figure 33 . The green curve is the original solution (R_e = 1.15, F_e =0.0736 and R_m = 2.6), and as this plot shows, it significantly over estimates the absorption, and thus, the retrieval process under estimates the true rain rate and wind speed.

To validate these results, an independent collocated data set consisting of surface wind estimates from GPS dropsondes and the AOC SFMR deployed on N43RF WP-3D aircraft in 2005 were used. This is the same data set that was published by [Uhlhorn et al., 2006]. Note that the excess emissivity SFMR GMF (or wind GMF) was trained on this data set in [Uhlhorn et al, 2007]. The GPS dropsonde surface wind speed estimates were derived using the lowest 150-m averaged wind speeds reported from each drop profile and scaling the data according to [Franklin et al, 2003]. For details, see [Uhlhorn, et al, 2006]. The SFMR surface wind speeds were derived using the 2005 absorption GMF and the excess emissivity model as reported by [Uhlhorn et al, 2007].

Figure 34 plots a histogram of the retrieved rain rate for these data. Although rain rates greater than 40 mm/hr were sampled, the majority of the data was collected in lower rain conditions (approximately 70 percent of these data were acquired under rain conditions less than 20 mm/hr).

Figure 35 plots the GPS surface wind estimates versus the collocated SFMR surface wind estimates using the 2005 absorption GMF. The mean difference between the SFMR wind speed estimates and the GPS dropsonde surface wind estimates is approximately 1.0 m/s. The solid circles represent the bin averaged data (7 m/s bin size). A linear fit between these data is shown by the dashed curve and the slope and offset are given. The slope is consistent with that reported by [Uhlhorn et al, 2007]. Besides the SFMR slightly under reporting the surface wind speeds, the difference between the dropsonde surface winds and the SFMR error grows with wind speed.

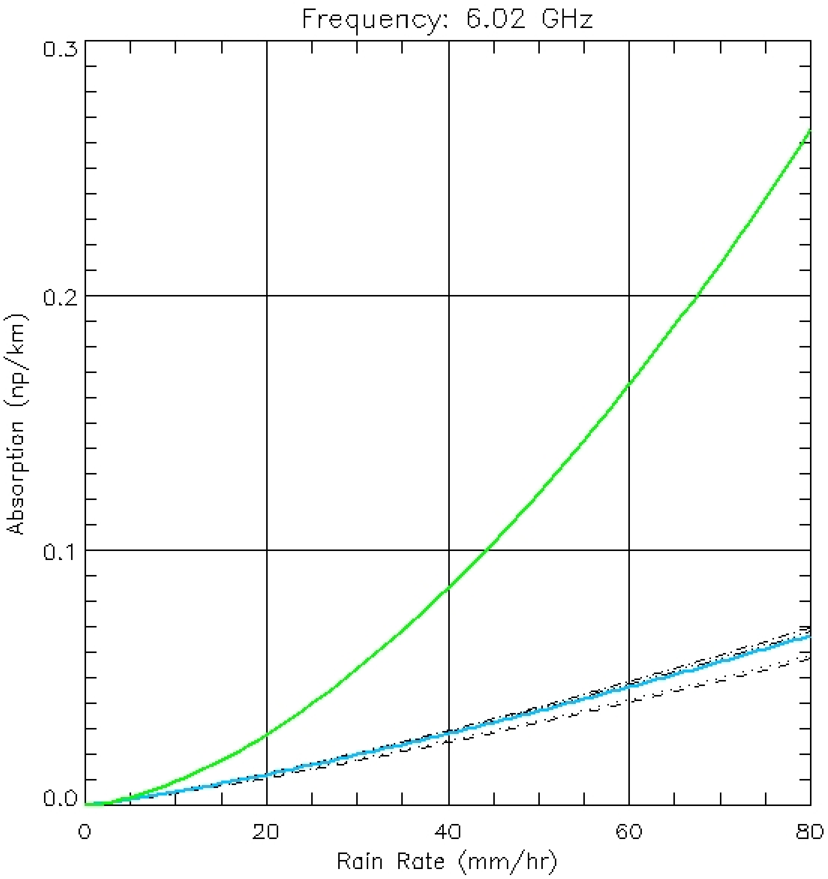

Figure 33: Absorption at 6.02 GHz plotted versus rain rate. The green curve is the original solution. The dashed dotted curves are from Table 2 and the blue curve is the selected solution.

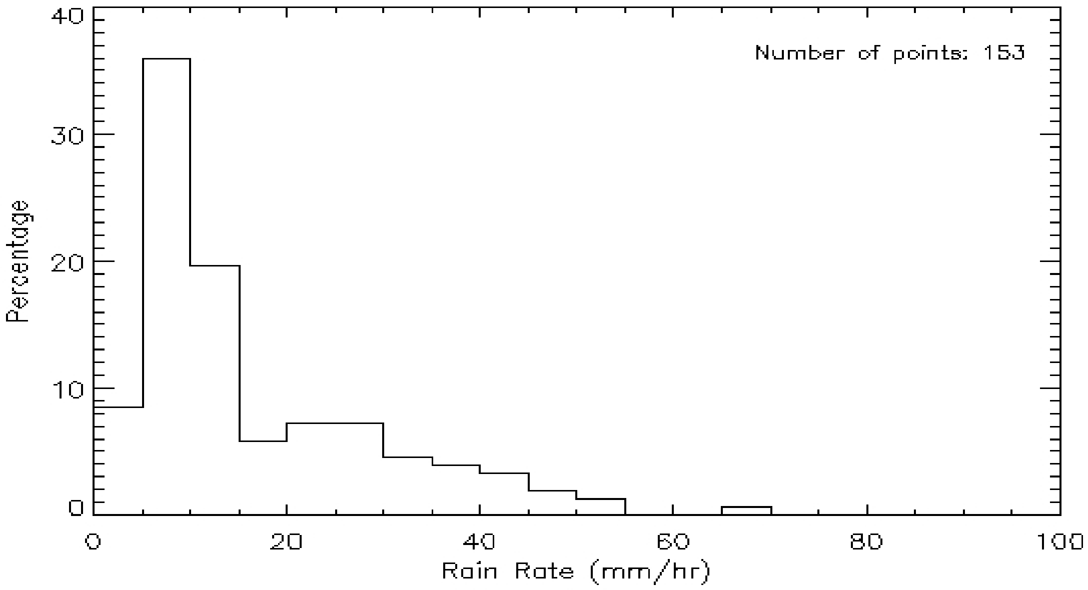

Figure 34: Histogram of rain rate measurements for figures 33 and 34. Bin size is 5 mm/hr.

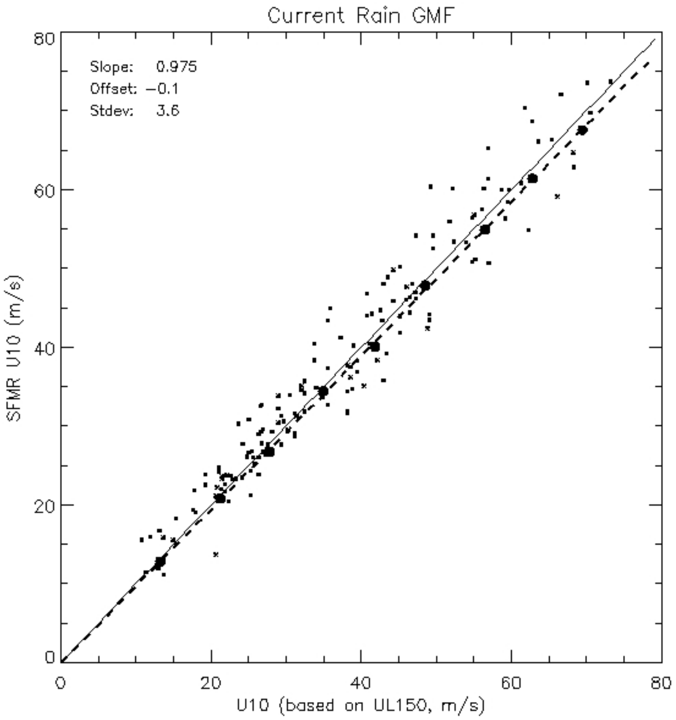

Figure 35: SFMR wind speed retrievals derived using the 2005 absorption GMF are plotted versus collocated GPS dropsonde surface wind speed estimates. See Uhlhorn et al, 2007 for details on processing of the dropsonde data and collocation scheme. The large solid circles represent the binned averaged data (7 m/s bins). The dashed line is a linear regression to the data.

Figure 36 plots this residual error (green circles) versus wind speed. It clearly shows a more negative value as a function of wind speed. Assuming that the errors in the 2005 absorption GMF are the cause, this error would be larger if higher rain rates had been experienced. The solid green curve is a linear fit to these data. The correlation of this fit is approximately -78 percent.

Using the new absorption GMF reported above (R_e = 0.7, F_e =0.0756, R_m = 2.8), new SFMR wind speed estimates are derived from the same set of SFMR measurements. Figure 37 plots the comparison between the GPS dropsonde surface wind speed estimates and these new SFMR surface wind speed estimates. The mean difference between the new SFMR surface wind speed estimates and those derived from the GPS dropsonde measurements is 0.087 m/s. Once again the data are averaged into 7 m/s bins shown by the solid circles. A linear fit to these data now shows a slope of 1.0. The residual error, shown in Figure 36 (blue dots), and the fit to this error (blue line), show no significant dependence on wind speed. Thus, the new absorption GMF better represents the true absorption due to rain, and this model has removed the errors (bias) in the wind speed retrieval caused by the errors in the 2005 absorption GMF.

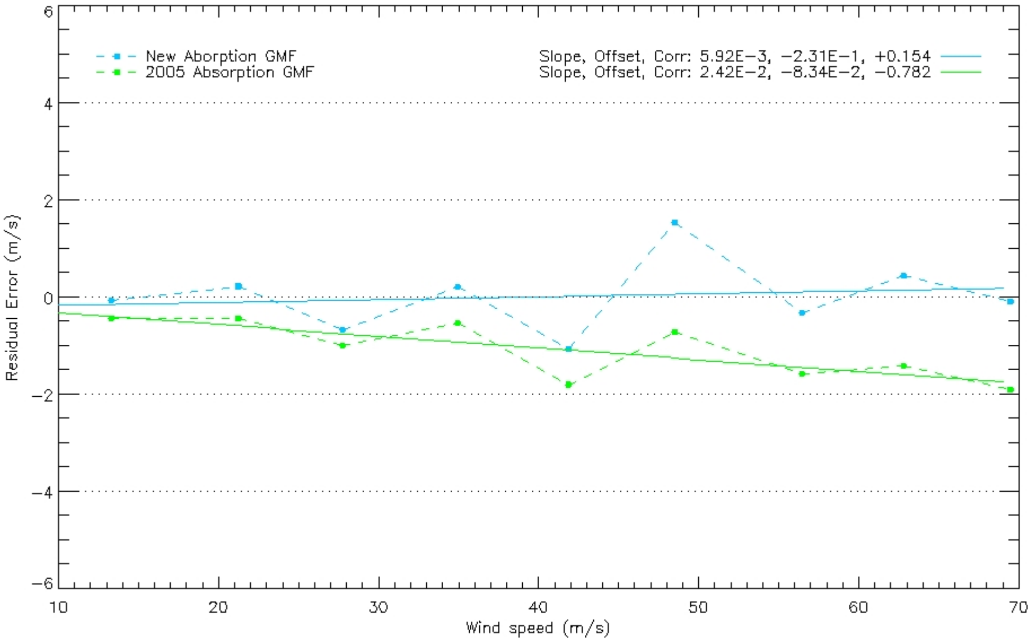

Figure 36: Residual error in retrieved wind speed. Blue and green lines are linear fits to the residual error when using the new absorption GMF and the 2005 absorption GMF, respectively.

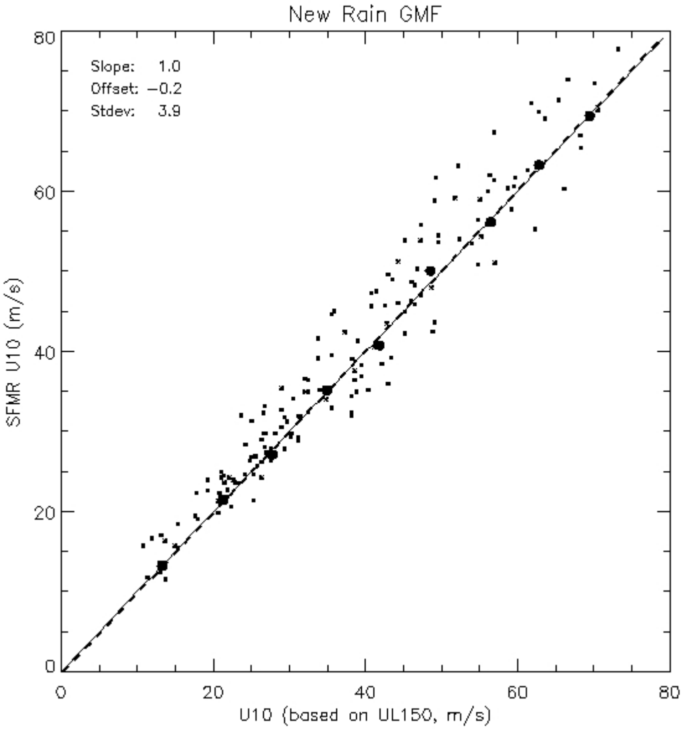

Figure 37: Same as Figure 35 except the new absorption GMF is used in the retrieval process (Re=.7, Rm=2.8, Fe=0.696)

2.3.2.2 Retrieval Error with 2005 Absorption GMF

Because the 2005 absorption GMF is incorrect, the SFMR wind speed and rain rate retrievals that were derived using this GMF are in error, and this error depends on wind speed, rain rate and altitude. At the 2007 IHC, the community requested that this error be determined. To accomplish this task, we simulated the brightness temperature measurements using the correct (new) absorption GMF over all rain and wind conditions and at two different altitudes. Using the 2005 absorption GMF in the retrieval process, the retrieved wind and rain rates are derived. Thus, this simulates the measurement and retrieval process for the 2005/2006 hurricane season. The error in the retrievals is simply the difference between the retrieved wind speed and rain rate and the actual wind speed and rain rate used to produce the simulated brightness temperature measurements.

Using the SFMR simulator, we derived a simulated brightness temperature data set over wind conditions from gale to category 5 hurricane force winds and rain rates from 0 to 100 m/hr. We assumed a 0.5 K measurement precision. For each wind speed and rain rate, we realized 1000 measurements at the six SFMR frequencies and a standard deviation of 0.5 K. The new absorption GMF was used in the SFMR brightness temperature model function to derive the mean values. A SST of 29 degrees, an ambient air temperature of 20 degrees C and an altitude of 1524 m were assumed. The SFMR retrieval process was run on each point using the 2005 absorption GMF. The mean errors between the retrieved wind speed and rain rate and the inputted wind speed and rain rate used to create the brightness temperature measurements were calculated and binned according to the wind speed and rain rate.

Figure 38 presents a contour of the wind speed retrieval error as a function of wind speed and rain rate assuming an altitude of 1524 m. The x-axis is the true wind speed in knots and the y-axis is the true rain rate in mm/hr. The SFMR retrievals under predict the true wind speed with the error growing with increasing rain rate and decreasing wind speed. For example if the true rain rate is 60 mm/hr, the SFMR using the 2005 absorption GMF would have reported 45 kt, 60.5 kt and 80 kt for a true wind speed of 50 kt, 64 kt and 83 kt, respectively.

As the aircraft flies higher, the error in the retrieved wind grows. Figure 40 presents the same contour except the assumed altitude is 3048 m. For the same example given above where the true rain rate was 60 mm/hr and the wind speeds were 50 kt, 64 kt and 83 kt, the retrieved SFMR wind speeds using the 2005 absorption GMF would have reported the surface wind speeds to be 43.2 kt, 59.4 kt and 88.9 kt. As these contour plots demonstrate, the uncertainty or error in the SFMR wind speed estimates, depends on altitude, wind speed and rain rate.

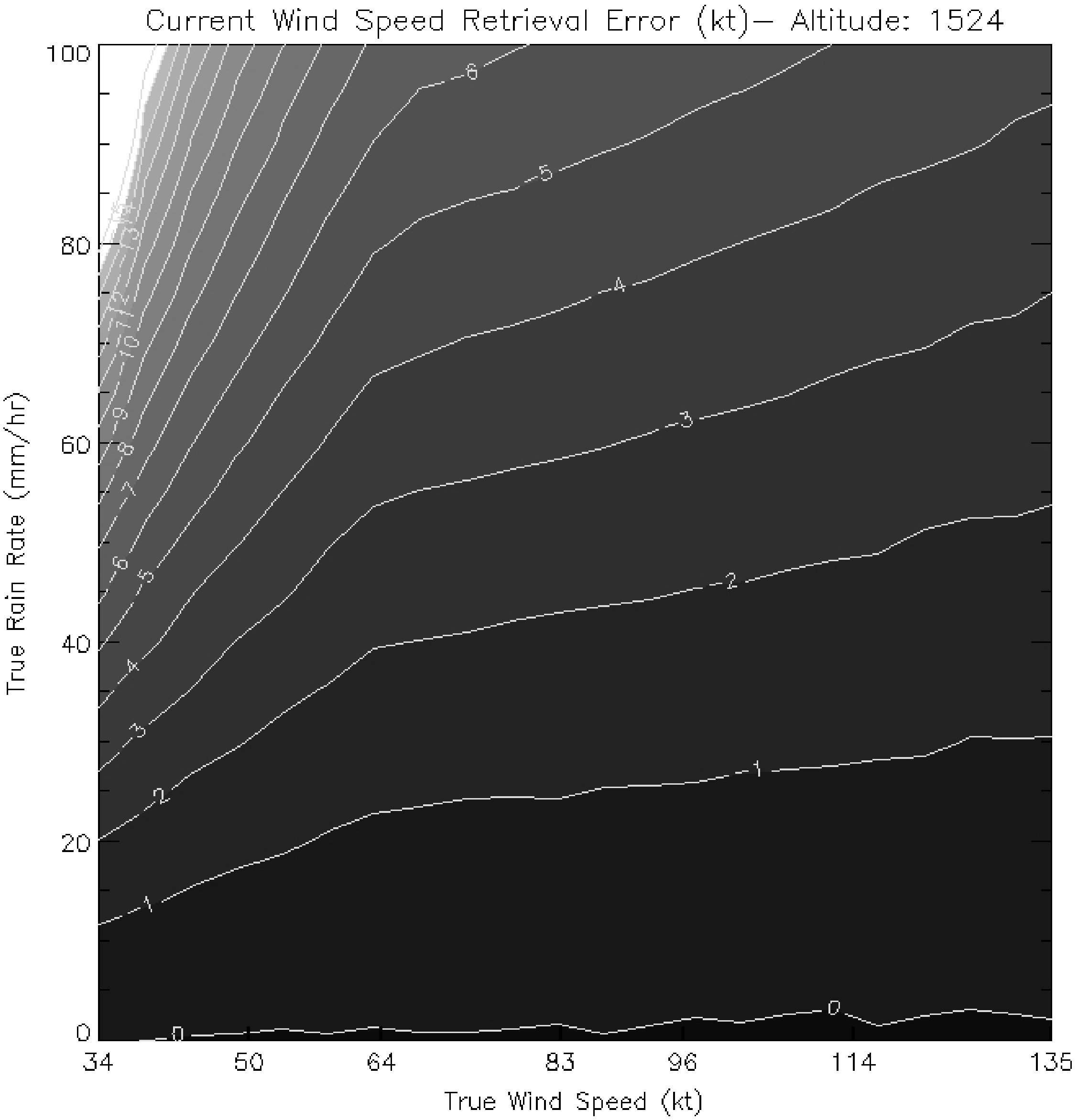

Figure 38: Contour of the SFMR wind speed retrieval error in knots using the 2005 absorption GMF in the retrieval process is shown over a range of wind speeds and rain rates. The reported error is calculated by subtracting the true wind speed from the retrieved wind speed. A negative value means that the SFMR retrieved winds under reports the true wind speed. A 1524-m altitude, 20 deg C ambient temperature and 29 deg C SST were assumed.

Likewise, the rain rate retrievals using the 2005 absorption GMF also under predict the true rain rates. However, unlike the wind speed retrieval error, the rain rate retrieval error is not dependent on wind speed or altitude. This is expected since it is a column averaged rain rate which accounts for the column height and the surface emissivity is modeled correctly. Figure 40 and Figure 41 plot the contours for the SFMR rain rate retrievals for 1524 m altitude and 3048 m altitude. The rain rate retrieval error depends only on the true rain rate growing with increasing rain rate. This agrees with the results shown in the comparison between IWRAP and SFMR rain rate retrievals (Figure 32).

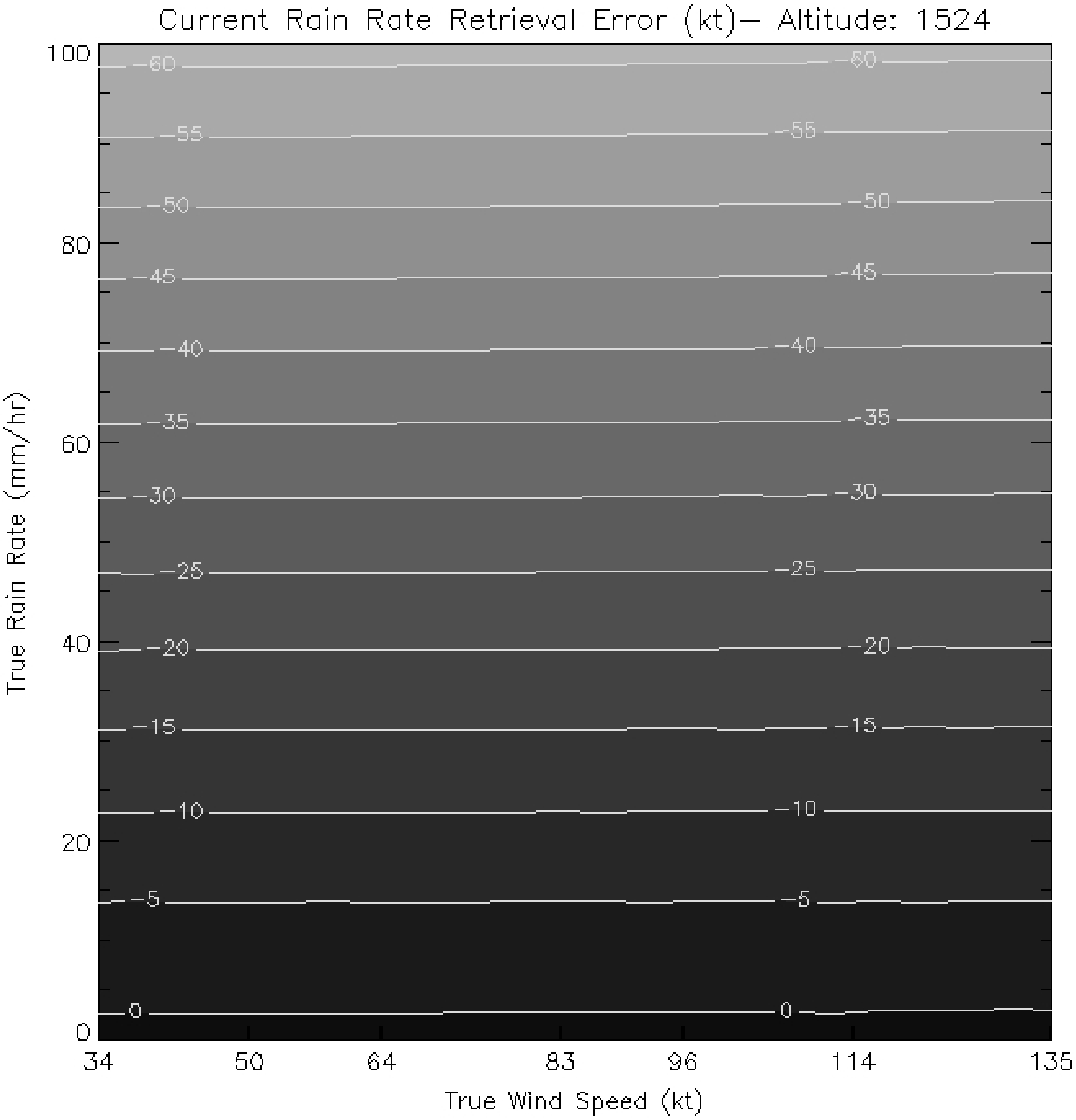

Figure 39: Contour of the SFMR rain rate retrieval error in mm/hr using the 2005 absorption GMF in the retrieval process is shown over a range of wind speeds and rain rates. The reported error is calculated by subtracting the true rain rate from the retrieved rain rate. A negative value means that the SFMR retrieved rain rate under reports the true rain rate. A 1524-m altitude, 20 deg C ambient temperature and 29 deg C SST were assumed.

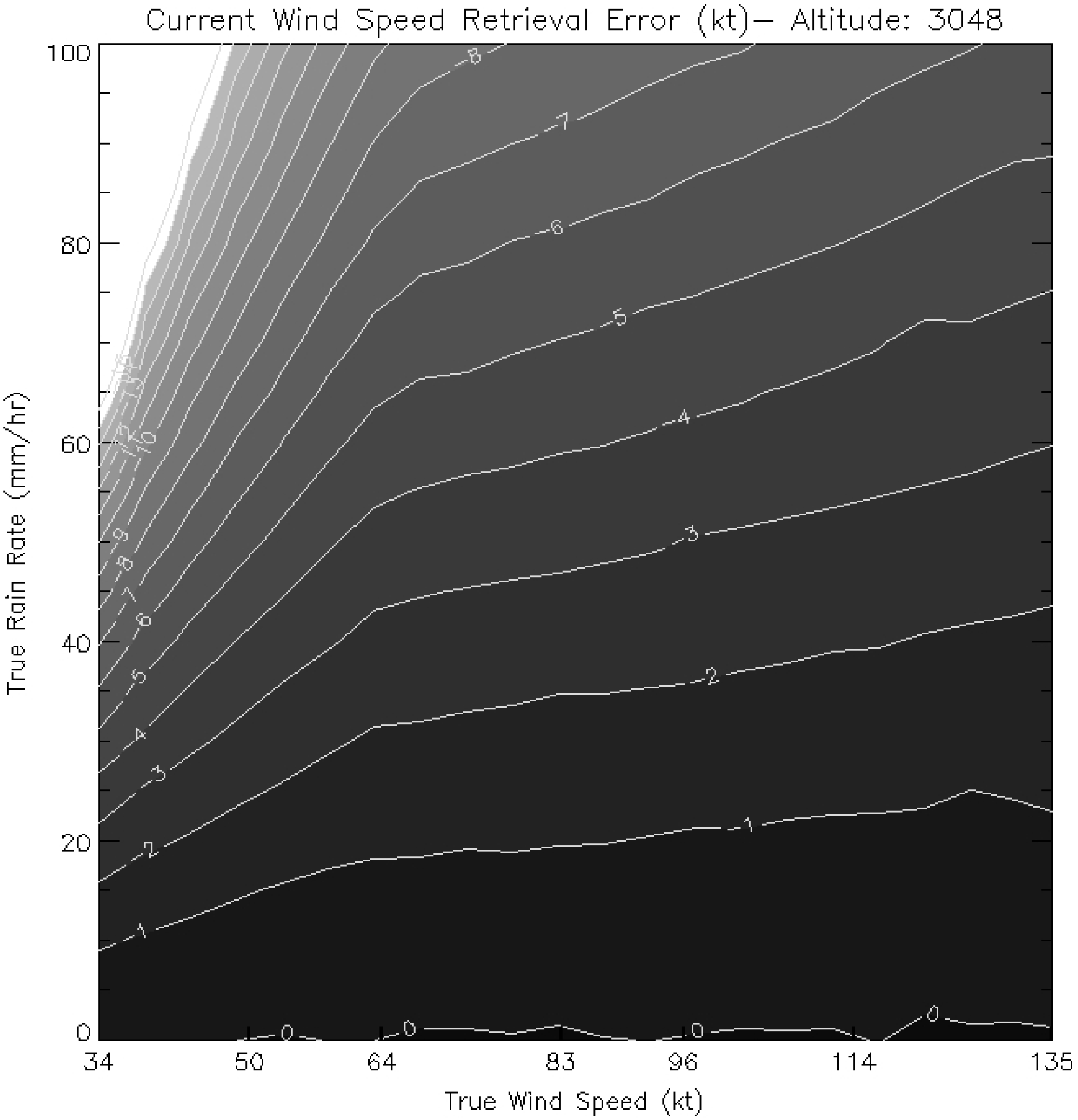

Figure 40: Same as Figure 38 except the altitude is now 3048 m.

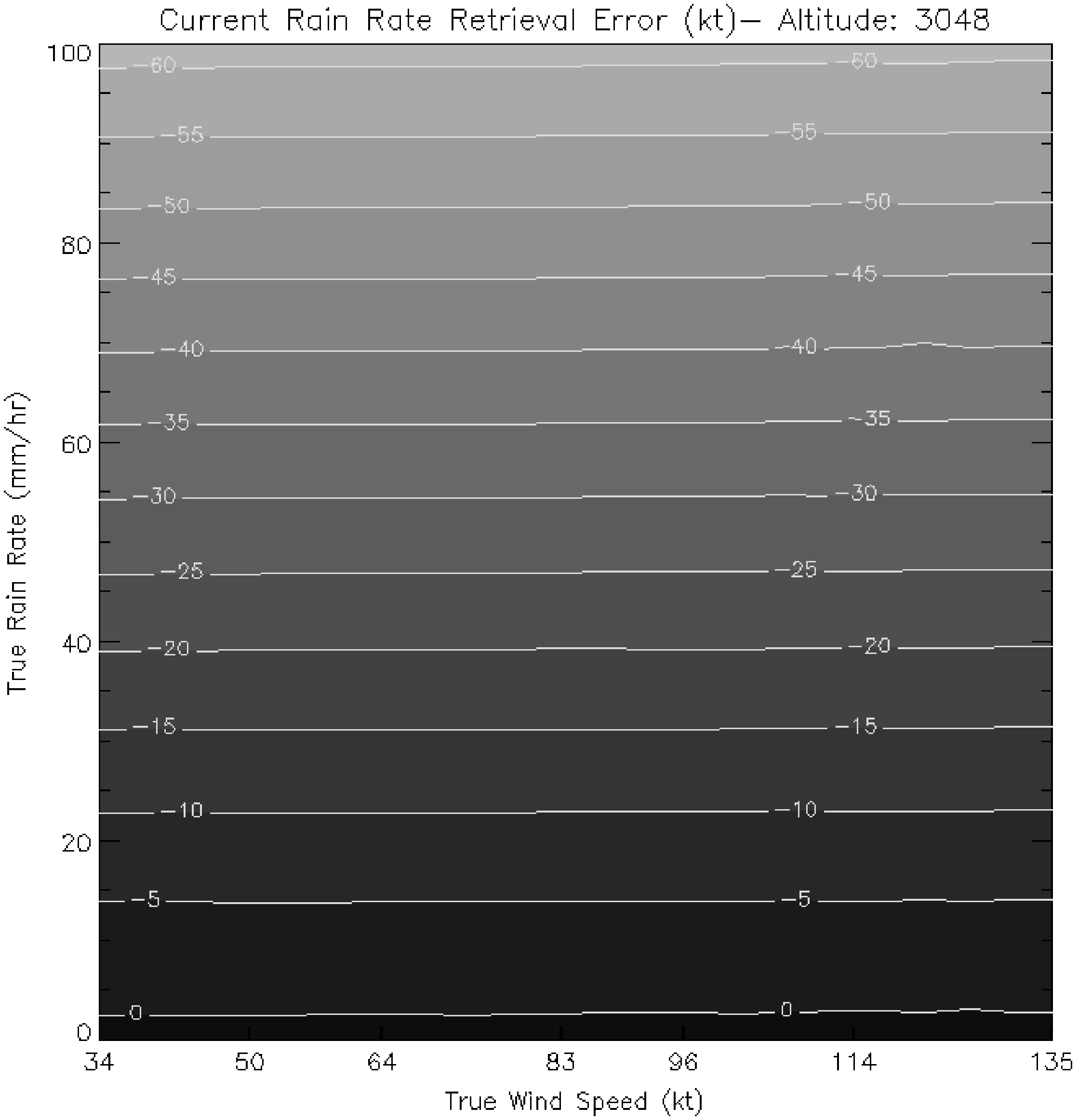

Figure 41: Same as Figure 39 except the altitude is now 3048 m.

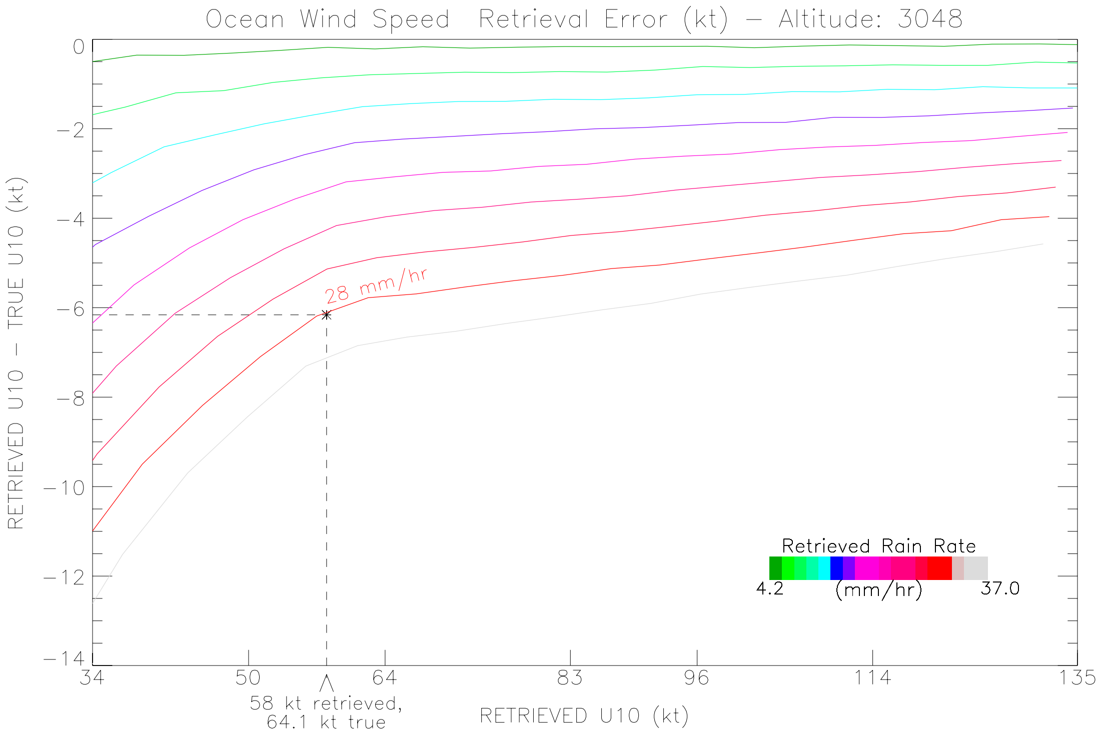

Figure 42: The error in the SFMR retrieved wind speed (retrieved – actual surface wind speed)

In order to determine the error in the 2005 and 2006 SFMR retrieval estimates from the retrievals themselves, a series of curves were generated. Each curve is at a constant SFMR retrieved rain rate and represents the error (SFMR retrieved surface wind – true surface wind) as a function of the SFMR retrieved surface wind speed. These curves are plotted in Figure 42. An altitude of 3048 m is assumed. From these curves the error in the retrieved SFMR wind speed can be determined based on the retrieved wind speed and rain rate. For example, if the retrieved rain rate was 28 mm/hr and the retrieved wind speed was 58 kt, the SFMR would have under estimated the true surface wind speed by 6.1 kt. That is, the true wind speed is really 64.1 kt, and the system is a category 1 hurricane rather than a tropical storm.

2.4 Retrieval Errors Caused by Sequential Sampling

The SFMR measures the brightness temperature of the scene at six frequencies from 4.74 GHz to 7.05 GHz. By measuring the scene at different frequencies, the SFMR retrieval process can individuate the contribution from the ocean surface wind speed and precipitation, and thus, these parameters can be retrieved. The current operational SFMR, designed and built by ProSensing Inc, is based on its predecessor built by Quadrant Engineering (now ProSensing) for the Hurricane Research Division. Both of these designs measure the brightness temperature at six frequencies by sequentially stepping through each of the (six) frequencies. With each step, the operational SFMR dwells for approximately 0.6 seconds as it integrates the brightness temperature measurement at a particular frequency.

Thus, it requires approximately 3.6 seconds in order to acquire all six brightness temperature measurements. If the observed scene is constant over this total integration time, no errors are introduced. However, since it is deployed on the NOAA WP-3D aircraft, the SFMR moves in the along track direction by approximately 450 m during this time. Because its footprint is much wider than this distance, it has been argued that even in the presence of gradients in the observed rain and/or wind fields, the sequential sampling approach does not introduce any significant errors in the retrievals. This assumption, however, is not true.

To demonstrate, the SFMR sampling, measurement and retrieval process are simulated for varying rain and wind conditions to evaluate the accuracy of the retrievals in the presence of gradients in the rain and wind fields. To properly model the measurements, the observed scene is integrated over the SFMR antenna pattern to account for the smoothing that the actual SFMR antenna pattern introduces. All errors are calculated based on the integrated scene (rain and wind) response.

Before evaluating the effects of the sequential sampling paradigm on the retrieval accuracy, Figure 43 presents an example of the effects of the antenna pattern on the observations. In this example, a rain band that is approximately 800 m in width (along track direction) with a peak rain rate of 40 mm/hr is observed. A constant rain rate of 5 mm/hr outside this band is assumed. It is common to observe such an event as the aircraft transects rain bands especially near the eye wall of tropical cyclones. Because the actual SFMR antenna patterns are not available, a Gaussian antenna pattern with a 3 dB antenna beam width of 22 degrees is assumed (SFMR’s antenna 3 dB beam width is approximately 22 degrees). The observed precipitation field is convolved with the antenna pattern as the SFMR flies through the rain band. The solid line shows the true precipitation field and the dashed line shows the precipitation field as viewed through the SFMR antenna. The latter is broader and has a lower peak due to the smoothing affects of the SFMR antenna pattern. For all simulations to follow, the effects of the antenna pattern on the precipitation and wind fields are accounted for prior to inputting these fields into the simulator. Once again, the retrieval errors will be calculated based on the antenna pattern weighted precipitation and wind fields, not the actual precipitation and wind fields. Thus, the errors that will be presented are solely due to sequential sampling (i.e. the stepped frequency approach).

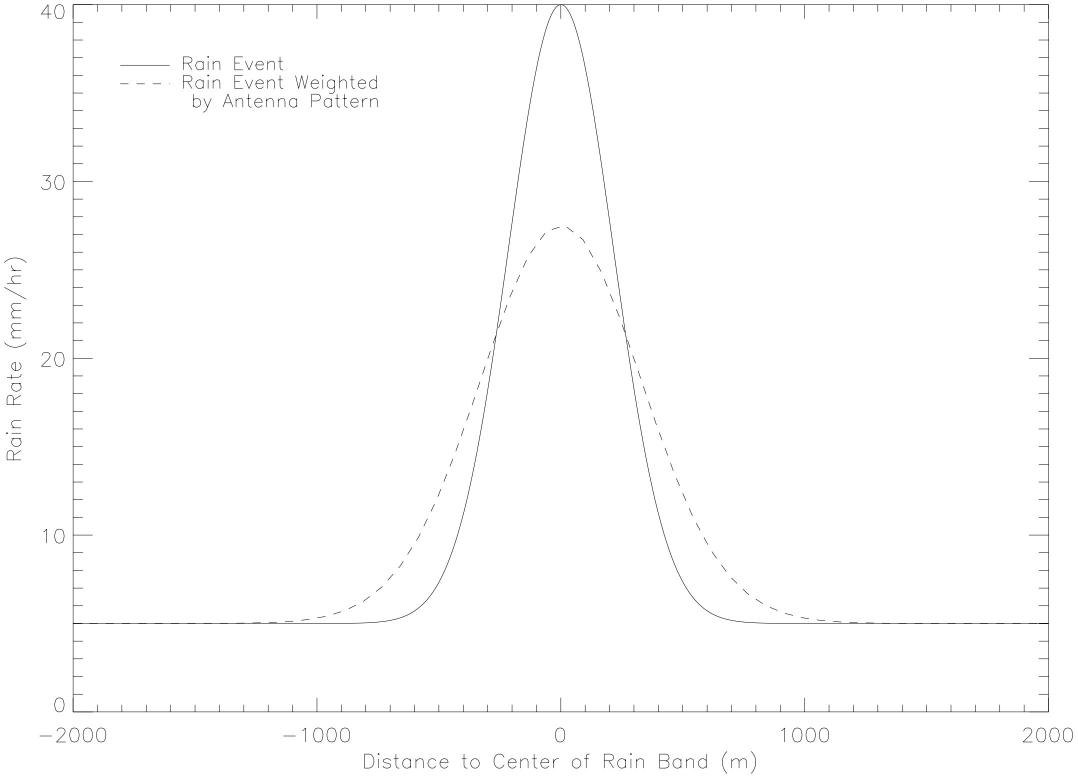

Figure 43: An example of the effects of the SFMR antenna pattern is shown. A precipitation rain band of roughly 800 m width that goes from 5 mm/hr to 40 mm/hr is shown by the solid curve. The dashed curve is the precipitation field viewed through the antenna. That is, it is the precipitation field convolved with the antenna pattern. Because the SFMR antenna patterns are not available, a Gaussian antenna pattern with a 22 degree beam width (approximate beam width of the SFMR) is assumed. The altitude is 1524 m for this case.

2.4.1 Sequential Sampling: Effects of Rain Events on Retrieval Errors

Figure 44 illustrates how the operational SFMR samples the scene. For this example, the precipitation field shown in Figure 43 is used. The wind speed will be assumed constant so that only the gradients due to the rain event are evaluated. The solid line presents the observed precipitation field that has been convolved with the SFMR antenna pattern as the SFMR files over the event. The numbers on the plot show the channel for which the brightness temperature measurements are being gathered at any given time. The SFMR steps through its six frequency channels every 3.6 seconds. As shown by the dashed lines, channels 0, 1, 2, 3, 4 and 5 observe rain rates 9.92, 12.0, 14.6, 17.6, 20.6 and 23.5 mm/hr, respectively, during one cycle through all six frequencies. If the retrieval process was run just following the last sample, the six brightness temperature measurements inputted into the retrieval process would each have observed a different mean rain rate. As will be shown, this produces significant errors in the mean retrieved rain and wind estimates. These are mean errors (i.e. biases), not random errors.

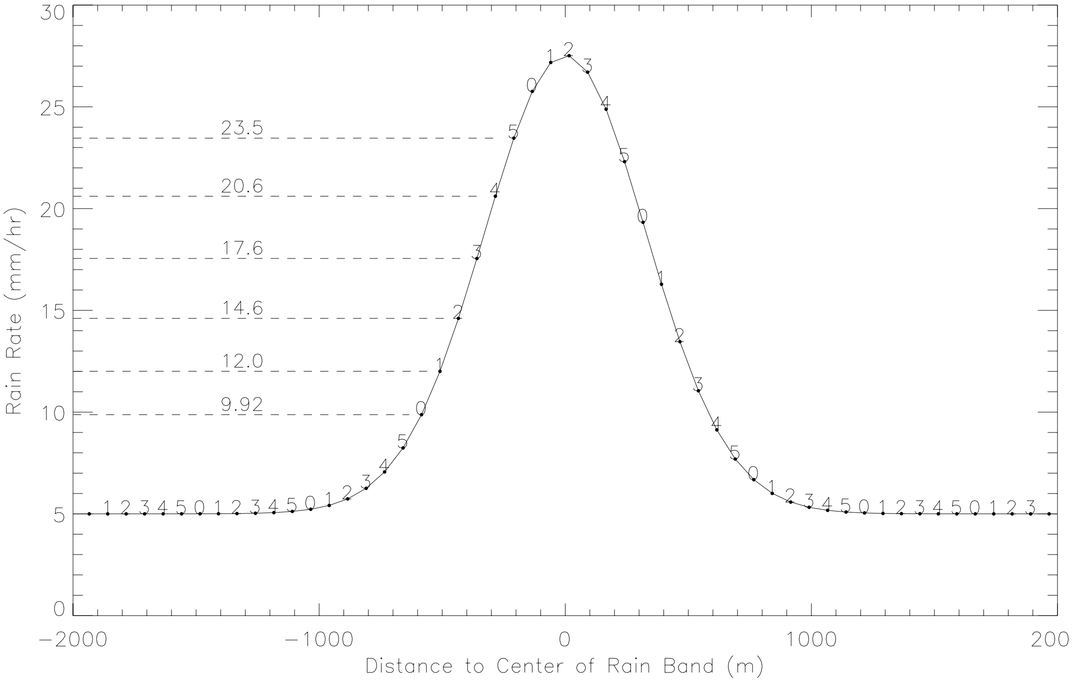

Figure 44: SFMR sequential sampling is illustrated above. The solid line presents an observed precipitation field that has been convolved with the SFMR antenna pattern. As the SFMR over flies this scene, it steps through its six frequency channels every 3.6 seconds. The numbers on the plot show which channel is being observed at any given time. As shown by the dashed lines, channels 0 through 5 observe rain rates 9.92, 12.0, 14.6, 17.6, 20.6 and 23.5 mm/hr during one cycle through all six frequencies. The assumed altitude is 1524 m for this plot.

To replicate the actual SFMR sampling and retrieval process, a simulated brightness temperature data set is derived using the SFMR simulator assuming a constant wind speed of 25 m/s, an altitude of 1524 m, a SST of 29 deg C and an ambient temperature of 20 deg C. For each sample in time (single frequency measurement), the mean brightness temperature for the channel being sampled is derived from the SFMR model function and the observed rain rate shown in Figure 44. For each of the last six brightness temperature measurements, one hundred realizations are created by adding random Gaussian distributed noise with a 0.5 K standard deviation to the mean brightness temperature values in order to fully simulate the actual measurements. For each realization, the rain rate and wind speed retrievals are derived using the real-time SFMR retrieval algorithm. The retrievals for this set of simulated measurements (6 channels * 100 realizations per channel) are averaged to estimate the mean retrieved rain rate and wind speed. For example, if the last measurement is made at approximately -200 m from the center of the rain band, the brightness temperatures for SFMR channels 0, 1, 2, 3, 4 and 5 are derived using rain rates 9.92, 12.0, 14.6, 17.6 20.6 and 23.5 mm/hr, respectively. Note that in practice the retrieval process is typically run once a second (roughly every two measurements) rather than at each point. The end result is the same; the only difference is that the results presented here are over sampled (sampled every 75 m rather than 125 m assuming a 125 m/s ground speed).

Figure 45 presents the results. Panel (a) plots the observed precipitation field (solid black line) and wind field (dashed black line) and the SFMR rain and wind retrievals (blue and red dots). The 10-second averaged SFMR rain and wind estimates are shown by the blue and red curves. Between the two dotted vertical lines is the observed rain event (i.e. rain rate is 5.25 mm/hr or greater). Panel (b) plots the error in the rain retrievals. This error is defined as the difference between the mean retrieved rain rates (blue points in panel (a)) and the observed rain field (black line in panel (a)). Note that this error is a mean error not a random error. The channel number for each measurement within the rain event is shown and corresponds to those in Figure 44. The six numbers in red correspond to the exact same six shown in Figure 44 whose rain rates were marked. This is done to provide an easy reference point between the figures. Panel (c) plots the error in the wind retrievals. This error is defined as the difference between the mean retrieved wind speed (red points in panel (a)) and the observed wind field (dashed black line in panel (a)). Once again this is a mean error (i.e. bias), not a random error.

Clearly the sequential sampling approach employed by the operational SFMR results in significant errors in both the rain and wind speed retrievals when gradients in the observed rain field are present. This is consistent with the oscillations in the retrievals noted in section 2.1 of this report. Once again the reader is reminded that the observed rain and wind already includes the weighting of the antenna pattern which lessens the actual gradients. As the gradient becomes steeper the oscillation in the errors becomes greater. The error for any one sample depends on the gradient in the rain rate and the phase of the sampling (i.e. which channel was last sampled). As will be shown, the error also depends on the rain rate, wind speed and altitude. In general, when the rain rate is over estimated, the wind speed is under estimated and vice versa. Also note that even for small changes in the observed rain rate over the six channels, significant retrieval errors occur. For example, the error in the wind speed retrieval at approximately -650 m is approximately -2 m/s even though the rain rate has only changed from approximately 5 mm/hr to 8 mm/hr over the six brightness temperature measurements acquired from -1050 m to -650 m.

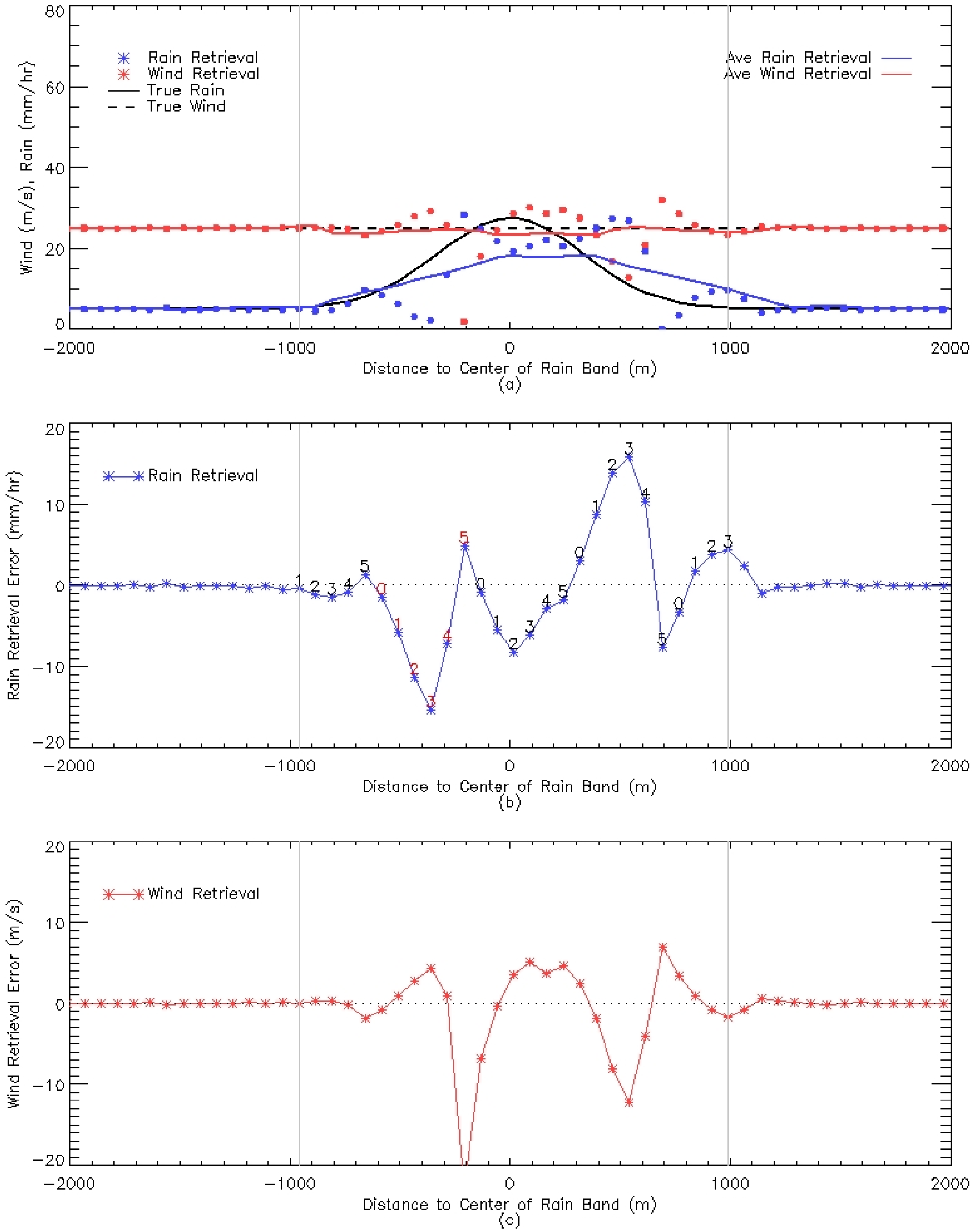

Figure 45: (a) Plots the observed precipitation field (solid line), wind field (dashed line) and the SFMR rain and wind retrievals (blue and red dots). The 10 second averaged rain and wind estimates are shown by the blue and red curves. (b) The difference between the rain retrievals (blue points in (a)) and the observed rain field is plotted. (c) The difference between the wind speed retrievals (red points in (a)) and the observed wind field is plotted.

Figure 46 presents the same analysis and results as presented by Figure 45 except that the observed wind speed for all measurements is set to 50 m/s (category 3 force winds) rather than 25 m/s (storm force). At the higher observed wind speed, the error in the wind retrievals is smaller, although still very significant. The reduction in the error is primarily due to the fact that the brightness temperature sensitivity to wind speed is much greater at hurricane force winds than at storm force winds. Thus, the errors introduced by sequential sampling have a smaller effect on the wind speed retrieval error. The error in the rain rate retrieval for the higher observed wind speed case is the same as for the lower observed wind speed case.

Finally, Figure 47 presents results for the same conditions as presented in Figure 46, but for a much broader rain event. In this case the change in magnitude in the observed rain event is the same but occurs over 4 km rather than less than 2 km. Once again, significant retrieval errors are experienced due to sequential sampling.

2.4.2 Sequential Sampling: Effect of Wind Events on Retrieval Errors

To evaluate the effects of sequential sampling in the presence of wind gradients, the same approach taken above is used except that the observed rain field is held constant at 5 mm/hr and a wind gradient similar in shape to the rain gradient above is observed. Figure 48 and Figure 49 present two cases: an observed wind event that is approximately 800 m in width that goes from 25 m/s to 42 m/s and an observed wind event that is approximately 800 m in width that goes from 50 m/s to 67 m/s. For these cases, the mean retrieved rain rate and wind speed errors are unaffected by sequentially sampling the wind gradient. Unlike absorption due to rain, the emission of the ocean surface and its dependence on wind speed is only weakly dependent on frequency. Thus, sequentially sampling the wind gradient over time (i.e. distance), does not introduce significant errors in the retrieval process.

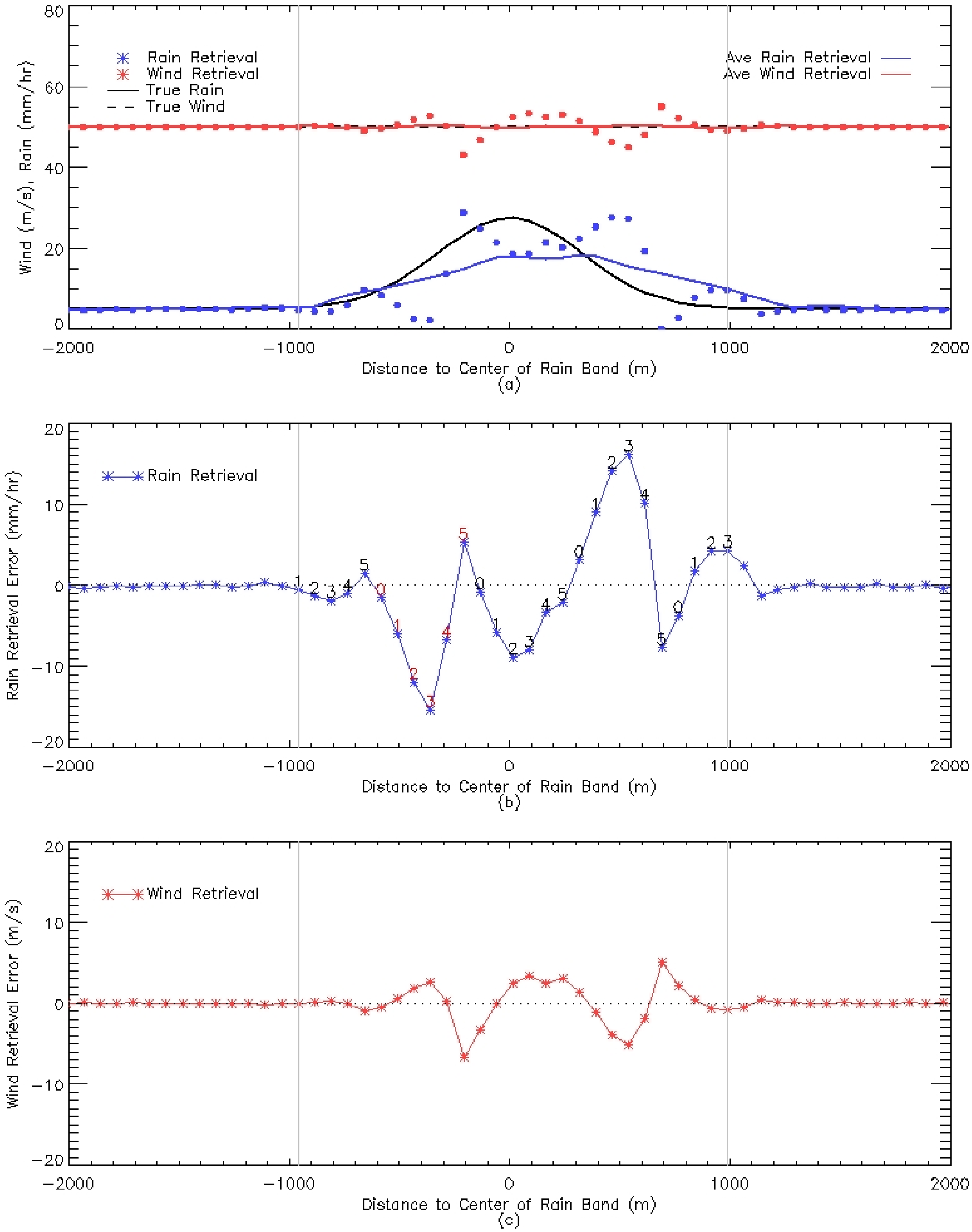

Figure 46: (a) Plots the observed precipitation field (solid line), wind field (dashed line) and the SFMR rain and wind retrievals (blue and red dots). The observed precipitation field is the same as in Figure 45 and the wind field is constant at 50 m/s. The 10 second averaged rain and wind estimates are shown by the blue and red curves. (b) The difference between the rain retrievals (blue points in (a)) and the observed rain field is plotted. (c) The difference between the wind speed retrievals (red points in (a)) and the observed wind field is plotted.

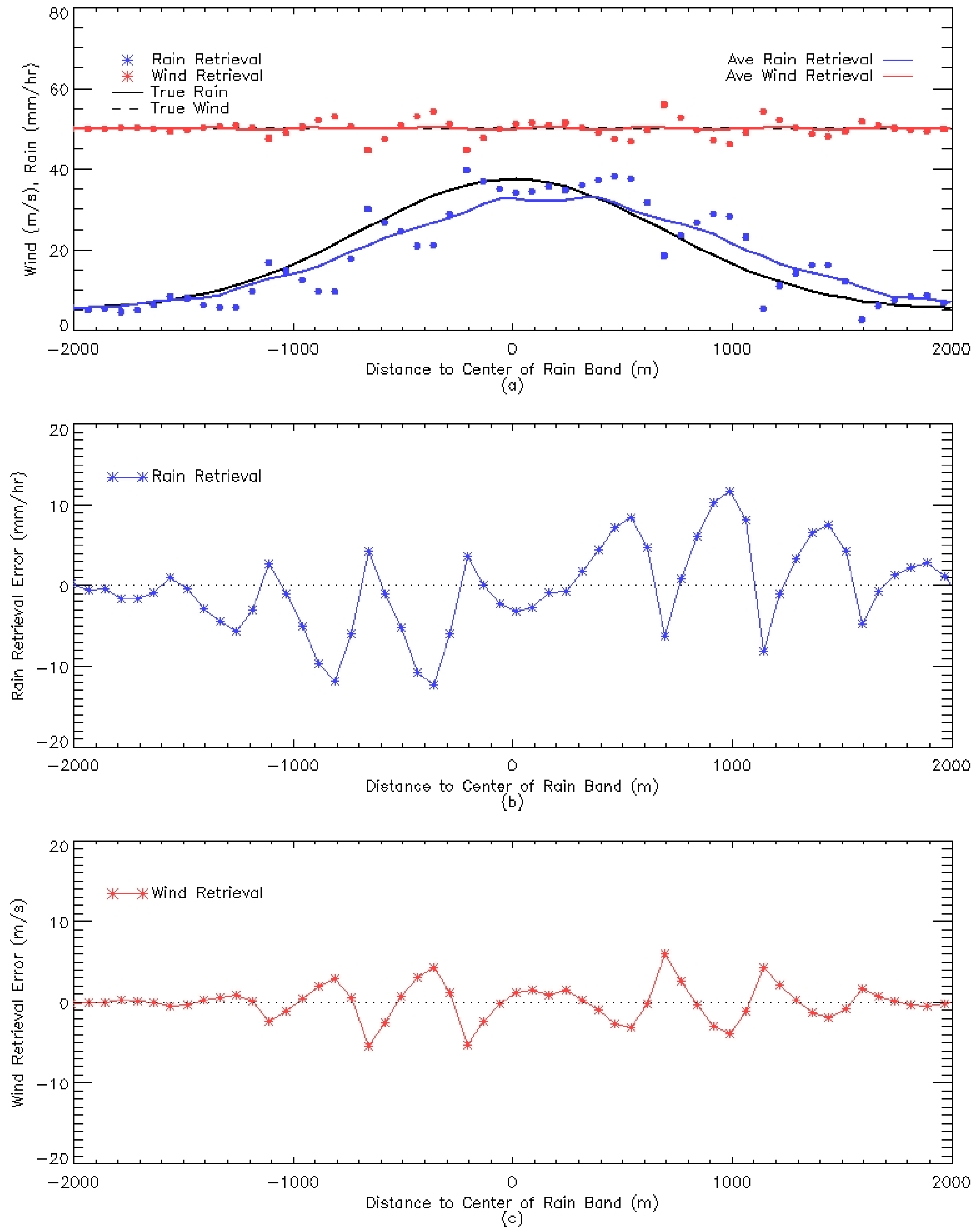

Figure 47: (a) Plots the observed precipitation field (solid line), wind field (dashed line) and the SFMR rain and wind retrievals (blue and red dots). The observed precipitation field is much broader than in Figure 45. The wind field is constant at 50 m/s. The 10 second averaged rain and wind estimates are shown by the blue and red curves. (b) The difference between the rain retrievals (blue points in (a)) and the observed rain field is plotted. (c) The difference between the wind speed retrievals (red points in (a)) and the observed wind field is plotted.

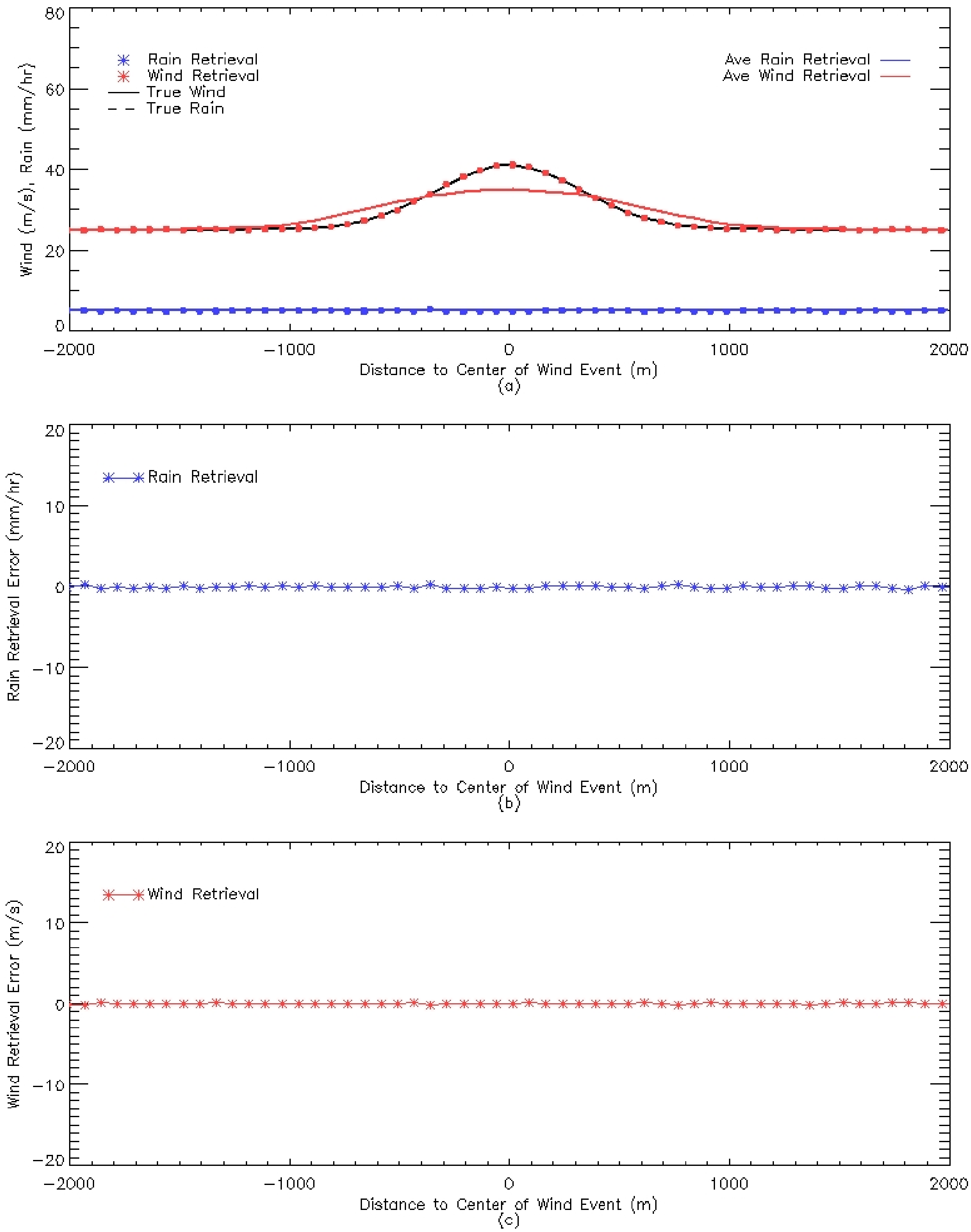

Figure 48: (a) Plots the observed precipitation field (dashed line), wind field (solid line) and the SFMR rain and wind retrievals (blue and red dots). A wind gradient is observed while the rain rate is constant. The 10 second averaged rain and wind estimates are shown by the blue and red curves. (b) The difference between the rain retrievals (blue points in (a)) and the observed rain field is plotted. (c) The difference between the wind speed retrievals (red points in (a)) and the observed wind field is plotted

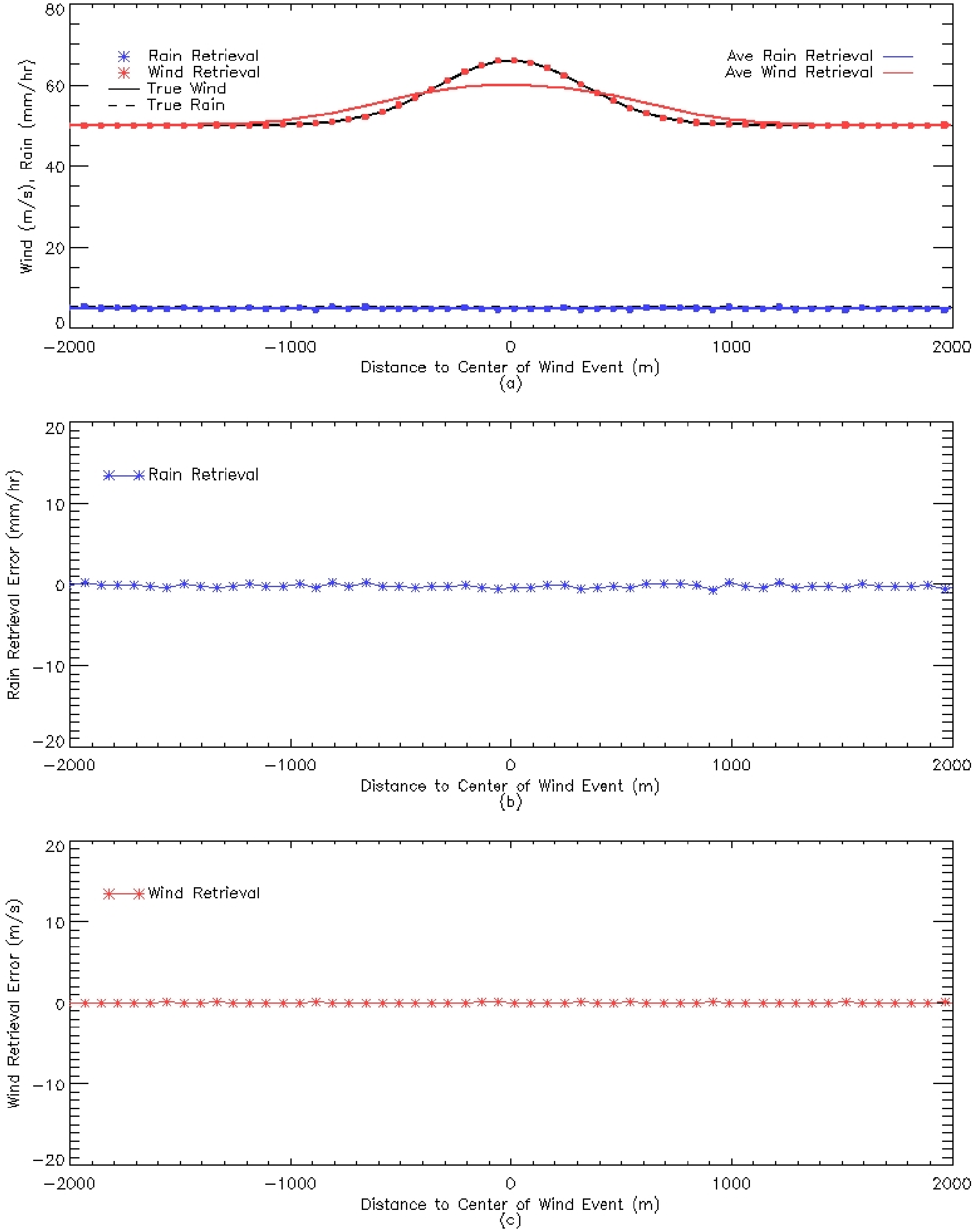

Figure 49: Same as Figure 48 except the wind gradient occurs at hurricane force winds.

2.4.3 Sequential Sampling: Minimizing Retrieval Errors

While sequential sampling appears to work in the presence of wind gradients, it introduces very significant errors in the presence of gradients in the observed rain field. For tropical storms and hurricanes, these gradients will be present and will often occur in high wind regions where it is critical to acquire accurate wind speed estimates. Further the retrieval errors caused by sequential sampling are dependent on rain and wind conditions, the steepness of the rain gradient, the altitude of the aircraft and the relative phase of the SFMR frequency channel sampling relative to the rain gradient. It should also be noted that the smoothed fields (10 second) averages also contained significant error. Because these errors oscillate based on the conditions and sampling phase, they have probably contributed to the uncertainty in the comparison of the SFMR wind retrievals to the collocated surface wind estimates derived from the GPS dropsonde measurements, since many of these measurements have been acquired in the presence of precipitation.

Ideally, the operational AOC SFMR should simultaneously sample all six channels as does the UMass SFMR. However, the current design for the operational system was based on a previous system used by the Hurricane Research Division for several reasons, and to modify these systems would not be cost effective. However, a simple and possible solution that can improve the accuracy of the retrievals in the presence of gradients in the rain field is to shorten the sampling period for the SFMR. In conversations with ProSensing, RSS discovered that the integration time for each SFMR channel can be programmed in software and shortened such that all six channels are measured within a 1 second period. The simulations presented in section 2.4.1 were re-run using a dwell time of 1/6th of a second for each channel.

Figure 50 presents the results for the shorter integration time during storm force wind conditions. The observed rain and wind fields are identical to those presented in Figure 45. Although errors in the rain and wind retrievals are still present, they are significantly smaller. If the reported wind and rain estimates are averaged over 10 seconds (i.e. the current practice) the bias introduced is small.
Likewise, the same is true at hurricane force winds. Figure 51 presents the results for the shorter integration time and hurricane force wind conditions. The error in the mean rain and wind retrievals are significantly reduced to that presented in Figure 46 where the integration time per channel was 3/5th of a second rather than 1/6th of a second.

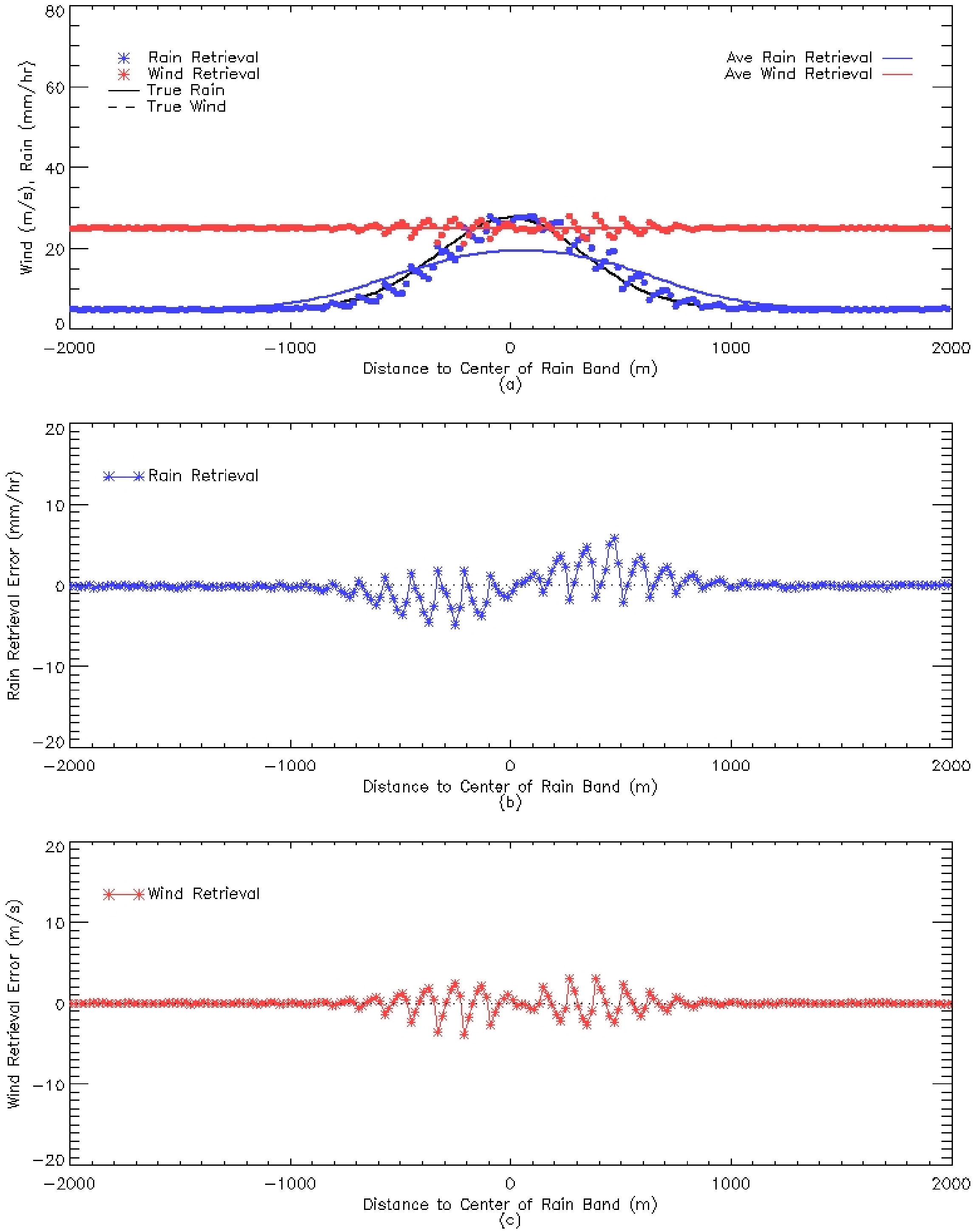

Figure 50: a) Plots the observed precipitation field (solid line), wind field (dashed line) and the SFMR rain and wind retrievals (blue and red dots). The SFMR integration time is set to 1/6th of a second per channel. The observed winds are constant at 25 m/s. The 10 second averaged rain and wind estimates are shown by the blue and red curves. (b) The difference between the rain retrievals (blue points in (a)) and the observed rain field is plotted. (c) The difference between the wind speed retrievals (red points in (a)) and the observed wind field is plotted

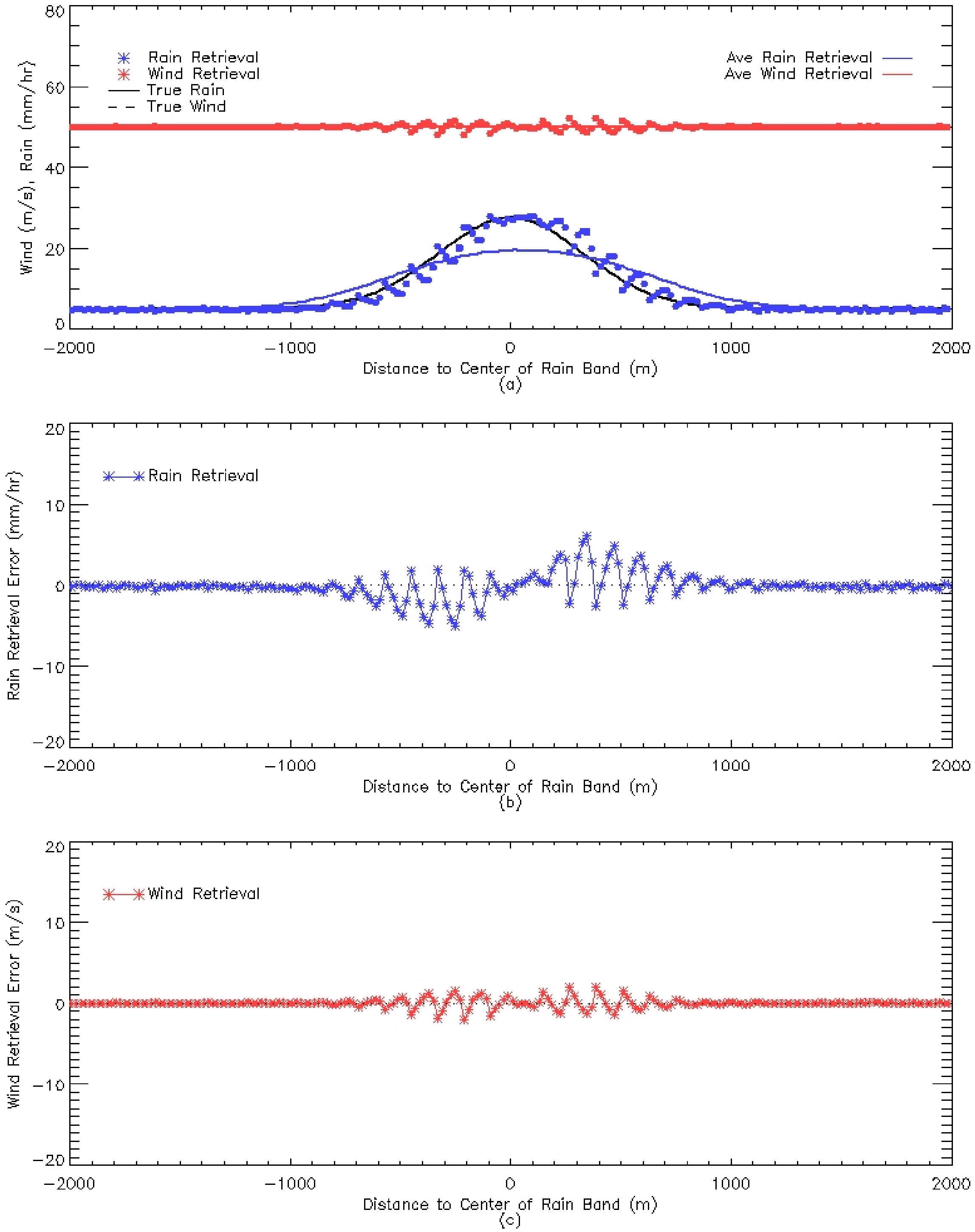

Figure 51: a) Plots the observed precipitation field (solid line), wind field (dashed line) and the SFMR rain and wind retrievals (blue and red dots). The SFMR integration time is set to 1/6th of a second per channel. The observed winds are constant at 50 m/s. The 10 second averaged rain and wind estimates are shown by the blue and red curves. (b) The difference between the rain retrievals (blue points in (a)) and the observed rain field is plotted. (c) The difference between the wind speed retrievals (red points in (a)) and the observed wind field is plotted

There is a small compromise to this solution. As the SFMR steps through its channels, there is overhead in the process such that not all the time can be allocated to the measurement due to switching noise and other setup issues. As the integration time becomes smaller, this time becomes a larger fraction of the total measurement time. Thus the precision (effective ∆T) will increase. In conversations with ProSensing, RSS was advised that reducing the channel integration time to 1/6th of a second would not significantly decrease the precision of the measurements over the 10 second averaging period for reporting the averaged retrieval values.

2.5 SFMR-Bathymetry Flight Tracks

In the annual report from the first year of this project, in subsequent technical reports and in section 2.1 of this report, higher than expected SFMR wind speed retrievals have been documented in regions where the water depth is less than 50 m. Several mechanisms may be the cause of these anomalies, but the largest is believed to be enhanced wave breaking due to shoaling. As ocean waves enter shallower water their height increases as their speed and length decrease. At a certain point the wave becomes unstable and begins to curl forward and break. This generates foam at the surface. Since this foam is not directly generated by the local wind and the ocean surface emission is dependent on the amount of foam, the SFMR retrieval process over estimates the wind speed. As a rule of thumb, breaking will occur when the water depth is equal to the wave height, however, the gradient in the water depth, the direction of the waves, the complexity of the wave field and other parameters will affect this process. To begin to understand and characterize these effects, SFMR observations and "in situ" ocean surface wind observations in different water depths, ocean states and wind conditions are required.

RSS and HRD designed flight modules that would obtain ocean surface wind observations collocated with the SFMR observations in water depths ranging from 50 m to 10 m. Potential wind observations from ocean wind scatterometry would not suffer from the same effects, and thus ocean surface backscatter observations collected by the IWRAP system were included in the flight modules. Utilizing IWRAP for this purpose has the advantage of requiring less resources since GPS dropsondes would not be needed and IWRAP would provide continuous wind observations rather than point observations that are obtained with the GPS dropsondes.

The flight modules described below were recommended for inclusion, and were included in the HRD Hurricane Field Program for 2007. Unfortunately, HRD priorities were focused on other objectives and these modules were not executed in 2007. Because the ocean vector wind science community would be interested in these measurements, we have held initial discussions with Dr. Paul Chang to include these flight modules in this ocean storms field program.

2.5.1 Proposed Bathymetry Flight Module

The objective of the bathymetry flight modules is to obtain collocated SFMR and GPS dropsonde estimates of the 10-m wind speed measurements at different water depths (less than 50 m). In addition to the SFMR, IWRAP observations are desired. Flight modules for both single and dual aircraft missions are described. To be most effective, these modules must be executed for different wind and bathymetry conditions. Ideally the flight module(s) should be executed at water depths of 10 m, 20 m, 30 m, 40 m and 50 m under gale, storm and hurricane force winds. Each flight module is designed to obtain in situ measurements of the 10 m wind speed that are collocated within approximately 200 hundred meters of the center point in the SFMR footprint. Because the wind and bathymetry might be changing spatially and because the SFMR observations are time sequenced with its finite beam widths, each module executes orthogonal cross patterns over the GPS dropsonde splash point. This pattern allows the effects of bathymetry on the SFMR to be separated from spatial gradients in the wind field and bathymetry.

2.5.1.1Single Aircraft

2.5.1.1.1 Required Instruments

NOAA AOC SFMR and GPS dropsondes are required for this flight module. IWRAP is desired but not required. Ocean wave measurements from the scanning radar altimeter (SRA) and/or from buoys are also desired but not required. Wind measurements from buoys are desirable but not required.

2.5.1.1.2 Single Aircraft Bathymetry Flight Module

Figure 52 presents a proposed flight track pattern for a single aircraft mission. Below is a description:

1. Aircraft enters pattern heading in the direction of the bathymetry gradient (increasing or decreasing water depth). If the bathymetry gradient is not known, this pattern is still recommended as the orthogonal cross pattern will allow us to determine if the bathymetry was changing and in which direction.
2. At time t = 0 seconds, GPS dropsonde (Drop 1) is launched. Aircraft maintains a level flight.
3. GPS dropsonde 2 (Drop 2) is launched 2 minutes later (t = 120 seconds).
4. Aircraft maintains level flight until the splash location of the Drop 1 is determined. At 5000 ft altitude, the dropsonde will take approximately 150 seconds to fall to the surface.
5. With the splash location known, the aircraft executes a series of three 90 degree turns to align for a pass over the splash location of Drop 1. Each turn should be sharp (30 degree bank) to minimize turning time and non-level flight. Between turns the aircraft should maintain level flight. This will

maximize the amount of valid observations collected with the SFMR (and IWRAP).

6. An 8 km level flight leg centered on the Drop 1 splash location is executed. The heading of this leg should be orthogonal to the original flight track as depicted in the figure.
7. By this time the splash location of Drop 2 should be known. The aircraft should execute two 90 degree turns (30 degree bank angle) to align for the pass over the second splash location. Once again, between turns the aircraft should maintain level flight.
8. An 8 km level flight leg centered on the Drop 2 splash location is executed. Again, the heading of this leg should be orthogonal to the original flight track as depicted in the figure.
9. After this leg, the aircraft can exit this flight module.

This flight track module can be embedded in another flight track module as a sub module or part of a flight track dedicated to analyzing bathymetry effects on the SFMR. For the latter, the aircraft should be heading in the direction of increasing or decreasing water depth. Figure 53 illustrates the flight track for a dedicated flight.

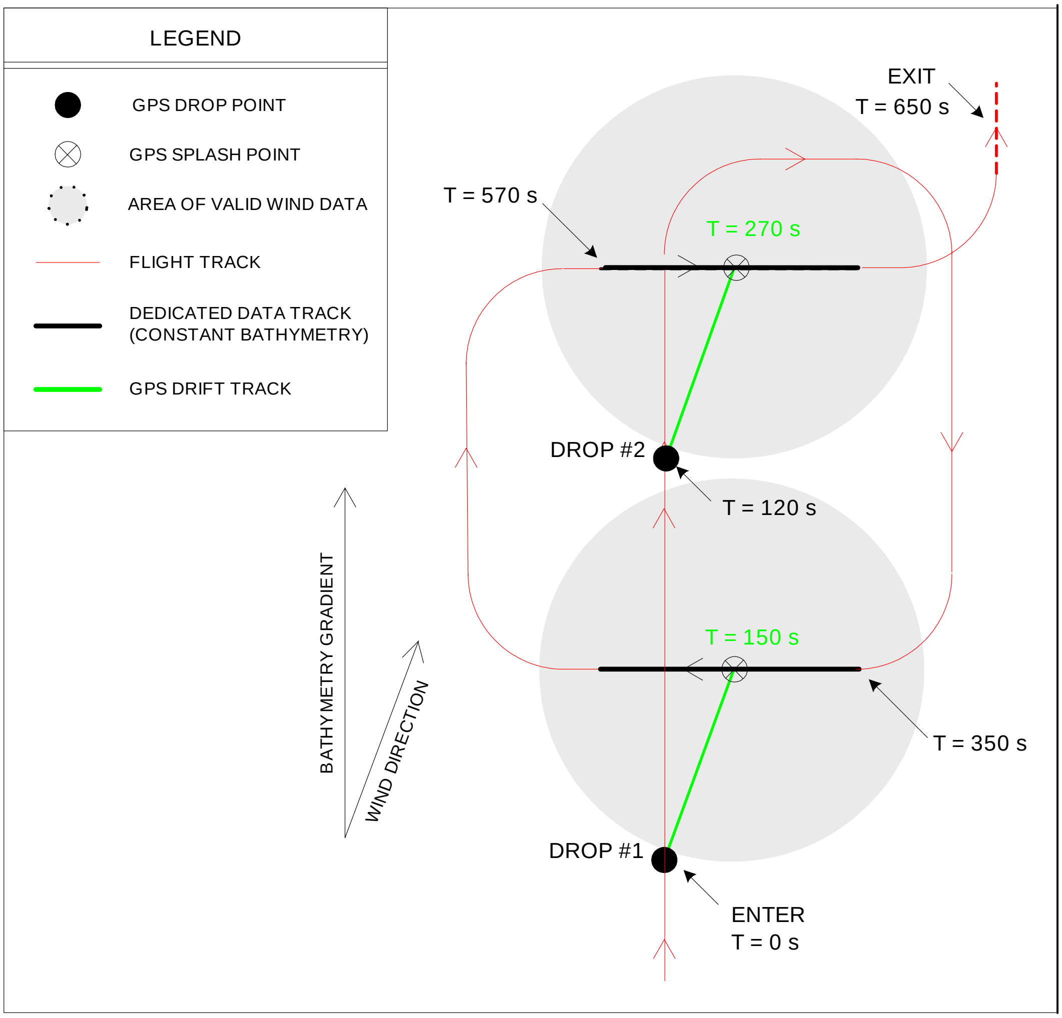

Figure 52: Proposed single aircraft flight module designed to collect the necessary observations for determining the impact bathymetry has on the SFMR retrievals.

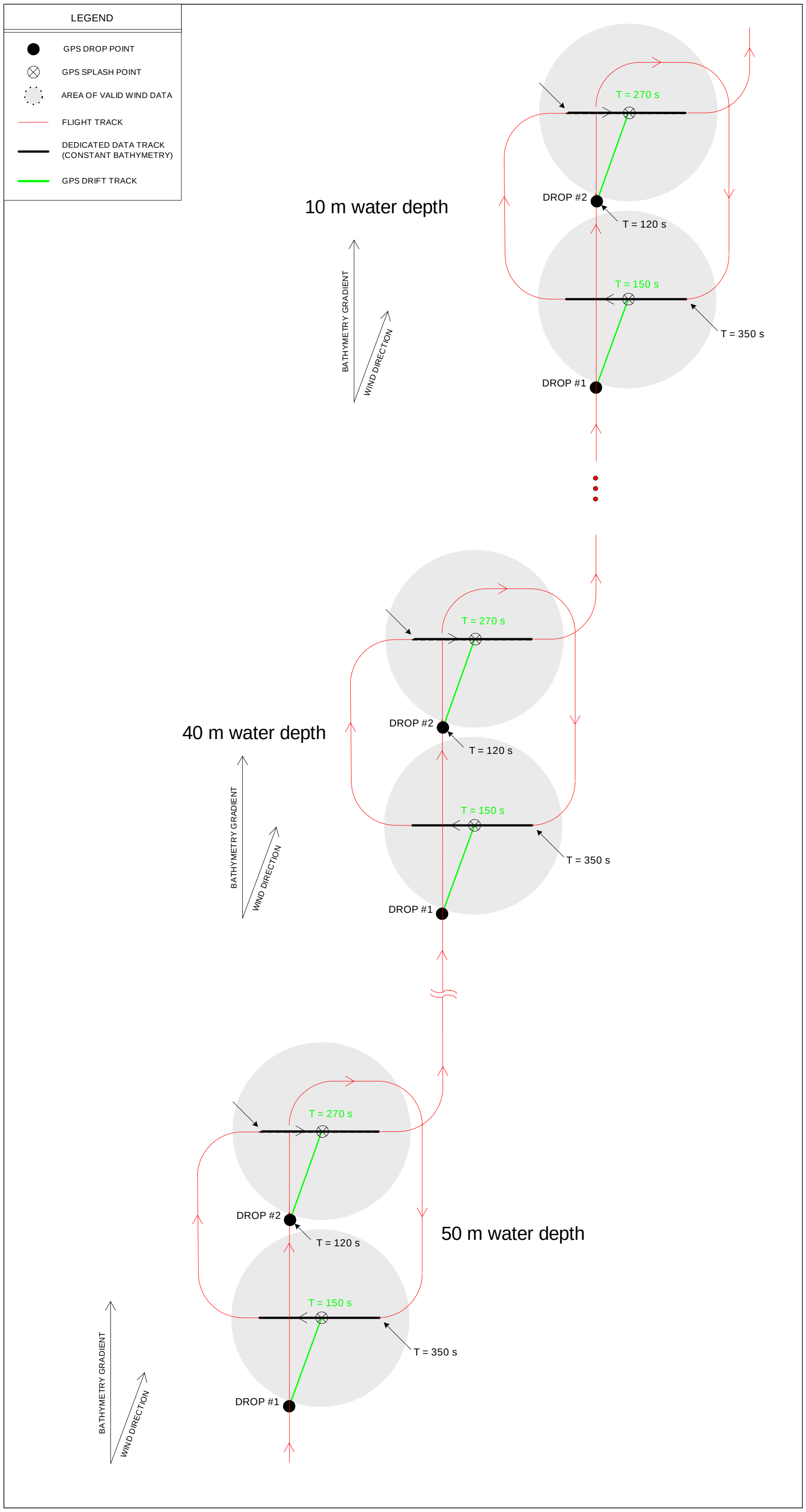

Figure 53: Single aircraft dedicated bathymetry flight track is shown. Each submodule (Figure 52) is executed at water depths of approximately 50 m, 40 m, 30 m, 20 m and 10 m.

2.5.1.2Multi-Aircraft

2.5.1.2.1 Required Instruments

NOAA AOC SFMR and GPS dropsondes are required for this flight module. IWRAP is desired but not required. Ocean wave measurements from the scanning radar altimeter (SRA) and/or from buoys are also desired but not required. Wind measurements from buoys are desirable but not required.

2.5.1.2.2 Dual Aircraft Bathymetry Flight Module

Figure 54 presents the dual aircraft bathymetry flight module. The orthogonal cross patterns over the splash locations of each dropsonde are achieved by flying orthogonal legs with the two aircraft rather than each aircraft. This reduces the total flight time to execute the module and simplifies the pattern for the higher altitude aircraft. Below is a description.

Low Aircraft (5000 feet):

1. Aircraft enters pattern heading in the direction of the bathymetry gradient (increasing or decreasing water depth). If the bathymetry gradient is not known, this pattern is still recommended as the orthogonal cross pattern will allow us to determine if the bathymetry was changing and in which direction.
2. At time t = 0 seconds the aircraft executes a 90 degree turn (30 deg bank) and then holds level flight. At time t = 90 seconds GPS dropsonde 1 is launched (Drop 1).
3. GPS dropsonde 2 (Drop 2) is launched 2 minutes later (t = 210 seconds).
4. Aircraft maintains level flight until the splash location of the Drop 1 is determined (~ t = 270 seconds). The aircraft executes a 180 degree turn to over fly splash location of Drops 1 and 2. Splash location of Drop 2 is estimated from splash location of Drop 1. Since the drop points are separated by approximately 12 to 15 km, both dropsondes should advect similarly.
5. The aircraft maintains level flight as it over flies the splash locations of Drop 2 and Drop 1 at approximately t = 390 seconds and t = 510 seconds, respectively. After flying a minimum of 4 km past the splash location of Drop 1, the aircraft then executes a 90 degree turn to resume the original flight track exiting this flight module at t = 580 seconds.

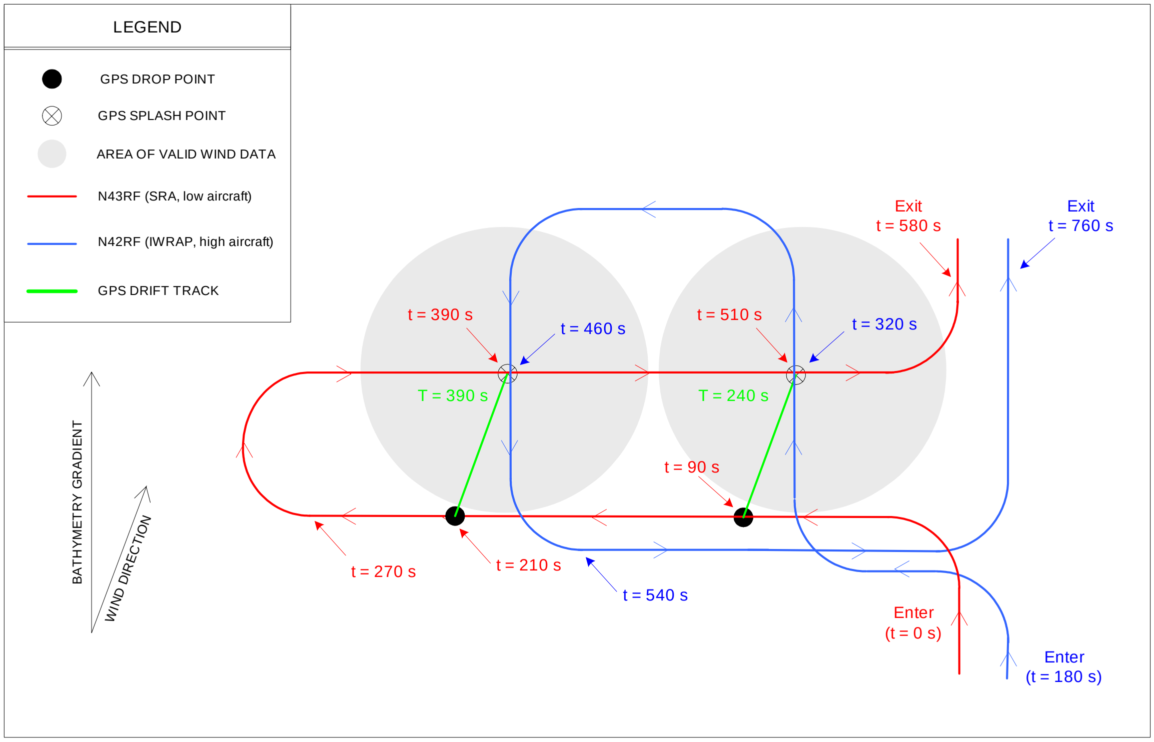

Figure 54: Dual aircraft bathymetry flight module 1.

High Aircraft (IWRAP, 7000 to 10,000 feet):

1. The high altitude aircraft enters pattern at the same location as the low aircraft but delayed by 180 seconds. It may be offset slightly so that it is over flying the splash locations of GPS dropsondes launched by the lower aircraft.
2. With knowledge of the splash location of Drop 1, a box pattern is executed to over fly the splash locations of Drops 1 and 2. Each leg over each drop splash location is a minimum of 8 km centered on the splash location. The length can be extended in order to keep the timing of both aircraft aligned at the exit of the flight pattern. During the 8 km legs, the aircraft must maintain level flight. Note that in this case the splash location of Drop 2 will already be known and therefore does not need to be estimated.
3. After completing the box pattern the aircraft executes a 90 degree turn to resume the original track with the lower aircraft.

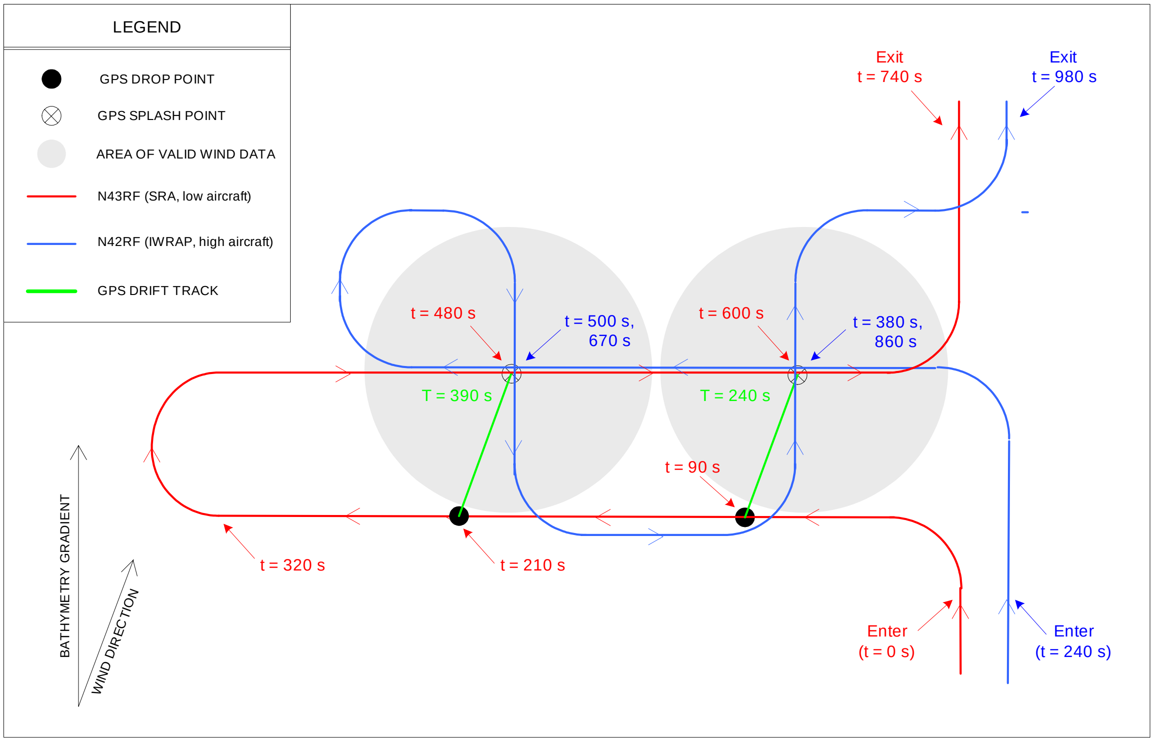

Figure 55: Dual Aircraft bathymetry flight module 2.

An alternative flight pattern is shown in Figure 55. With this pattern, the higher altitude aircraft executes orthogonal cross patterns over each location and over flies the same track as the lower aircraft as it over flies the two splash locations. This pattern has several advantages:

- Small calibration biases between the two SFMR units on the lower and higher altitude aircraft can be calculated since the two aircraft over fly the same track between the splash locations of Drops 1 and 2.
- The orthogonal legs are executed by the same aircraft, and thus measurement uncertainty caused by calibration biases between instruments is removed.
- More observations in the presence of the splash locations are collected by the additional passes of the higher altitude aircraft and by the coincident legs between the splash locations. This reduces the statistical uncertainty in the analysis.
- The splash location of Drop 2 does not need to be estimated since the track of the lower aircraft is extended giving the lower aircraft more time to determine the splash location.

The tradeoff is that this pattern is slightly more complex for the higher altitude aircraft (albeit probably attractive to the pilots) and the total flight module takes 2 minutes longer to execute.

2.6 Real-time Lower Fuselage Data Display System

RSS developed a Python and IDL based data distribution and visualization system for viewing data collected from instrumentation on the NOAA aircraft. This novel system was evaluated by forecasters and scientists at the National Hurricane Center (NHC) and Hurricane Research Division (HRD) as well as NOAA Weather Field Offices (WFOs) and various research institutes across the country during the 2005 and 2006 hurricane seasons. The system dynamically configures and transmits data from aircraft based instrumentation over satellite links with as little as 1200 bps throughput to a ground-based relay server. Processes onboard the aircraft and within the ground-based server monitor the flow of data and link to the aircraft, reporting the status of the satellite link and data transmission. A transmission subsystem determines the available bandwidth of the satellite links and dynamically alters the rate of data sent so that it fits within the available bandwidth to continue providing information in real-time. The ground server maintains a list of “subscribers” which it publishes this data to via the internet. Each subscriber specifies the type of data it wishes to receive, and the relay server complies by publishing only that data for which it has subscribed, further boosting the efficiency of the system.

An IDL-based user interface was created for NHC to display the critical parameters their forecasters are most interested in. This display presents a GIS map showing the aircraft track, flight level wind vector, flight level wind speed, SFMR wind speed, surface pressure estimates, boundary layer wind ratio and vertical wind speed. It also displays these parameters in real-time and historical mode XY plots around the GIS view.

In 2005 for the first time, aircraft were able to send continuous reflectivity profiles measured by the Lower Fuselage Radar on NOAA aircraft. These profiles were sent in real-time to a ground-based server. From there they were distributed to users through a subscription relay server and were even sent back up to the NOAA aircraft. These data along with the 33 scientific measurements were sent using on a 9600 baud satellite link. The latency measured from the time the data was acquired on the aircraft to the time it was displayed on the ground was only 1.5 seconds. In 2006 this application was expanded; see **Figure 56**, to provide the user with GIS viewing capability of parameters along with single and multiple parameter X-Y plots for comparison. This application included a novel feature allowing hurricane researchers and forecasters to display parameters overlaid on the actual flight path of the aircraft. The user was also given the ability to manipulate these flight tracks into a storm relative mode, whereby the rendering of the flight tracks were plotted as though the storm remained stationary. This feature along with the capability of point-and-click interaction between the X-Y plots and GIS display and simple measurement functions allowed researchers to directly measure the storm and hurricane wind radii on the GIS view. The X-Y plots were also linked to the GIS view. By clicking with the mouse on a data point within an X-Y plot, its actual location on the GIS plot was indicated. This allowed the user to zoom in to a particular section of the time series plot and determine the location of the event being studied automatically on the GIS view. One immediate use was for center fixing. By zooming in on the flight and SFMR wind profiles, the minimum wind speed could be easily determined and its location automatically transferred to the GIS view which showed the larger spatial picture. The user was then able to mouse drag from that point to the perimeter of hurricane force winds on the GIS view, and thereby measure the wind radii.

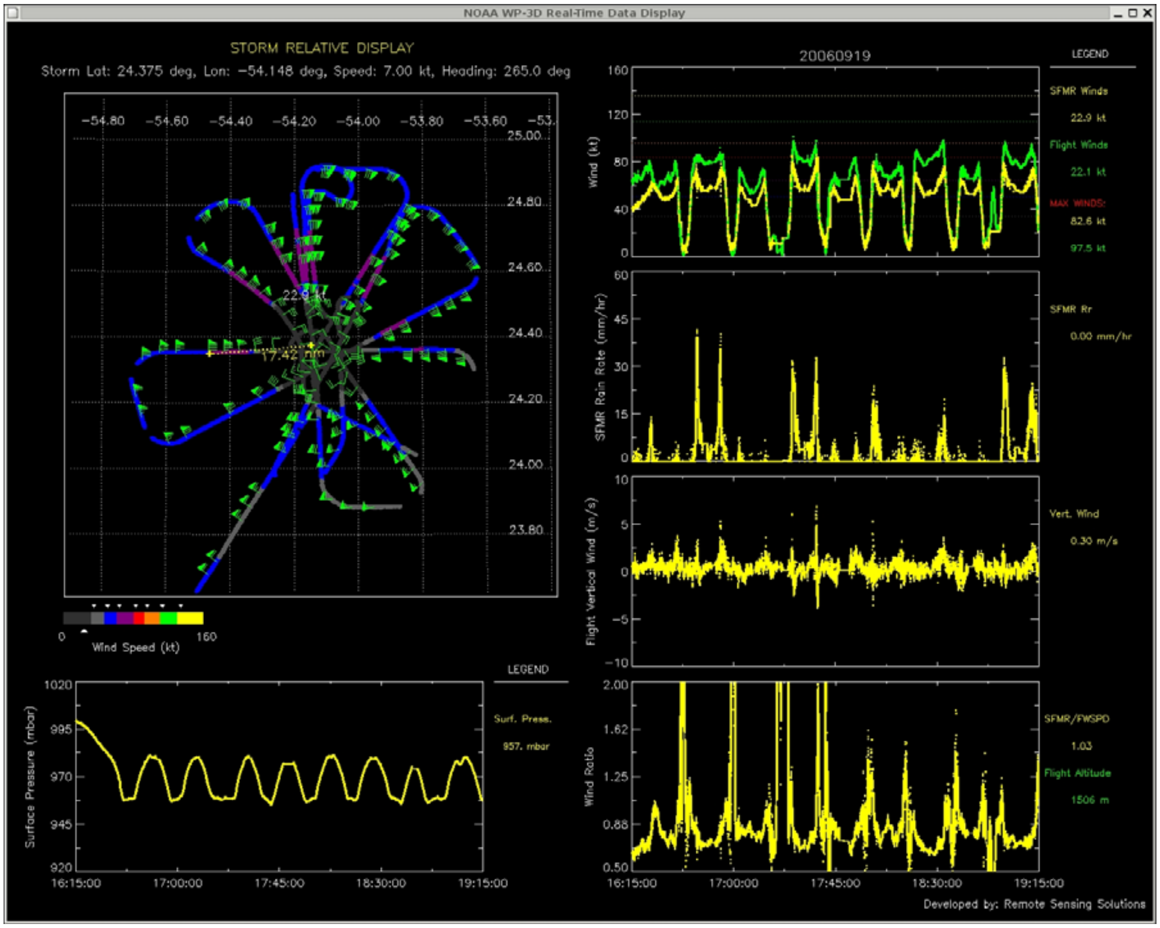

Figure 56: Real-time Data Display System in Storm Relative Mode

RSS received positive feedback on this application. Users remarked that it was very useful and powerful but its capabilities would be better utilized if it could be transferred to the NAWIPS environment. RSS is now developing such capabilities for the forecasters which will be available in a test mode in the spring of 2008.

3 Recommendations

With the deployment of the operational SFMR on the NOAA WP-3D aircraft in 2005, and in 2007 on the Air Force WC-130 aircraft, a critical wind and precipitation measurement capability has been realized. Forecasters are now provided with continuous ocean surface wind speed observations from these aircraft. The SFMR ocean surface wind observations have been cited in several forecast discussions and have aided in improving warnings and watches. However, as the work and results presented in this document and in the annual report from the first year of this effort show, further steps are required to remove performance limitations, improve accuracy and reduce uncertainty in the SFMR ocean surface wind speed observations. For the majority of issues presented, Remote Sensing Solutions has identified and developed solutions to overcome them. In sum, the primary issues are: calibration process, SFMR geophysical model function, SFMR sequential sampling, SST induced errors, radio frequency interference and bathymetry and real-time analysis tools. Below each topic is summarized and recommendations are presented.

3.1 SFMR Calibration Process

For the SFMR to produce unbiased estimates of the ocean surface wind speed, its measurements must be well calibrated and agree with the SFMR geophysical model function used in the retrieval process. ProSensing, Inc. provides an initial calibration of each instrument. They perform the calibration at their facility using standard radiometric loads. However, when deployed on the NOAA WP-3D aircraft, the SFMR reports brightness temperatures that do not agree with the SFMR GMF. Comparisons with buoy and GPS dropsonde winds have verified this problem. Initially AOC would fly in high wind conditions to collect measurements in order to tune the calibration of each SFMR channel. Remote Sensing Solutions analyzed this approach and found flying in low wind conditions is better suited for detecting and removing calibration biases. As discussed in our annual report from the first year of this effort, the SFMR is not very sensitive to low wind speeds. When calculating errors in the calibration, collecting measurements in low wind speed conditions helps because small variations in the true wind speed and measurement errors in the collocated in-situ wind observations do not produce significant variations in the brightness temperature measurements. Thus, accurate estimates of calibration biases can be determined. Remote Sensing Solutions recommended to AOC that they fly initial calibration flights over a buoy in wind conditions less than 10 m/s (15 m/s is upper limit), and AOC has adopted this approach. Remote Sensing Solutions recommends that this practice continues.

In addition to flying in low wind conditions to determine the calibration biases, another useful tool can be applied to determine the accuracy of the calibration. Due to the nature of the problem, the SFMR brightness temperature measurements naturally fluctuate even while all environment parameters are constant (i.e. ocean wind speed, rain rate, SST, air temperature). The measurements have a standard deviation of 0.5 K. This fluctuation in the brightness temperature measurements translates to zero mean noise f in the ocean surface wind speed and rain rate retrievals. In cases where no precipitation is observed, the SFMR should report positive and negative rain retrievals. Because the retrieval process zero-thresholds the rain retrievals, 50 percent of the rain retrievals reported should be zero when precipitation is not present irregardless of the wind speed. In the first year annual report, Remote Sensing Solutions showed that this parameter (percent of rain rate retrievals that are zero when precipitation is not present) is very sensitive to calibration biases and can be used to detect biases as small as 0.2 K. Also shown in this analysis is that calibration errors on the order of 0.2 K can produce significant biases and errors in the ocean surface wind speed retrievals even at hurricane force winds. Table 2 summarizes the error in the SFMR retrievals assuming that the total absolute calibration error (i.e. sum of absolute calibration error of each channel) is 1 K. For hurricane force conditions, this calibration error causes biases in the retrieved ocean surface wind of 4 to 6 knots. Larger calibration errors would cause larger errors. Because the parameter discussed above (percent of rain retrievals that are 0 mm/hr) is extremely sensitive to calibration errors, Remote Sensing Solutions recommends that the calibration-tuning process (i.e. the measurement and removal of calibration biases) use an additional criterion. This being that the rain rate retrievals in the presence of zero rain, produce 0 mm/hr estimates 50 percent of the time over reporting intervals of five minutes. Because such a procedure only requires access to the SFMR retrievals and not the brightness temperature measurements, and knowledge that precipitation is not present (radar systems on board can provide this information when not visually determinable), implementation would be very simple. In fact, this procedure could be run continuously to serve as a quality control parameter for monitoring the calibration of the instrument. Additionally, since NOAA AOC will be deploying its new data system, developed by Remote Sensing Solutions, on its aircraft during 2008, this data system could easily implement such a procedure.

Table 2: Maximum retrieval errors caused by 1 K maximum tuning error.

Warning Thresholds	Wind Speed	Rain Rate	Wind Speed Bias		Rain Rate Bias		Correlation
			min	max	min	max	
	knots	mm/hr	knots	knots	mm/hr	mm/hr	%
Tropical Storm Force / Gale	33	0	-12.6	8.9	0.0	4.6	-90.7
	33	5	-11.6	7.8	-3.7	2.4	-93.8
	33	10	-11.3	7.7	-1.9	1.7	-93.7
	33	20	-11.9	7.8	-1.2	1.2	-93.0
	33	30	-13.5	8.3	-1.0	1.1	-92.4
	33	40	-16.0	9.2	-1.1	1.1	-91.8
Storm	50	0	-6.0	5.9	0.0	4.7	-89.3
	50	5	-5.5	5.2	-3.8	2.4	-94.4
	50	10	-5.6	4.9	-2.0	1.8	-94.2
	50	20	-5.8	5.0	-1.2	1.3	-93.4
	50	30	-6.3	5.4	-1.1	1.2	-92.8
	50	40	-7.2	6.0	-1.1	1.2	-92.4
Hurricane Category 1	64	0	-4.3	4.6	0.0	4.9	-89.0
	64	5	-4.0	4.0	-4.3	2.6	-94.5
	64	10	-4.1	3.9	-2.1	1.9	-94.3
	64	20	-4.2	3.9	-1.3	1.4	-93.6
	64	30	-4.6	4.2	-1.2	1.2	-93.0
	64	40	-5.2	4.7	-1.2	1.3	-92.6
Hurricane Category 2	83	0	-3.8	4.4	0.0	5.3	-88.6
	83	5	-3.5	3.9	-4.6	2.9	-94.7
	83	10	-3.5	3.6	-2.4	2.1	-94.6
	83	20	-3.6	3.8	-1.5	1.6	-93.8
	83	30	-4.0	4.2	-1.5	1.5	-97.3
	83	40	-4.5	4.6	-1.4	1.4	-92.9
Hurricane Category 3	96	0	-3.8	4.5	0.0	5.6	-88.6
	96	5	-3.7	4.1	-4.8	3.2	-94.8
	96	10	-3.6	3.8	-2.7	2.3	-94.8
	96	20	-3.7	3.8	-1.8	1.7	-94.0
	96	30	-4.1	4.1	-1.5	1.6	-93.5
	96	40	-4.5	4.6	-1.5	1.6	-93.2
Hurricane Category 4	114	0	-3.9	4.8	0.0	6.2	-88.8
	114	5	-3.7	4.4	-4.9	3.6	-95.1
	114	10	-3.7	3.9	-3.3	2.7	-95.1
	114	20	-3.8	3.8	-2.1	2.0	-94.4
	114	30	-4.1	4.2	-1.8	1.8	-93.9
	114	40	-4.7	4.7	-1.8	1.9	-93.5
Hurricane Category 5	135	0	-4.1	5.0	0.0	7.1	-88.8
	135	5	-3.9	4.7	-4.9	4.4	-95.7
	135	10	-3.9	4.1	-4.3	3.3	-95.5
	135	20	-4.0	4.1	-2.6	2.5	-94.9
	135	30	-4.3	4.4	-2.3	2.2	-94.4
	135	40	-4.5	4.7	-1.8	1.8	-92.9
Maximum Wind	165	0	-4.5	6.2	0.0	9.2	-88.7
	165	5	-4.3	5.8	-4.9	6.2	-95.9
	165	10	-4.3	4.8	-8.1	4.8	-96.2
	165	20	-4.4	4.6	-4.2	3.6	-95.9
	165	30	-4.8	4.9	-3.6	3.3	-95.5
	165	40	-5.5	5.4	-3.5	3.4	-95.3

3.2 SFMR Geophysical Model Function

The SFMR geophysical model function predicts the brightness temperature as a function of frequency, ocean surface wind speed, rain rate, altitude, ambient air temperature and SST. This is an empirical model that was originally developed during the 1980s with limited data. The SFMR retrieval process determines the ideal ocean surface wind speed and rain rate that minimizes the error between a set of brightness temperature measurements (six brightness temperature measurements at the six SFMR frequencies) and those predicted by the SFMR geophysical model function. Thus, errors in this model will result in errors in the retrieval process.

In 2005, the portion of this geophysical model function that describes the ocean surface emissivity's dependence on the ocean surface wind speed, along with the rain exponent parameter in the absorption model, were updated [Uhlhorn et. al, 2006]. However, as reported in this document, it was found that the absorption model is still in error. Using independent, collocated rain rate estimates from IWRAP, Remote Sensing Solutions derived new coefficients for the absorption model that provide an optimal solution. Using an independent SFMR data set published by [Uhlhorn, et al, 2006] and the new coefficients in the absorption model, the SFMR ocean wind speed retrievals improved (bias between the SFMR ocean surface wind retrieval and GPS dropsonde surface winds was no longer present – i.e. slope of 1.0 in comparison) and the residual error no longer depended on wind speed or rain rate. Remote Sensing Solutions recommends that the operational retrieval process be updated to use these new coefficients:

$R_m = 2.8$
$R_e = 0.7$
$F_e = 0.0756$,

which are used in the equation:

$$K = \alpha\left(f^{R_m R_r{}^{F_e}}\right)\left(R_r^{R_e}\right).$$

During the 2007 IHC, questions were raised regarding the extent of the impact changes in the absorption model would have on the retrievals. Remote Sensing Solutions ran simulations to produce error contours and graphs that present these errors in the retrievals based on 2005 model function. Dr. Carswell plans to present an abstract and presentation to review this new model and the improvements in the retrievals that will result during the 2008 NHC conference.

3.3 SFMR Sequential Sampling

The operational SFMR developed by ProSensing, Inc. uses a sampling approach such that the six frequency brightness temperature measurements are gathered sequentially as the instrument steps through its six frequencies. The duration of this process is approximately 3.6 seconds. In the presence of gradients in the rain field, sequentially sampling over this long time period introduces significant errors in the ocean surface wind speed as documented in section 2.4. To substantially reduce these errors, Remote Sensing Solutions recommends that the total integration time to step through all six brightness temperature measurements be reduced to 1 second. In conversations with ProSensing, Inc., it was determined that a one second integration time period is acceptable and that the system can be modified to do so through a software configuration parameter only. Therefore no hardware changes are required.

3.4 SST Errors

The SFMR retrieval process requires knowledge of the SST. In the past, this value was manually entered or held constant for an entire flight despite the understanding that the SST will often vary substantially over the regions sampled in a single reconnaissance flight. Errors in the SST are known to cause significant errors in the retrieved ocean surface wind speed. For example, if the SST is under estimated, the ocean surface wind speed is over estimated and vice versa. This relationship is documented in the first year annual report.

To minimize this error, Remote Sensing Solutions worked with NOAA NESDIS and AOC to develop a process for gathering gridded SST values. Alan Goldstein at AOC modified the SFMR retrieval process to use a look up table that retrieves the SST value from the gridded SST values based on latitude and longitude. Starting in the winter of 2007, the AOC SFMR retrieval process began using this approach. Remote Sensing Solutions recommends that this procedure continues, and becomes an operational requirement. Note that ProSensing’s retrieval processor uses a table lookup to determine if land is present in the field of view. Therefore, SST values may be added to this database so that ProSensing’s retrieval process can also use the same approach. In conversations with ProSensing, Inc., it was determined that this technique could be accomplished.

3.5 Radio Frequency Interference

Since the SFMR is essentially a very sensitive C-band microwave receiver, it is susceptible to radio frequency interference. Detection schemes have been implemented by AOC and ProSensing, Inc. to identify RFI and prevent those channels containing RFI from being used in the retrieval process. Remote Sensing Solutions worked with UMass and NOAA NESDIS to acquire an RFI data set in 2007 during winter storm missions. This data set was provided to ProSensing in order for them to validate their RFI mitigation procedure. Remote Sensing Solutions also analyzed these data to determine frequency operation requirements for existing and future radar systems on board the NOAA WP-3D aircraft.

Remote Sensing Solutions also analyzed the impact that RFI has on the uncertainty of the SFMR ocean surface wind retrievals when it forces a particular channel or set of channels to be removed in the retrieval process. This analysis showed that the precision of the SFMR ocean surface wind speed is significantly degraded when the lowest or highest frequency channel is disabled (i.e. not used in the retrieval process). As a result, Remote Sensing Solutions recommends that NOAA AOC require that radar systems flown on their aircraft do not operate in 300 MHz bands around the lower and upper frequencies of the SFMR (4.74 GHz and 7.05 GHz), when the SFMR is collecting measurements. Further that the out-of-band transmit spectrum of these systems be measured and filtered to reject transmission in the protected bands. The amount of rejection will depend on the peak and average transmit power and the antenna pattern of each radar system. The integrated RFI within the protected bands needs to be less than -120 dBm at the SFMR antenna port. This assumes a 50 MHz integration bandwidth for the SFMR and a 10 dB rejection level.

Based on these criteria, a high pass filter was used during the operation of IWRAP. Results showed that without the filter IWRAP interfered with the SFMR’s lowest frequency channel. However, with the filter in place, no interference was detected.

3.6 Bathymetry

Shallow water depths can affect the accuracy of the SFMR retrievals due to enhanced wave breaking. Analysis presented in the first year annual report and observations shown in section 2.1 of this document show the negative effects that shallow water depths can have on the SFMR ocean surface retrievals. Both the AOC and ProSensing retrieval processors utilize land masks to help prevent land contamination and to some extent shallow water, due to the conservative tendencies of these land masks. Nevertheless, errors are still present in retrievals over shallow water. Unfortunately the current data set does not provide enough information to develop more advanced algorithms to detect errors introduced by shallow water or the ability to set fixed limits on an acceptable water depth for confidence in the SFMR retrievals. As noted this problem is very complex.

To address this issue, Remote Sensing Solutions has designed several flight modules that could be executed in order to gather the required data for analyzing this situation further. Working with HRD, these flight modules were incorporated into the hurricane field program during 2007. Unfortunately, due to other HRD priorities, these flight modules were not executed. Remote Sensing Solutions recommends that NHC incorporate these flight modules into their operational plans. Performing the flight modules would present a fairly low impact to existing missions and could be executed by the NOAA aircraft during the 2008 hurricane season and even during other field programs. Besides the requirement of some additional flight hours, the allocation of GPS dropsondes would to be necessary for these flight modules.

3.7 Real-time Analysis Tools

Remote Sensing Solutions developed a real-time data display application that allowed end users to visualize and interact with the SFMR data and other aircraft data as it flowed into NHC over a satellite data link. This application provided both time series and GIS views that allowed the end user to interact with for not only visualizing the data, but also viewing data at various averaging times, performing center fix operations and calculating wind radii. Feedback that we received indicated that these capabilities were very useful but that they needed to be integrated into the NAWIPS environment. Based on this request Remote Sensing Solutions is developing a subset of the real-time applications that will enable NAWIPS to display the SFMR data in a storm relative coordinate system as part of its JHT project focused on the Air Force SFMR system. If during this project, it is determined that the stand-alone version of the real-time display application should be implemented operationally, Remote Sensing Solutions will enable this deployment. The options for the standalone system would to provide the source code and documentation so that this application can be developed in the appropriate software language, alter the existing application to run automatically or develop the application for NHC in the environment and software language that is preferred. Note that the current application is based on Python and IDL and runs on a Linux operating system.